SYNTHETIC JET ACTUATOR FOR ACTIVE FLOW CONTROL

SYNTHETIC JET ACTUATOR FOR ACTIVE FLOW CONTROL

By

SHERIF ABDOU, B.SC.

A Thesis

Submitted to the School of Graduate Studies

in Partial Fulfillment of the Requirements

for the Degree

Master of Applied Science

McMaster University

MASTER OF APPLIED SCIENCE — McMaster University

(Mechanical Engineering) — Hamilton, Ontario

TITLE: Synthetic Jet Actuator for Active Flow Control

AUTHOR: Sherif Abdou, B.Sc. (Ain Shams University, Cairo, Egypt)

SUPERVISOR: Dr. S. Ziada

NUMBER OF PAGES: xv, 143.

ABSTRACT

This thesis investigates the characteristics of a long aspect ratio synthetic jet actuator and its application for the active control of the vibrations of the downstream cylinder in a tandem cylinder arrangement.

A long aspect ratio synthetic jet is produced through an axial slit along part of the length of a cylinder. The jet is excited acoustically by a pair of loudspeakers mounted at the cylinder terminations. The study compares between the performance of two different slits with aspect ratios of 273 and 773. The comparison is based on the spanwise distribution of the mean jet velocity and phase between the jet velocity fluctuations and the excitation signal. Three different frequencies and amplitudes are used to excite the speakers covering the range of frequencies used in the control application.

For both cases studied the mean centerline velocity of the jet increases with increasing the amplitude of the exciting signal, but decreases with increasing its frequency. Moreover, velocity deficits of up to 30% are evident as the midspan of the cylinder is approached from either end. Similar trends are also observed for the centerline phase distributions of the velocity fluctuations, with deficits of up to 130°. However, it is observed that for the long slit case the deficits in both the velocity and phase distributions are much larger than those for the short one.

The synthetic jet is then mounted in the upstream cylinder of a tandem cylinder arrangement to be used as a control actuator for controlling the vibrations of the downstream cylinder. A simple feedback control mechanism is used at a Reynolds number of about 6.3×10^4. This Reynolds number corresponds to the case where the

downstream cylinder's response is dominated with two frequency components, one at the resonance frequency of the cylinder, which is excited by broadband turbulence in the flow, and the other at the vortex shedding frequency. Both slits studied for the characterization experiments are used to compare their performance as control actuators.

Both jets produce comparable reductions in the vibration of the downstream cylinder. A reduction of about 20% in the total RMS amplitude of the vibrations signal is achieved. This amounts to a reduction of about 50% in the resonant peak and an average value of about 40% in the vortex shedding peak. The optimal values of gain and time lag of the controller are then used to investigate the effect of the jet on the flow. It is found that the short slit jet produced an effect that was traced up to 1.875 diameters downstream, while the effect of the long slit jet dropped dramatically very close to the upstream cylinder.

ACKNOWLEDGEMENTS

I would like to dedicate this work to my parents, my wife and my grandparents for their continuous guidance, backup and support. I would not be where I am today if it wasn't for them.

The author would also like to thank the following people for their contributions to this work:

Dr. S. Ziada, my supervisor, for his continuous guidance, support and his invaluable advice throughout the course of my master's work. Also, for his priceless help in editing the thesis.

Dr. D. S. Weaver for his useful guidance and suggestions as well as allowing me to use the wind tunnel and the spectrum analyzer.

Ron Lodewyks, Joe Verhaege, Andrew Buyers and Dave Shick for their technical guidance and help.

My friends Tarek Sadek, Iman Aouf, Rafael Bravo, Erik Naczynski, and Wael Hasan for their precious help with editing the thesis and their technical help with the lab equipment and the experiments.

TABLE OF CONTENTS

LIST OF FIGURES

NOMENCLATURE

A	Projected area of downstream cylinder.
b	Synthetic jet half width.
C_L	Lift coefficient.
D	Characteristic length of bluff body.
D_i	Inner diameter of cylinder.
D_o	Outer diameter of cylinder.
f	Driving frequency of the synthetic jet.
F_L	Lift force.
f_r	Resonance frequency of the downstream cylinder.
f_v	vortex shedding frequency.
h	Width of jet producing slit.
K_c	Controller gain.
l	Length of jet producing slit.
L_d	Length of downstream cylinder.
L_o	Stroke length of synthetic jet.
L_u	Length of upstream cylinder.
L_{wt}	Distance between parallel sides of the wind tunnel.
M	Magnification factor.
Re	Reynolds number.
$St.$	Strouhal number.
T_d	Controller time delay.
U	Free stream velocity.
U_{cl}	Average centerline velocity of issuing jet.
δ	Logarithmic decrement.
ζ	Damping ratio.
μ	Fluid viscosity.
ρ	Fluid density.

CHAPTER 1

INTRODUCTION

1.1. MOTIVATION

In 1998, Glezer et al. introduced the concept of synthetic jets and the prospect of using them as active control actuators. Since that time many applications have been developed in flow control using synthetic jets as the control actuator including jet vectoring, mixing enhancement, lift and drag manipulation, boundary layer separation control, cavity resonance, and vortex shedding control.

The characteristics of synthetic jets and how they compare to continuous and pulsed jets have been addressed in the literature both experimentally and numerically (e.g. Glezer et al. 1998; Glezer and Amitay 2002; Smith and Swift 2001, 2003 and many others). The emphasis was always on the steady state features of the jet, e.g. velocity profiles, jet width, momentum and volume flux of the jet as well as the downstream progression of the jet. Hence, the measurements do not take into account spanwise variations in the synthetic jet characteristics and the jet was always generated uniformly along the length of the jet-producing slit.

Currently, synthetic jets are used in many applications to control flow oscillations (e.g. Hsiao and Shyu 1991; Huang 1995; Ziada 1995,1999; Wolfe and Ziada 2003), including the control of vortex shedding from single and tandem cylinders. These applications entail the production of synthetic jets from an axial slit along part of the length of a cylinder by excitations provided at the terminations of the cylinder. Different

positions along the slit may be excited at different amplitudes and phase from other positions. It is therefore necessary to study the spanwise characteristics of these jets in order to analyze and understand the effect of this uneven excitation on the performance of the control actuator.

The application of synthetic jets in the control of the dynamic loading on the downstream cylinder of a tandem cylinder arrangement is of interest for the current study. The process can be briefly explained by Figure 1.1. Initially, without control, flow passes over the upstream cylinder, causing vortex shedding from the cylinder, which then convects downstream causing the downstream cylinder to vibrate due to the turbulence in the flow. Wolfe (2000) proposed a method to control these vibrations of the downstream cylinder using a synthetic jet actuator mounted on the upstream cylinder. Velocity perturbations induced by the synthetic jet manipulate the boundary layer of the upstream cylinder; hence, the vortex shedding process is altered. When the modified flow in the wake of the upstream cylinder reaches the downstream cylinder, it causes a reduction in the vibrations of the cylinder. Wolfe managed to substantially suppress the turbulent buffeting response of the downstream cylinder. The mechanism by which the synthetic

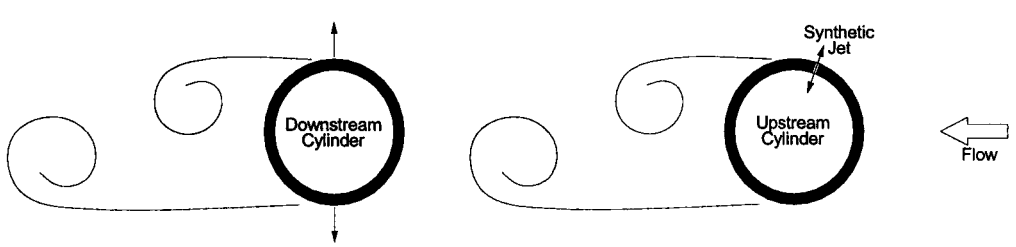

Figure 1.1. Schematic layout of the use of a synthetic jet actuator mounted on the upstream cylinder to control the dynamic loading on the downstream cylinder of a tandem cylinder arrangement.

jet manipulates the flow, however, is still not known and requires further investigation.

1.2. OBJECTIVES

From the above discussion, the main objectives of the present research are outlined in the following:

1. The first objective is to investigate the spanwise characteristics of a synthetic jet produced through a long narrow slit. The slit extends along the length of a cylinder and the jet is produced by acoustical excitations at the cylinder terminations. These characteristics include:
    a. The response of the synthetic jet to different excitation amplitudes and frequencies.
    b. The spanwise distribution of the mean centerline velocity of the issuing synthetic jet for the different excitation amplitudes and frequencies.
    c. The spanwise distribution of the phase of the velocity fluctuations for different excitation amplitudes and frequencies.
    d. The effect of changing the length of the slit on the characteristics of the synthetic jet.
2. The second objective of this study is to better understand the mechanism by which the turbulent buffeting of the downstream cylinder is attenuated by means of the synthetic jet. This requires investigating the effect of the controller gain and phase on the control performance of the synthetic jet. Hotwire measurements in the gap

between the cylinders is also needed to clarify the effect of the synthetic jet on the flow exciting the downstream cylinder.

1.3. THESIS LAYOUT

This thesis is presented in six chapters followed by a conclusion and four appendices. Chapter 1 introduces the motivation behind carrying out the work discussed in this thesis and the objectives of the research. In Chapter 2, the available literature discussing the topics covered through this thesis are surveyed. The chapter starts with vortex shedding from single cylinders and the different parameters governing the process. A discussion of vortex shedding from two cylinders then follows introducing the different patterns studied and emphasizing on the tandem cylinder arrangement. Flow control concepts are then introduced with emphasis on active flow control of vortex shedding and vortex-induced vibrations of single and tandem cylinders. Finally, synthetic jets are introduced and their characteristics and applications to flow control are discussed.

Chapters 3 and 4 discuss the experimental facility used, its different components and their characteristics. The description and specifications of the different components used in the test setup are described in Chapter 3. The chapter includes schematic diagrams of the experiments carried out as well as construction drawings of the different parts of the test section. Detailed description of the instrumentation used and the data acquisition system are also provided. Chapter 4 deals with the dynamic characteristics of the test setup components and their response to flow. The chapter includes the frequency response of the upstream cylinder synthetic jet production system, the dynamic

characteristics of the downstream cylinder, the lift coefficient, and the force transducer. Finally, the response of the tandem cylinder arrangement to flow is discussed.

Chapters 5 and 6 deal with the experimental results obtained and their analysis. The synthetic jet characterization is dealt with in Chapter 5 where a description of the experimental procedure is outlined followed by the analysis of the experimental results. In Chapter 6, the characterized synthetic jet is used as an actuator for controlling the downstream cylinder vibrations in a tandem cylinder arrangement. Analysis of the optimal control parameters used are discussed followed by a study of the effect the controller on the flow past the cylinders.

Last but not least, Chapter 7 summarizes the conclusions and contributions of this thesis, as well as introducing ideas for future research.

The appendices contain the data sheet of the speakers used to generate the synthetic jet as well as calibration data of the hotwires and the strain gages used. Detailed spectra and coherence measurements used for the results discussed in Chapter 6 are also included in the appendices.

CHAPTER 2

LITERATURE REVIEW

2.1. INTRODUCTION

This chapter provides a survey of the literature related to the topics covered in this thesis starting with vortex shedding from single and tandem cylinders. Following that, flow control mechanisms and applications will be discussed. Finally, synthetic jets are introduced along with their applications and characteristics.

2.2. VORTEX SHEDDING

Vortex shedding is a natural phenomenon that develops around bluff bodies when subjected to flow. It occurs due to the separation of the boundary layer into two shear layers around the body that roll-up in the near field forming a periodic vortex street knows as the Von Karman vortex street.

The history of vortex shedding probably dates back to ancient times as it was observed that wind causes the production of sound in an Aeolian harp. However, this was merely based on observations with no scientific basis. In the fifteenth century Leonardo da Vinci produced the first step in trying to understand vortex shedding with a sketch of vortices being shed from a piling in a stream. Later on, in 1878, the scientific study of vortex shedding started when Strouhal performed experiments on wires and discovered that the Aeolian tones produced by a wire in wind were proportional to the wind speed

divided by the wire thickness. It was not probably until 1912 with Von Karman's establishment of the Von Karman vortex street that a well established scientific basis for the study of vortex shedding was set forth.

The phenomenon of vortex shedding is dependent on many parameters related to the bluff body, e.g. the shape, orientation, and size, or flow related parameters, e.g. the velocity of the flow as well as the viscosity and density of the fluid, as well as being dependant on a wide range of small disturbances, like the turbulence in the flow, the blockage ratio for flow in ducts and the aspect ratio of the body. (Zdravkovich 1997)

The following sections discuss vortex shedding from single and tandem cylinders and the parameters and flow regimes that govern the process.

2.2.1. Vortex Shedding from a Single Cylinder

Although vortex shedding occurs from different bodies having different geometries and cross sections, circular cylinders have attracted a great amount of research due to their abundance and importance in all aspects of engineering applications.

Vortex shedding from a single cylinder is probably one of the most heavily studied topics with numerous reference published describing the phenomenon and analyzing different parameters that affect the process. Two textbooks by Zdravkovich (1997) and Blevins (1994) provide a very comprehensive and detailed analysis of the vortex shedding phenomenon from circular cylinders. They also contain a collection of references that thoroughly cover the topic. Several other references provide more information on this topic including reviews by Lienhard (1966), King (1977), Sarpkaya

(1979) and Matsumoto (1999). Lienhard (1966) provides an introduction to vortex shedding from cylinders, while King (1977) presents a review of, not only the phenomenon of vortex shedding but also the effect of different parameters as the length/diameter ratio, surface roughness, correlation length, as well as the wake interactions between a cylinder and another cylinder or a splitter plate.

The process of vortex shedding is affected by many parameters as mentioned earlier, the most important of which are discussed below:

2.2.1.1. Reynolds number

When a cylinder is subjected to a uniform flow a Von Karman vortex street will be observed to form in the wake of the cylinder due to the separation of the boundary layer from both sides of the cylinder. The process is mainly a function of the Reynolds number, Re, defined as the ratio between inertial to viscous forces in the boundary layer and is provided by

$$\mathrm{Re} = \frac{\rho U D}{\mu}$$

where,

ρ is the fluid density,

U is the free stream velocity,

D is the characteristic length (the cylinder diameter in case of flow around a cylinder), and

μ is the fluid viscosity.

Lienhard in 1966 summarized the different flow regimes of vortex shedding according to Reynolds number as shown in Figure 2.1. More in depth analysis of the different regimes observed in the figure can be found in the textbooks by Blevins (1994) and Zdravkovich (1997).

2.2.1.2. Strouhal number

As mentioned earlier, Strouhal in 1878 was the first to conclude that the Aeolian tones produced by a wire were proportional to the wind speed divided by the wire thickness, thus establishing what is now known as the Strouhal number. However, it was not until 1926 when Benard proposed to call this dimensionless parameter the Strouhal number (Zdravkovich 1997).

The Strouhal number can be defined as the proportionality constant between the frequency of vortex shedding from a body and the ratio between the free stream velocity to the characteristic length of the body (the diameter of the cylinder in this case), where

where,

$$St = \frac{f_v D}{U}$$

St is the Strouhal number,

f_v is the frequency of vortex shedding,

D is the characteristic length (the cylinder diameter in this case), and

U is the free stream velocity.

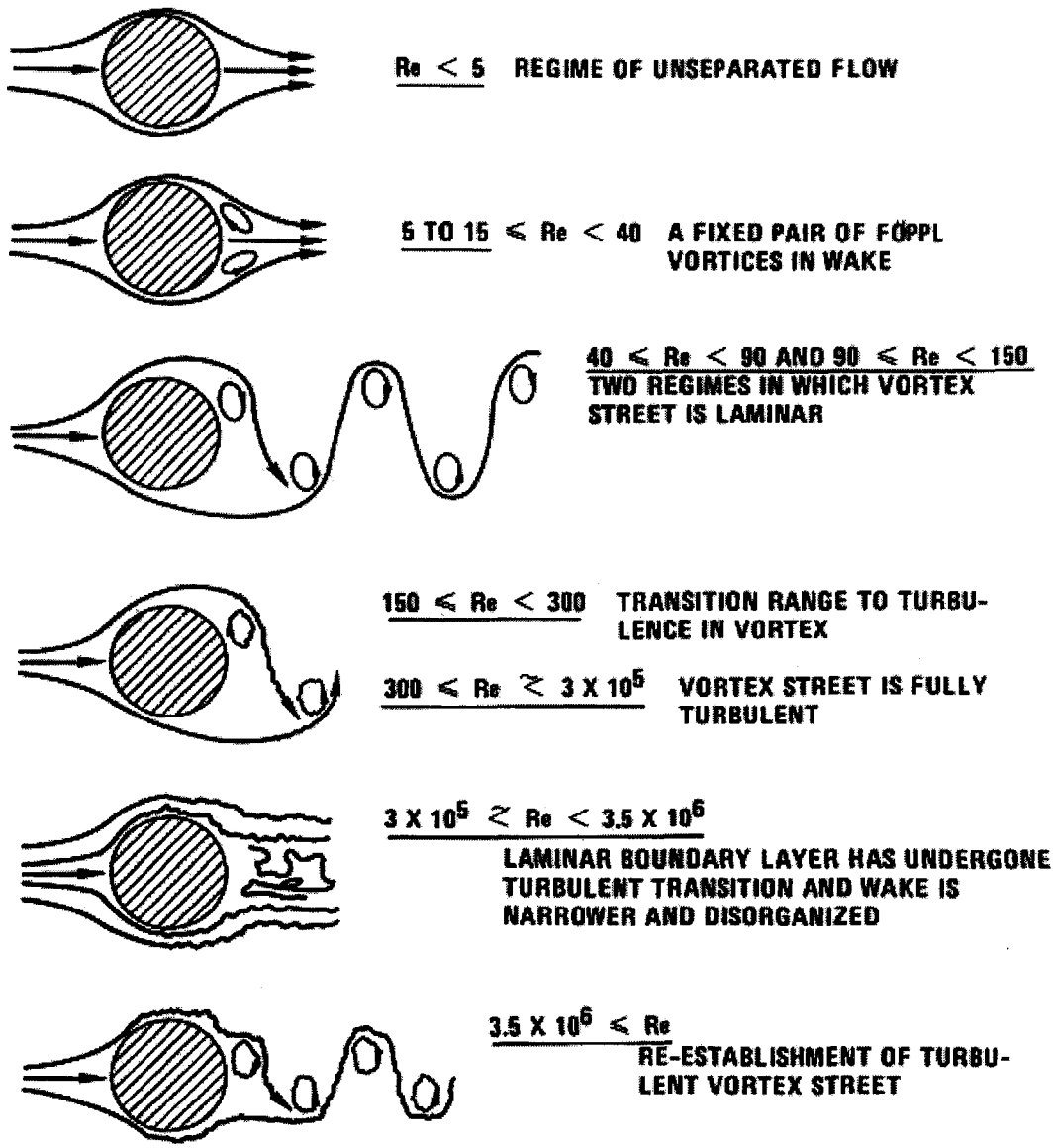

Figure 2.1. Flow regimes for flow across rigid smooth circular cylinders. [Lienhard (1966)]

Strouhal number is mainly a function of the Reynolds number as well as other parameters including the geometry of the body, the surface roughness, length to diameter ratio and turbulence levels in the flow. Figure 2.2, after Lienhard (1966), shows the variation of Strouhal number with Reynolds number for circular cylinders.

2.2.1.3. Correlation length

Although one might assume that vortex shedding from a circular cylinder is a steady, harmonic two-dimensional process, this is not entirely true. It was observed (e.g. Bloor 1964; Blevins 1985, 1994; Zdravkovich 1997) that the vortex shedding process is

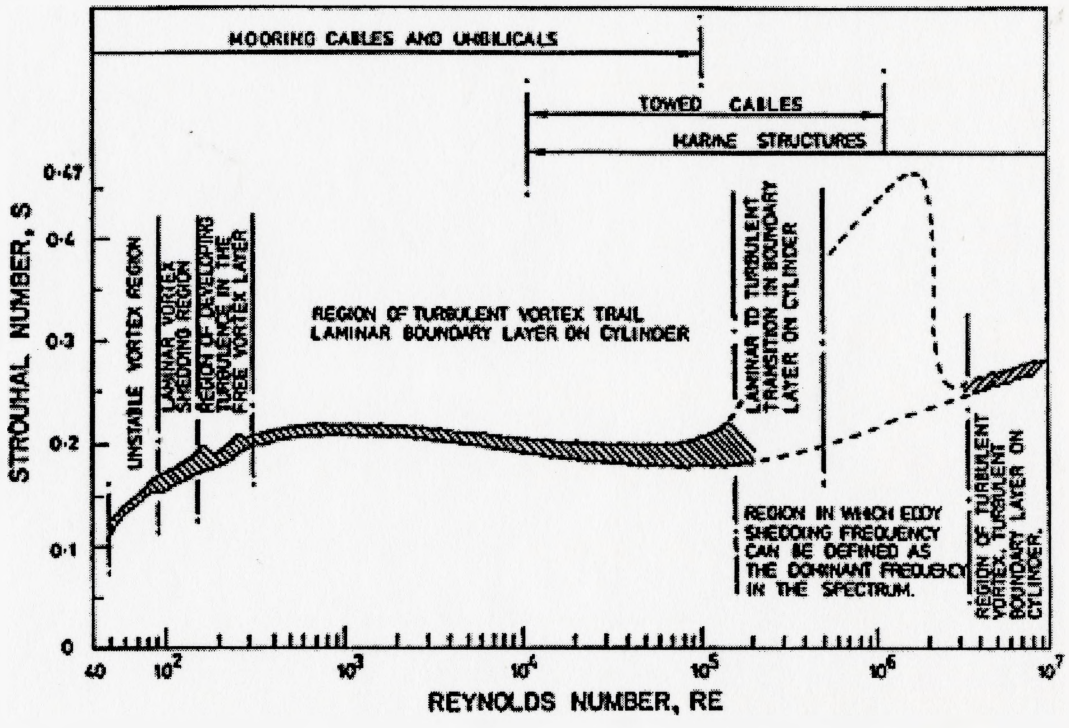

Figure 2.2. Strouhal number vs. Reynolds number relationship for circular cylinders. [Lienhard (1966)]

not constant along the span of cylinder and does not occur at a single frequency, but rather wanders over a narrow band of frequencies. This occurs due to the initiation and growth of irregularities in the wake of the cylinder. These three-dimensional effects are characterized by the correlation length.

The correlation length can be defined as the spanwise length along which the velocity fluctuations in the near-wake are still correlated (Zdravkovich 1997). King (1977) indicates that the correlation length varies with Reynolds number, turbulence, length to diameter ratio and surface roughness. Typical values of correlation length were also provided as a function of Reynolds number for smooth cylinder. Correlation length values of 15 to 20 diameters were typical for low Reynolds numbers ($40 < Re < 150$), while this value drops to 3 to 6 diameters for Reynolds numbers of the order of 10^4.

2.2.1.4. Effect of cylinder vibration on vortex shedding

Previous discussions were concerned with vortex shedding from rigidly fixed circular cylinders, thus preventing cylinder vibration due to fluctuating lift and drag. Nonetheless, it is of major importance to study the effect of having a flexibly mounted cylinder on the vortex shedding process as this represent a more realistic case in application. The presence of a flexible cylinder in cross flow allows the interaction between the vortex shedding process and the cylinder vibration.

Due to vortex shedding the cylinder is subjected to fluctuating lift and drag forces and experiments show that the fluctuating lift occurs at the shedding frequency, while oscillations in the drag force occur at twice the shedding frequency (Blevins 1994). This

occurs due to the nature of the vortex shedding process where the pressure fluctuations on the surface of the cylinder cause lift forces to repeat whenever a vortex pair is shed, while the drag forces repeat whenever a vortex is shed. These fluctuating lift and drag forces cause cylinders to vibrate both in the cross-flow direction and in-line with the flow respectively. Cross-flow oscillations, however, are the most common and are thus the mostly studied.

Transverse vibrations caused by the fluctuating lift occur at or near the vortex shedding frequency and have a strong effect on the vortex shedding process. These effects range from increasing the spanwise correlation due to better organization of the wake, to changing the vortex shedding frequency due to lock-in, changing the drag and lift on the cylinder, and changing the phase, sequence, and pattern of vortices in the wake. Many references discussing vortex-induced vibrations of cylinders cover these topics (e.g. Sarpkaya 1979; King 1977; Bearman 1984; Blevins 1994; Zdravkovich 1997; as well as many others)

The change in vortex shedding frequency accompanied by the interaction between cylinder vibration and vortex shedding in what is know as Lock-in is one of the most important results of vortex-induced vibration. Initially, as the flow velocity is increased the vortex shedding frequency increases accordingly to match a Strouhal number of about 0.2 (Figure 2.3). When the vortex shedding frequency approaches the resonance frequency of the cylinder, the cylinder resonates and large amplitude vibrations are observed. Further increase in flow velocity, however, does not change the vortex shedding frequency, which keeps being locked-on to the natural frequency of the

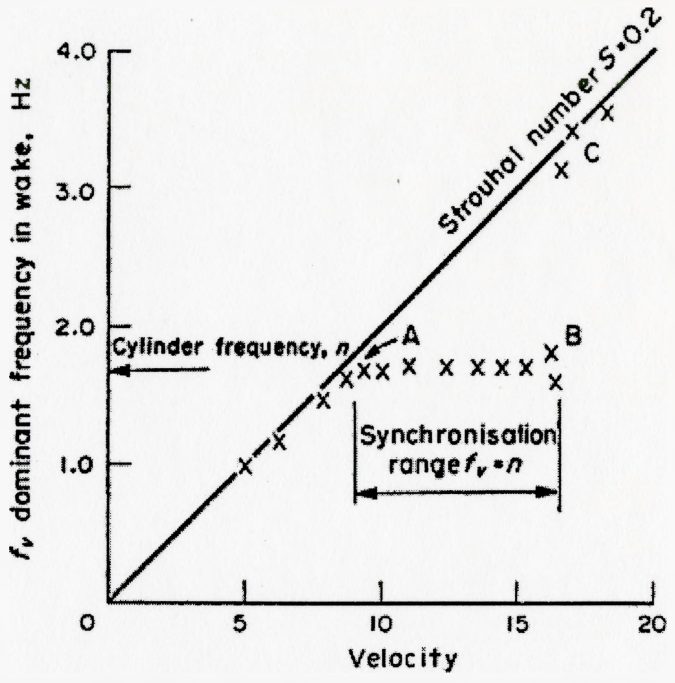

Figure 2.3. Cross-flow lock-in of vortex shedding oscillations.
[King (1977)]

oscillating body. Large amplitude oscillations of the cylinder are observer over the whole lock-in range and usually the maximum amplitude is reached in the middle of the lock-in range rather than at the initial resonance (Zdravkovich 1997).

2.2.2. Vortex Shedding from Tandem Cylinders

In practical applications, cylinders are usually found close to one another in either two or more cylinder arrangements. Thus the study of the interaction between two cylinders in proximity is of great importance. It can easily be assumed that two cylinders would behave in a similar manner to a single cylinder. However, this assumption is justified only if the two cylinders are sufficiently apart, i.e. one cylinder is not affected by

the wake of the other and there is no interference between the two cylinders (Zdravkovich 1977). It was found that the interference between two cylinders at close proximity changes the flow around them greatly.

The topic of vortex shedding from tandem cylinders receives much less attention than the case for single cylinders and hence fewer references are available on the topic. Zdravkovich published reviews in 1977, 1985, and 1987 that cover the topic extensively. Arie et al. (1983) discusses pressure fluctuations as well as lift and drag coefficients. Other references also cover the topic, e.g. Okajima (1979), Igarashi (1981, 1984), Lin et al. (2002), and Mahbub Alam et al. (2003). King (1977) includes a short section on the subject as well. Fitzpatrick and Nitti (1997) discuss noise generated from tandem cylinders in cross-flow.

2.2.2.1. Cylinder arrangement and flow regime

There is an infinite number of possible arrangements that two parallel cylinders in cross-flow can have. However, these arrangements can be grouped into three main categories being tandem (one cylinder directly behind the other), side-by-side, or staggered (which includes all other possible arrangements). Zdravkovich (1985, 1987) categorizes the interference regions (Figure 2.4) and provides the different flow regimes accompanying the different arrangements of the two cylinders in tandem and side-by-side arrangements (Figure 2.5).

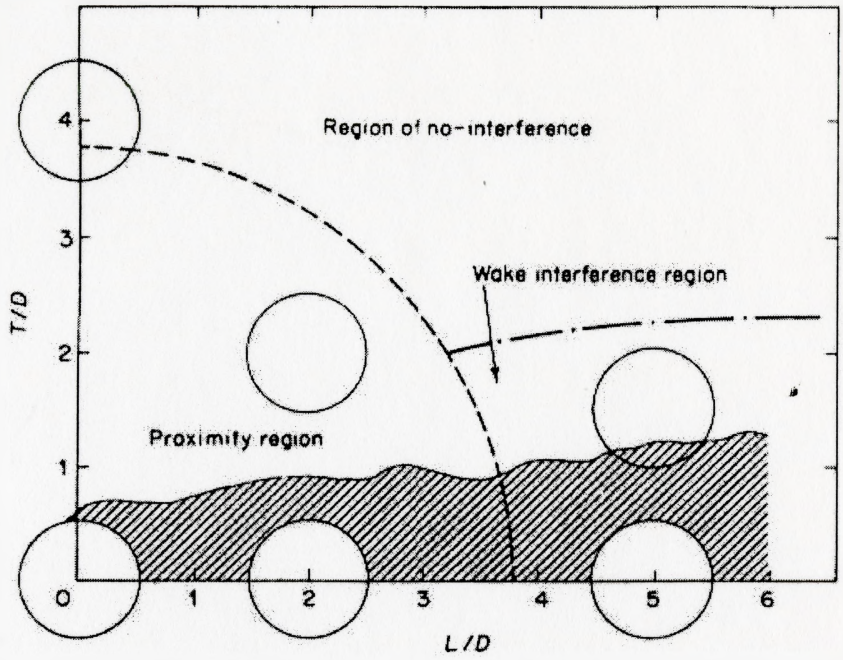

Figure 2.4. Classification of interference regions for a two cylinder arrangement. [Zdravkovich (1985)]

Figure 2.5 shows that for spacing up to some critical *L/D* ratio in the downstream direction, one vortex street forms behind the cylinders and vortex shedding is suppressed behind the upstream cylinder. Above this critical spacing, both cylinder shed vortices and coherent vortex shedding occurs between the cylinders. The critical spacing was reported by different references to be around an *L/D* value of 3.8 as reported by Zdravkovich (1977). Other references have observed critical values ranging from 3.5 to about 4. (Arie et al. 1983 and others). Lin et al. (2002) report that this critical spacing appears to be a function of Reynolds number as well as turbulence intensity of the flow.

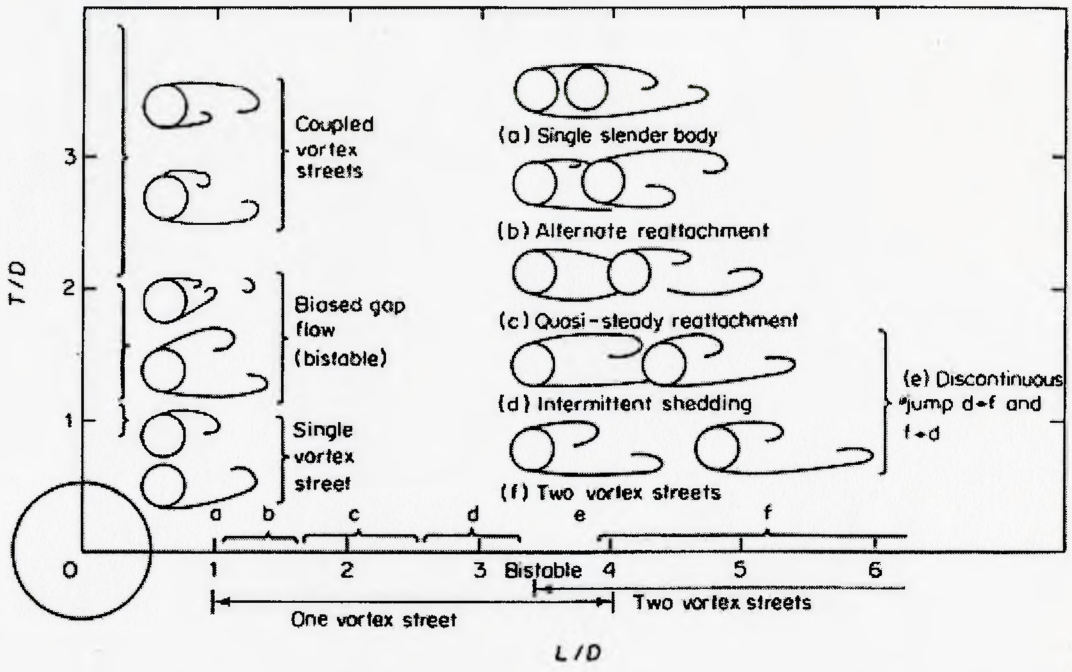

Figure 2.5. Classification of flow regimes for a two cylinder arrangement. [Zdravkovich (1985)]

2.2.2.2. Strouhal number

Introducing a cylinder in the wake of another alters the Strouhal number measured behind each cylinder. Mahbub Alam (2003) discusses the variation of the Strouhal number for different cylinder spacing for a subcritical Reynolds number of 6.4×10^4 (Figure 2.6). Very low values of Strouhal number, around a value of 0.14, were reported for spacing below the critical value. Above the critical value, however, Strouhal number values jump to about 0.18 and approach the value for a single cylinder with increasing the spacing. Zdravkovich (1987) discusses the variation of Strouhal number with Reynolds number for two spacings of 3 and 5 and provides data in agreement with the findings of Mahbub Alam et al.

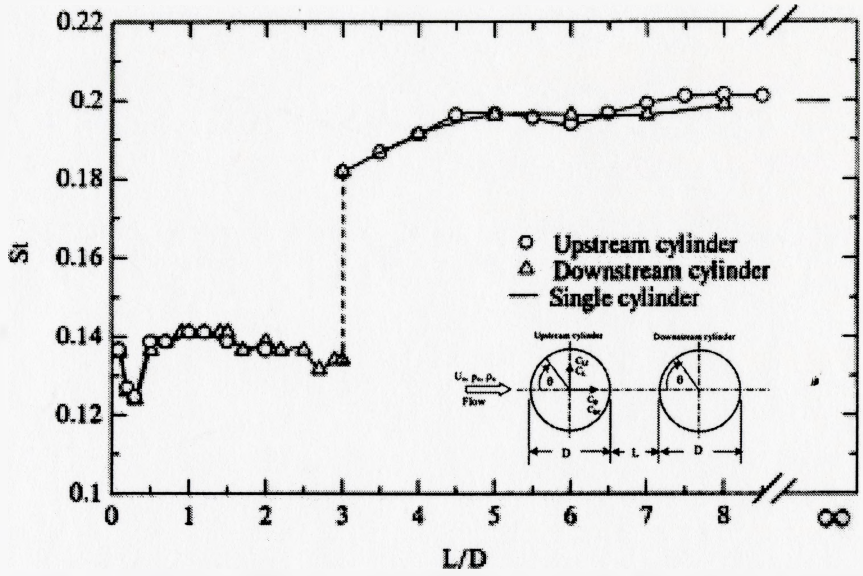

Figure 2.6. Strouhal number variation with cylinder spacing for a tandem cylinder arrangement. [Mahbub Alam et al. (2003)]

2.2.2.3. Lift and drag

Lift and drag characteristics of both cylinders when arranged in tandem differ greatly from one another and from those of the single cylinder. Arie et al. (1983) discusses the variation of lift and drag with varying the cylinder spacing for a Reynolds number of 1.57×10^5. Figure 2.7 shows that the downstream cylinder experiences much higher lift and drag compared to the upstream one. For small spacing, when no vortex shedding occurs behind the upstream cylinder, lift coefficient values for the upstream cylinder are very low. This value increases as the critical spacing is reached when vortex shedding starts in the gap. As cylinder spacing is further increased, values of lift and drag for both cylinders tend to approach the values measured for a single cylinder. Mahbub Alam et al. (2003) provide more detailed measurements for the lift and drag coefficients

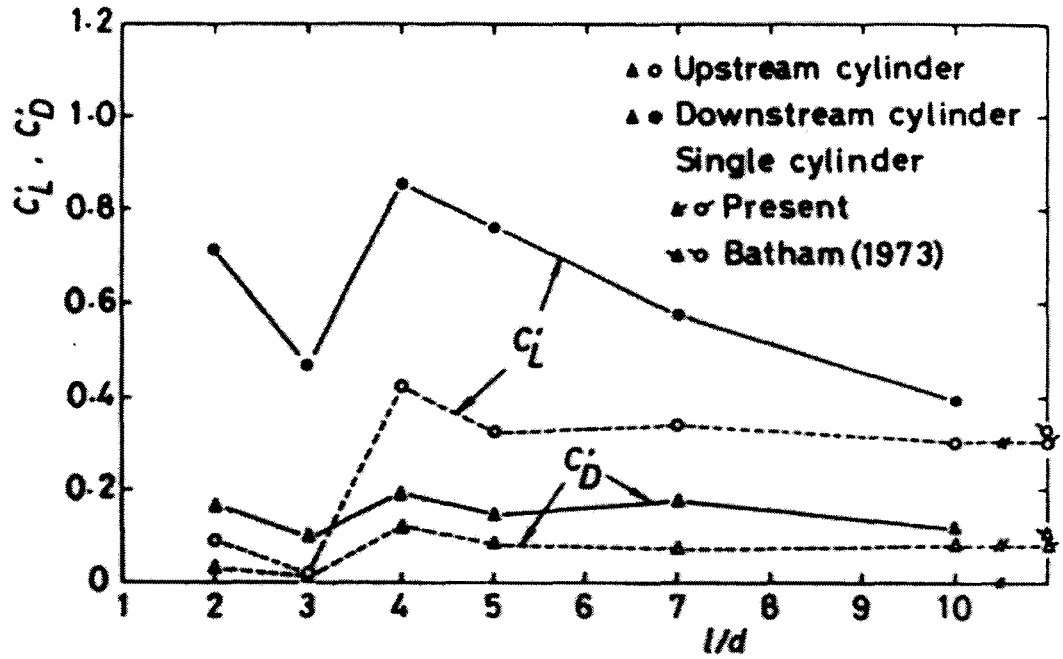

Figure 2.7. Lift and drag coefficients vs. cylinder spacing for a tandem cylinder arrangement. [Arie et al. (1983)]

for a comparable Reynolds number. Figure 2.8 shows the data they obtained which are in good agreement with the data provided above for Arie et al..

The increased lift observed for the downstream cylinder at post-critical spacing is attributed to the vortex impingement due to the shedding of vortices from the upstream cylinder, which creates an upstream feedback effect that enhances the vortex shedding process (Lin et al. 2002)

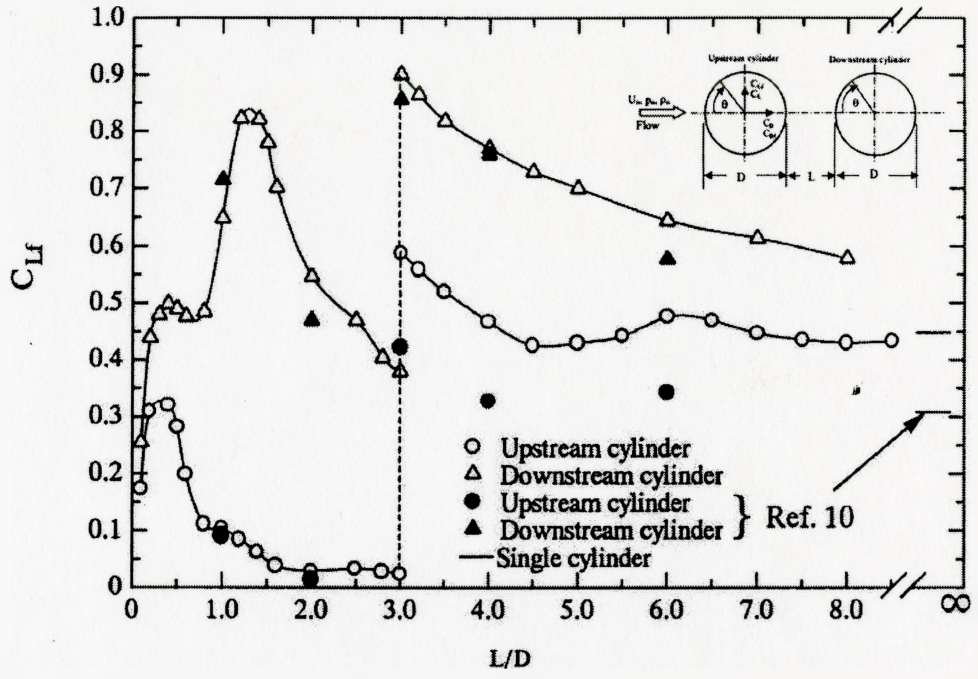

Figure 2.8. Variation of lift and drag coefficient with cylinder spacing for a tandem cylinder arrangement. (Ref. 10 in the figure points to Arie et al. (1983)) [Mahbub Alam et al. (2003)]

2.3. FLOW CONTROL

The art of flow control probably originated in prehistoric times when man used streamlined spears, sickle-shaped boomerangs, and fin-stabilized arrows. Furthermore, the establishment of an agriculture way of life followed and complex systems of irrigation were built along inhabited river valleys to control the water flow. The science of flow control, on the other hand, evolved with Prandtl (1904), who introduced the boundary layer theory, explained the physics of flow separation phenomena and described several boundary layer control experiments. (Gad-El-Hak 1996)

Flow control may involve active or passive mechanisms to affect a change in shear flows. Whether flow control is used to affect transition, turbulence, or flow separation, the resulting benefits include drag reduction, lift enhancement, mixing augmentation, heat transfer enhancement, and flow-induced noise suppression. Gad-El-Hak (1996) provides an excellent review of flow control technology.

2.3.1. Flow Control Methods

Flow control methods can be classified according to the way they consume energy and the control loop involved as shown in Figure 2.9 (Gad-El-Hak 1996). A flow control system may be passive, i.e. requiring no external power, or active, i.e. requiring energy input. Passive control systems include geometric shaping to manipulate pressure gradients, the use of fixed mechanical vortex generators for separation control, and

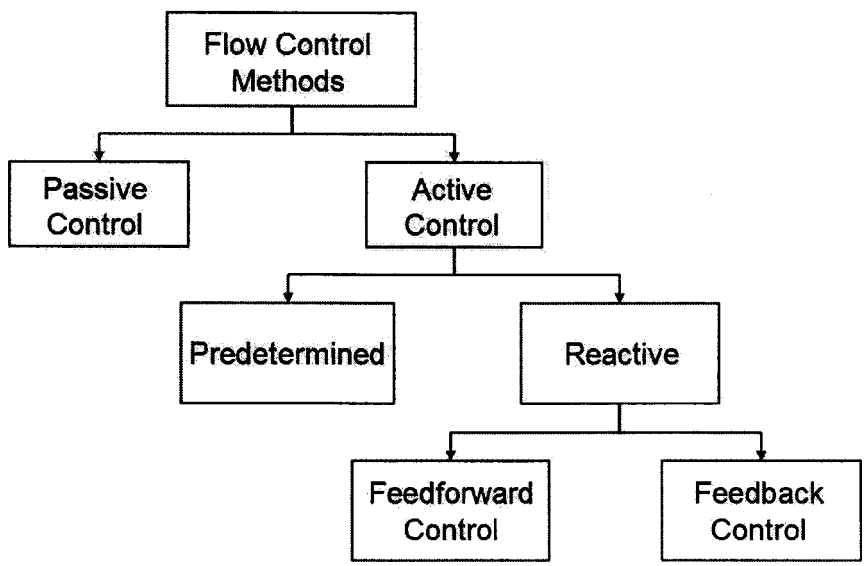

Figure 2.9. Classification of flow control methods.
[Gad-el-Hak (1996)]

placement of longitudinal grooves on a surface to reduce drag. Passive control of vortex shedding is widely used and includes the use of shrouds, helical strakes and splitter plates. These devices act by disrupting or preventing the organized vortex shedding process (Blevins 1994). Several references address this topic including zdravkovich (1981), Every et al. (1982), Rogers (1983), Kwon and Choi (1996).

Active control systems can be further divided into predetermined or reactive systems. Predetermined control involves the introduction of steady or unsteady energy to the system without consideration for the particular state of the flow. Thus the control loop is open, and no sensors are required. In reactive control, however, the control input is continuously adjusted based on measurements of some sort. Hence the control loop may either be open, feedforward, or closed, feedback loop.

Recently, active flow control techniques have received a great deal of focus in research due to their advantages over passive techniques. Active flow control of vortex structures has been investigated by many researchers and has proven to be effective (e.g. Huang and Weaver 1991,1994; Ziada 1995, 1999) Active control of vortex shedding from cylinders has gained its share of interest recently with methods of control ranging from external acoustic forcing (Ffowcs-Williams and Zhao 1989; and Roussopoulos 1993), to rotary cylinder oscillations (Tokumaru and Dimotakis 1991; and Fujisawa et al. 2001), cross-flow oscillations (Schumm et al. 1994; Warui and Fujisawa 1996), and internal acoustic excitation (Huang 1995, 1996; Hsiao et al. 1990; and Hsiao and Shyu 1991). This last method will be discussed in more details later.

A recent breakthrough in actuator concepts which aided in the development of active flow control mechanisms is the synthetic jet actuator which is discussed in the following section.

2.4. SYNTHETIC JETS

2.4.1. INTRODUCTION

The discovery of the concept of synthetic jets dates back to as early as 1950. At that time, however, this idea was merely used to study the circulation effects and the impedance of orifices. Ingrad and Labate (1950) reported observing the formation of zero-net-mass-flux jets during their study of orifices. Later, Medinkov and Novistskii (1975) and Lebedeva (1980) reported creating zero-net mass flux jets with velocities up to 17 m/s. The first use of synthetic jets as flow manipulation devices, however, was not until 1994 by Smith and Glezer (1994). In 1995, Ziada used synthetic jets to suppress the oscillations of jet-edge and jet-slot oscillators. Further development was carried out at the Georgia Institute of Technology by Smith and Glezer (1998). Since then, synthetic jets have gained an increased amount of attention as a promising flow manipulation and control device.

A Synthetic jet is a mean fluid motion created by an oscillating flow through an orifice or a slit. The fluid oscillations necessary to synthesize the jet are typically provided by intermittent suction and blowing through the jet orifice or slit. The device which produces the jet usually consists of a neck driven by a pulsating diaphragm in a

cavity as shown in Figure 2.10. Flow enters and exits the cavity through the orifice. On the intake stroke, fluid is drawn into the cavity from the flow surrounding the orifice. As this fluid is driven out of the cavity, a shear layer is formed between the expelled fluid and the surrounding one. This layer of vorticity rolls up to form a vortex ring, a vortex pair in case of a 2-D slot. This vortex ring, or pair, convects downstream due to its induced velocity. By the time the diaphragm starts another intake stroke, the vortex ring has gained enough momentum and moved far enough away that it is virtually unaffected. Thus a train of vortex rings is created by the actuator. In the mean, the velocity profile appears similar to a steady jet.

The driver, or the diaphragm, that is responsible for the production of the oscillating pressure drop across the neck necessary for the formation of the jet, can take a number of different forms including acoustic waves, piezoelectric diaphragms, and electromagnetically driven pistons. Acoustic sources were the first to be used by Ingrad and Labate (1950) who used acoustic standing waves in a circular tube to produce

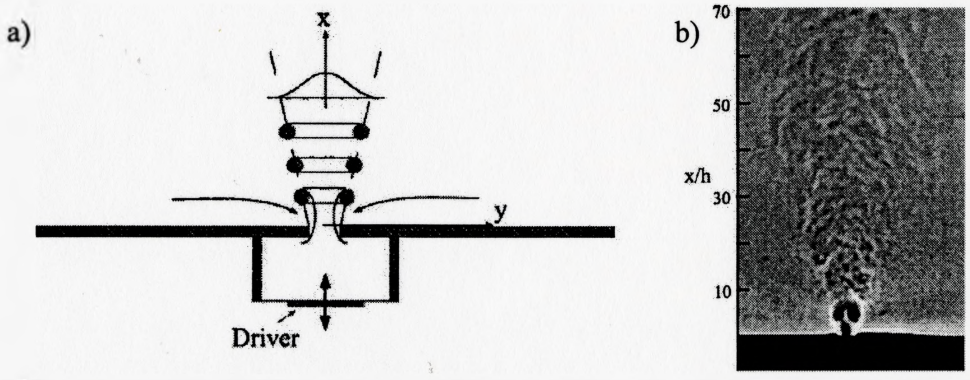

Figure 2.10. Synthetic Jet Actuator. a) Schematic of a synthetic jet actuator. b) Schlieren flow visualization of a synthetic jet. [Smith and Glezer (1998)]

oscillating velocity fields from an orifice endplate. Lebedeva (1980) reports creating a round synthetic jet through an orifice by using sound waves. Acoustically driven synthetic jets were also discussed or employed in other investigations (e.g. Ziada 1995, 1999; McCormick 2000; Smith and Swift 2001, 2003; Wolfe and Ziada 2003). Piezoelectric diaphragms are one of the mostly used drivers for synthetic jets and their use was reported in many experiments (e.g. Smith and Glezer 1997, 1998; Mallinson et al. 1999; Gilarranz and Rediniotis 2001; Utturkar et al. 2002, 2003; Gallas et al. 2003a, 2003b). Other sources used include electromagnetically driven pistons by Rediniotis (1999) and by Crook and Wood (2001). Since the dimensions of the synthetic jet scale with the dimensions of the orifice or slit producing the jet, it would be possible, theoretically, to produce jets over a wide range of scales including micromachined jets (e.g. Coe et al. 1994, 1995; Ho and Tai 1998).

2.4.2. Applications of Synthetic Jets

Synthetic jets possess a unique feature, that is, they are formed totally from the working fluid of the flow they are used in, and hence, require no external piping systems, making them a compact and low cost system. This feature enables the synthetic jet also to transfer linear momentum to the flow without any net mass injection. This unique property along with the fact that synthetic jets can exist in many different scales make the applications of synthetic jet numerous, especially in the area of flow manipulation and control.

The uses of synthetic jets cover a wide range of applications including active flow control (e.g. Hsiao and Shyu 1991; Ziada 1995, 1999; Huang 1995; Wolfe and Ziada 2003), separation control (e.g. McCormick 2000; Miller et al. 2000; Mittal et al. 2001; Gilarranz and Rediniotis 2001), virtual aeroshaping effects (e.g. Amitay et al. 1997; Smith et al. 1998; Glezer et al. 1999b; Mittal and Rampunggoon 2002), jet vectoring (e.g. Smith et al. 1997; Glezer and Smith 1999; Smith and Glezer 1997, 2002), cooling (e.g. Glezer et al. 1998, 1999) and mixing enhancement (e.g. Davis and Glezer 1999; Glezer et al. 1999a, 2000).

2.4.3. Characteristics of Synthetic Jets

As discussed above, synthetic jets are mainly formed by the successive blowing and suction of fluid through a narrow slit or orifice. Since their first application in 1994 for flow manipulation, a lot of research has been done to characterize synthetic jets and study their behavior both experimentally (e.g. Smith and Glezer 1997, 1998, 2002; McCormick 2000; Smith and Swift 2001; Glezer and Amitay 2002) as well as numerically (e.g. Rediniotis et al. 1999; Utturkar et al. 2002, 2003; Gallas et al. 2003a,b).

Several excellent studies have been published discussing the characterization of synthetic jets covering different geometries, slit sizes, actuators and operating conditions. The work of Smith and Glezer (1998), Smith and Swift (2001, 2003), Utturkar et al. (2003) and a review paper by Glezer and Amitay (2002) provide outstanding comprehensive analysis and characterization of synthetic jets.

The work of Smith and Glezer (1998) discusses the formation and characteristics of a high aspect ratio (aspect ratio of 150), piezoelectrically driven, synthetic jet formed in air. Schlieren images of the evolution of the synthetic jet are provided, (see Figure 2.10), which show the formation, convection and then break-up of the vortex pairs formed at the slit exit. Smith and Glezer start with introducing two primary dimensionless parameters, namely a dimensionless "stroke" length, L_o/h ($L_o = \int_0^{\tau} u_o(t)dt$, where $u_o(t)$ is the averaged streamwise velocity, τ is the period of discharge, i.e. half the actuator period, and h is the slit width) and a Reynolds number, Re_{Io} ($\mathrm{Re}_{I_o} = I_o/\mu h$, where $I_o = \rho h \int_0^{\tau} u_o^2(t)dt$, ρ and μ are the fluid density and viscosity respectively), based on the impulse per unit width as well as another Reynolds number based on the average orifice velocity Re_{U_o} (where $U_o = L_o f$ and f is the frequency of the driver). Following that, the near field characteristics of the jet are studied and are found to be dominated by the formation and advection of vortex pairs that ultimately undergo transition to turbulence, slow down and lose their coherence. This transition is then followed by the formation of a fully-developed turbulent jet in the far field of the jet.

The authors conclude that the synthetic jet is similar to conventional 2D turbulent jets in that cross-stream distributions of the time-averaged jet velocity components and their corresponding rms fluctuations collapse when plotted in the usual similarity coordinates. On the other hand, the mean centerline velocity of the synthetic jet decreases as we progress in the streamwise direction more rapidly than for conventional jets. Also,

the streamwise increase in the width and volume flow rate of the synthetic jet are lower. This was attributed to the adverse streamwise pressure gradient near the jet orifice.

In a more recent study, Smith and Swift (2001, 2003) compare synthetic jets to continuous and pulsed jets. They compare synthetic jets having different slot widths and formation parameters to both continuous and pulsed jets. The jets are acoustically excited and are formed in air. The synthetic jets are specified by the same formation parameters adopted by Smith and Glezer (1998); namely, the stroke length, L_o, and Reynolds number, Re_{Uo}, as discussed above. Continuous jets were characterized by a Reynolds number, Re_{Uave}, based on the mean velocity averaged over the cross stream of the jet.

The study starts with an analysis of the jet formation criteria whereby a threshold

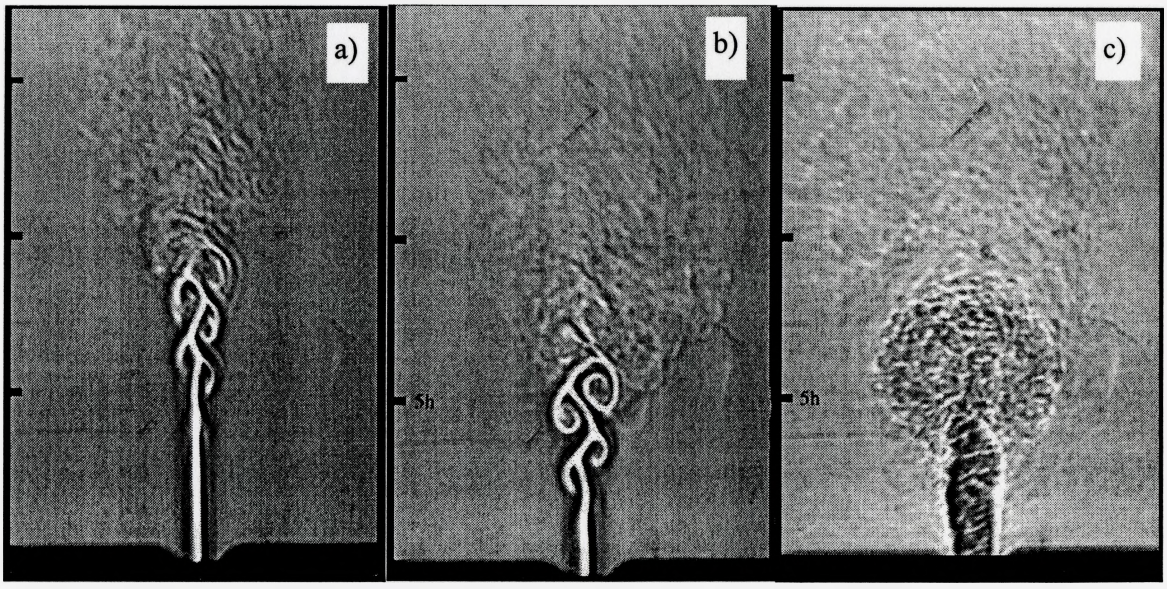

Figure 2.11. Schlieren images of: a) Continuous unforced jet Re_h=2200, b) Forced jet Re_h=2200 (forcing 5.5% of mean velocity), and c) Synthetic jet L_o/h=17 and Re_{Uo}=2200 at t/T=0.25. [Smith and Swift (2001, 2003)]

stroke length for the formation of the jet was introduced as $L_o/h = 4/\sqrt{\pi}$, where L_o is the stroke length and h is the characteristic length of the slit. Synthetic jets were then compared to similar continuous unforced and forced jets. The comparison was based on the same Reynolds number as discussed in the previous paragraph. The Schlieren images shown in Figure 2.11 show that synthetic jets start their growth much closer to the exit plane as well as being turbulent when exiting the nozzle.

Mean velocity profiles of the different jets were then plotted in similarity coordinates, as shown in Figure 2.12.(a), where it was obvious that all the jets collapse, being continuous or synthetic. The variation of the time-averaged centerline velocity with the downstream distance, shown in Figure 2.12.(b), shows that synthetic jets, start with a mean velocity of zero at the jet exit and increases to a value very close to that of continuous jets before the half-power-law decay, typical of plane jets. An interesting observation is that, despite the wide range of Reynolds number and stroke length covered in the data, the behavior is very similar for all the cases. Moreover, it can be observed that in the near field, synthetic jets consistently lie below continuous ones. This shows that they are wider and slower than the continuous ones. This is further elaborated by plotting the jet widths based on half the maximum velocity vs. the downstream distance (Figure 2.12.(c)). Synthetic jets are seen to exhibit wider jets than continuous ones.

The results discussed above are all in accordance to those observed by Smith and Glezer (1998) discussed earlier.

Utturkar et al. (2003) provide an investigation into the formation parameters of synthetic jets in search for a jet formation criterion. The study uses the same stroke length and Reynolds number based on U_o as discussed above. They conclude a formation criterion $1/St > K$, where St is the Strouhal number, $St = fh/U_o$, h is the width of the slot

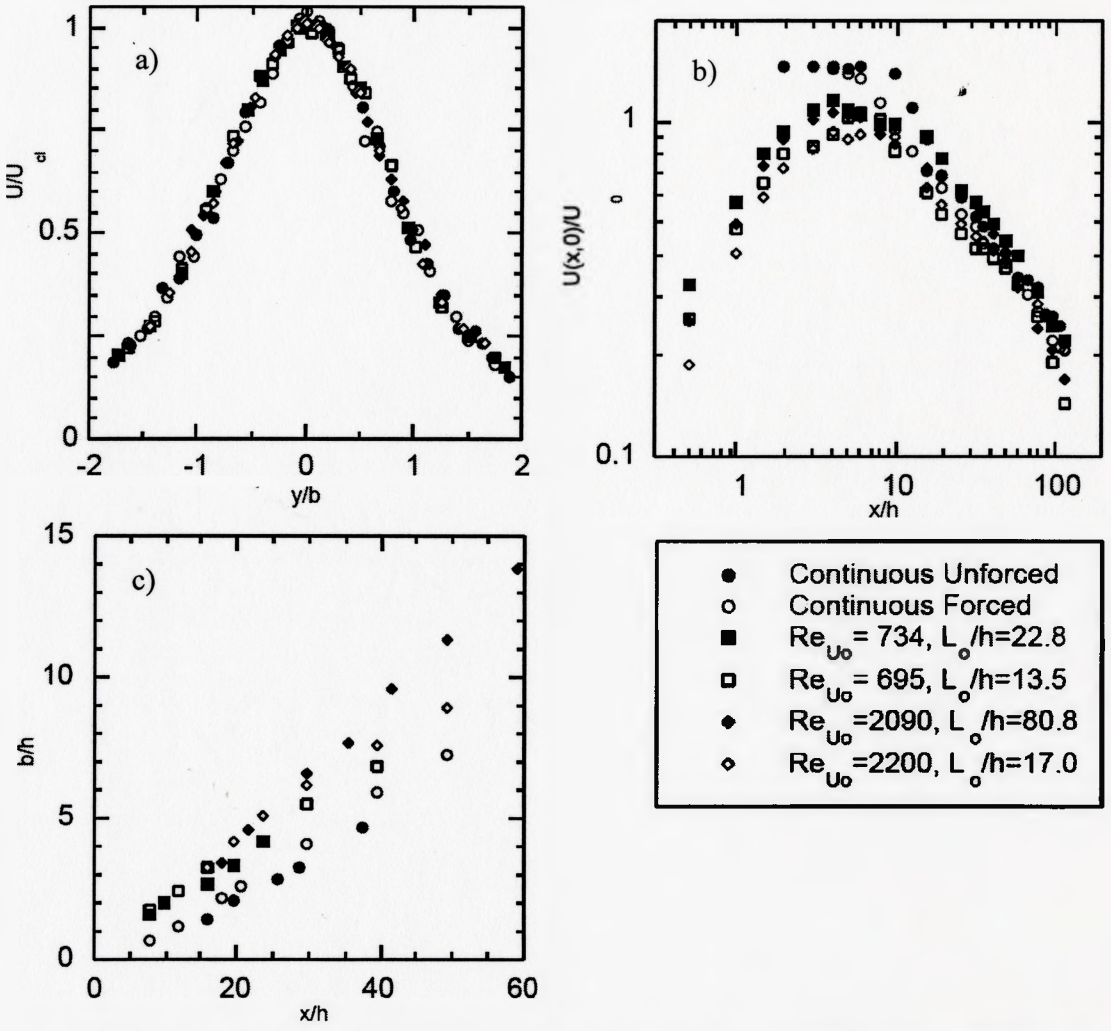

Figure 2.12. Different jet characteristics for different continuous and synthetic jets. a) Mean velocity profiles in similarity coordinates (profiles are taken at the downstream position where Ucl≈0.5Uo or 0.5Uave. b) Time-averaged centerline velocity vs. downstream distance. c) Width of jet based on half maximum velocity vs. downstream distance. [Smith and Swift (2001, 2003)]

(the diameter of the orifice in case of axysymmetric jets) and the constant K is approximately 2 for two dimensional synthetic jets and 0.16 for axisymmetric ones. The criteria they set is in good agreement with that suggested by Smith and Swift discussed above and with their experimental results as shown in Figure 2.13. The figure shows that most of the data lies above the limiting value of *1/St* of 2.

The characteristics of synthetic jets in comparison with continuous unforced as well as forced jets have been discussed above. Also, the different parameters involved in the formation of the jets were covered. While the literature provides an excellent and comprehensive analysis of the downstream evolution of uniformly excited synthetic jets, no references, to the author's knowledge, are available that provide the spanwise characteristics of a synthetic jet formed using high aspect ratio slits not excited uniformly

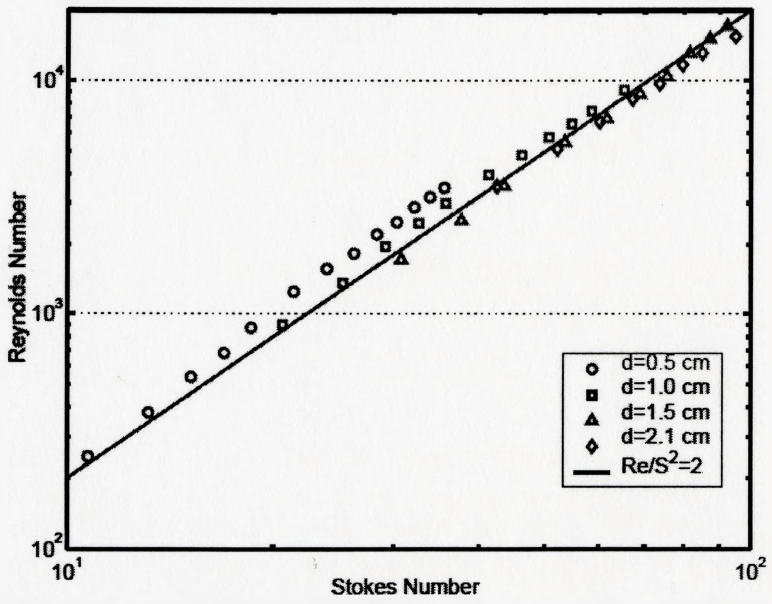

Figure 2.13. Reynolds number vs. stokes number for the experimental data obtained by Smith and Swift (2001) for different jet widths. [Utturkar et al. (2003)]

along the span as will be discussed below. Knowledge of these characteristics is essential for practical applications of flow control, as it is not always possible to generate synthetic jets by uniform excitations. The present work focuses primarily on the spanwise characteristics of synthetic jets.

2.4.4. SYNTHETIC JETS AND CONTROL OF VORTEX SHEDDING FROM CYLINDERS

It has been discovered recently that acoustic disturbances have a significant effect on shear flows. These effects include the ability of sound to correlate vortex shedding and modify the shedding frequency as well as its capacity to initiate transition to turbulence delaying separation. These findings encouraged researchers to use external acoustic disturbances to excite shear flows (e.g. Peterka and Richardson 1969; Collins and Zelenevitz 1975; Blevins 1985; and Zaman et al. 1987). These methods, however, required very strong sound fields of up to 140 dB. Internal excitation was then introduced, whereby sound emanates through a slit on the surface of the tested model. This concept of internal acoustic excitation was implemented for affecting different shear flows including aerofoils, cylinders and cavity resonance (e.g. Huang et al. 1987; Hsiao et al. 1989; Hsiao and Shyu 1991; Huang 1995; and Ziada 1995, 1999). Although these techniques do not state the use of synthetic jets, the concept used for the introduction of sound is basically a synthetic jet method as discussed below.

2.4.4.1. Active control of vortex shedding from a single cylinder

Controlling vortex shedding from a single cylinder by internal acoustic excitations is discussed by Hsiao and Shyu (1991) and Huang (1995).

Hsiao and Shyu (1991) introduced acoustic waves to the flow around a circular cylinder from a slot (having an aspect ratio of 80) on the surface of the cylinder. Reynolds numbers tested ranged from $4.2x10^2$ to $3.4x10^4$. The control was imposed at the shear layer instability frequency with sound pressure levels up to 130 dB. The study concludes that control is most effective when the jet is positioned around the separation point of the shear layer ($\theta \approx 80°$). Moreover, the excitation amplifies the shear layer instabilities causing the separated shear layers to reattach to the surface. This results in increased lift and reduced drag. Hsiao and Shyu also observe that the effect of the excitation frequency in the flow decays away from the cylinder. They conclude that internal excitation affects the flow locally rather than globally, which is the major difference between internal excitation and global forcing.

Huang (1995) performed experiments for Reynolds numbers in the range from 4000 to 8000. Control was affected by introducing sound through a narrow slit on the cylinder surface having an aspect ratio of 667. Acoustic pulsations were provided at the cylinder terminations by a pair of loudspeakers. The slit was positioned around the point at which the boundary layer separates and only one shear layer was controlled. The control input was a hotwire signal in the wake of the cylinder. Huang concluded that vortex shedding can be eliminated (reduction of up to 12 dB was achieved) in the wake of the cylinder when excited at the vortex shedding frequency using low sound levels up to 80 dB. These levels are much lower than those reported by Hsiao and Shyu (1991). Interestingly, he was able to produce such levels of attenuation while only exciting one of

the two shear layers and that the forcing slit should be positioned around the separation point as observed by Hsiao and Shyu (1991).

2.4.4.2. Active control of vortex shedding from tandem cylinders

A recent study by Wolfe (2000) investigates the use of a synthetic jet mounted on the upstream cylinder of a tandem cylinder arrangement to manipulate the dynamic loading on the downstream cylinder due to vortex shedding and turbulence excitations. This study provides the first attempt to investigate the effect of a synthetic jet on the shedding process from a tandem cylinder arrangement. An active feedback controller was used whereby the vibration signal of the downstream cylinder was used to excite a synthetic jet issuing from a narrow slit on the upstream cylinder surface. Two cases were studied at two different Reynolds numbers of 4.11×10^4 and 5.79×10^4. The first corresponds to a resonant case, where the vortex shedding frequency coincides with the resonance frequency of the downstream cylinder, and a non-resonant case, where the vortex shedding frequency is higher than the resonance one. The study also investigates the use of open loop control as well as tone and white noise excitations but results concerning the use of active control will be presented due to their relevance to the current study.

The implementation of feedback control resulted in significant reduction of the downstream cylinder response for both cases studied. For the resonant case, reduction of up to 70% was achieved with a slight shift in the shedding frequency, and for the non resonant case, a reduction of up to 75% was achieved for the resonance frequency

component of the cylinder's response and about 47% for the vortex shedding component. An interesting observation, though, was that no significant velocity fluctuations were observed at the resonance frequency in the wake of the upstream cylinder for the non-resonant case.

The results obtained by Wolfe provide a very promising future for the use of synthetic jet actuators in the control of vortex shedding from tandem cylinders especially for the control of the turbulent buffeting response as depicted by the reduction in the response of the downstream cylinder at the resonance frequency. However, the study does not discuss the actuator nor its characteristics. The mechanism by which the synthetic jet affects the flow and achieves the control has not been investigated either.

2.5. CONCLUDING REMARKS

Vortex shedding from single and tandem cylinders has been reviewed in this chapter including the governing parameters that affect the shedding process. Vortex shedding from flexible cylinders was then investigated along with the effect of cylinder vibration on the flow. Following that, flow control technologies were discussed with emphasis on active control techniques. Finally, the recently discovered actuator for flow control, the synthetic jet, was introduced. Applications and characteristics of synthetic jets were then analyzed with an interest in their use in control of vortex shedding from cylinders.

The topic of synthetic jets is a fairly new invention and its applications for active flow control are numerous. It has been gaining increased attention and more studies are

being published every day describing its characteristics or investigating its use in different areas and for different functions.

Recently this new actuator was used by Wolfe (2000) to control the dynamic loading on the downstream cylinder in a tandem arrangement of two cylinders. Promising results were obtained that warrant further investigation to explore the characteristics of this flow control actuator and better understand the mechanism by which it manipulates the flow and achieves the observed control.

To the author's knowledge, no studies have investigated the characteristics and the spanwise distribution of a synthetic jet that is excited non-uniformly along the span of the jet-producing slit. The present study considers a long aspect ratio synthetic jet to determine its characteristics and frequency response. This actuator will then be used for the active control of vortex shedding from a tandem cylinder arrangement to investigate the mechanism by which it affects the flow in the wake of the upstream cylinder such that the dynamic fluid loading on the downstream cylinder is reduced.

CHAPTER 3

EXPERIMENTAL SETUP

3.1. INTRODUCTION

Two groups of experiments are to be carried out in this thesis. The first group concerns the characterization of a long aspect ratio synthetic jet to investigate its use as a control actuator. The second involves the use of this actuator in the active control of vortex shedding from two tandem cylinders. The two groups are performed using almost the same setup with minor changes. The description and specifications of the different setup elements used are provided in details in this chapter.

Both experiments are performed inside a wind tunnel and a schematic diagram of the layout of the different components involved is shown in Figure 3.1. The layout for the synthetic jet experiment is shown in Figure 3.1.a. A cylinder with an axial slit along part of its length is supported to the sides of the test section walls. The excitation required to produce the jet is provided acoustically using a pair of speakers mounted on each side of the cylinder through adapters to match the diameter of the speaker's diaphragm to the cylinder's inner diameter. The speakers are excited by harmonic signals supplied from a signal generator through an amplifier. Velocity measurements of the issuing jet are performed using a hotwire anemometer mounted on a three-axis, computer controlled traversing mechanism, allowing measurements in the spanwise, streamwise, and transverse directions. The speakers' signal and that of the hotwire are sent to a PC data acquisition system for analysis and storage.

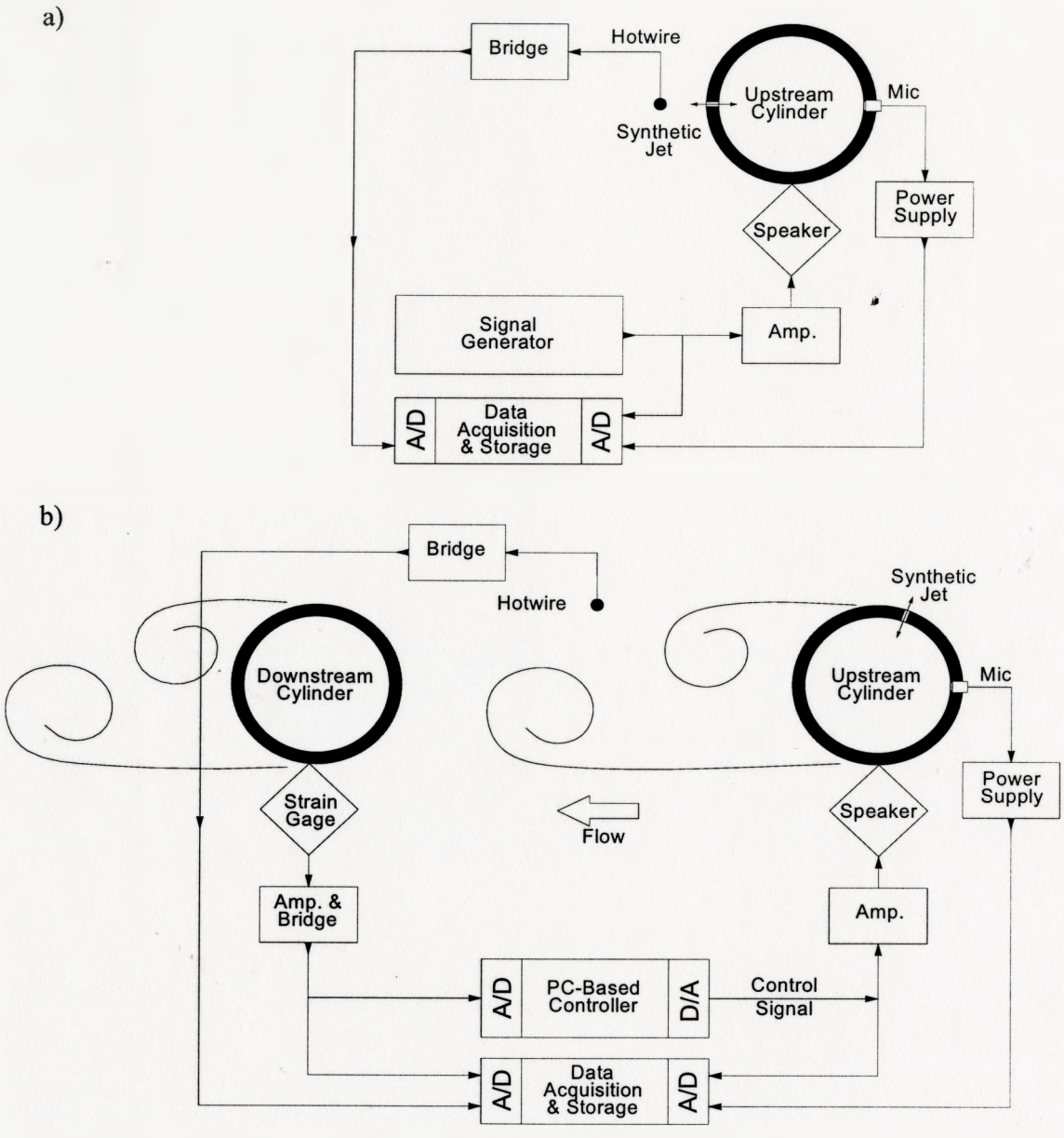

Figure 3.1. Schematic Layout for the experimental setup and equipment used.
a) Synthetic Jet Characterization. b) Tandem Cylinder Control Experiment.

The layout for the control experiments is shown in Figure 3.1.b. The upstream cylinder, the same cylinder as above, is rotated to position the slit at the required angle to achieve control and a downstream cylinder is installed in the setup. Strain gages are installed on the downstream cylinder to measure the fluctuating lift signal. This signal is fed into a PC based controller through an amplifier and an A/D converter card. The controller output is then fed back to the speakers through a D/A converter and an amplifier to excite the control actuator, thus forming a closed loop active control circuit. Hotwire measurements of the fluctuating velocity in the gap between the cylinders are also performed. The control signal, the lift signal and the hotwire signal are all fed into a PC through a data acquisition system for storage and analysis purposes.

Detailed description of the different components of the setup and the equipment used in the analysis and control are described in the following sections.

3.2. WIND TUNNEL

The wind tunnel used for the experiments in this thesis is located at McMaster University, in room JHE-208 in the Mechanical Engineering section of the John Hodgins Engineering Building. It is a suction type wind tunnel powered by a 9 kW electric motor, which drives an axial fan at the exhaust end of the wind tunnel. The Fan is capable of generating a maximum flow speed of approximately 25 m/s. The tunnel is approximately 10.5 m in length and has a contraction section at the inlet with an area ratio of 3.8 fitted with screens and honeycomb at the inlet. There is a removable test section constructed of acrylic with an octagonal cross-section. Figure 3.2 shows construction drawings of the

test section used in the control experiments. The test section has a cross-sectional area of 0.31 m^2, is 0.617 m between parallel sides and is approximately 0.69 m in length, with the tunnel maintaining the same cross sectional area for approximately 0.6 m upstream and downstream of the test section.

For the above-mentioned setup, the velocity profile upstream of the test section is flat within about 2% outside the boundary layer and the average turbulence intensity produced is approximately 0.5%.

3.3. UPSTREAM CYLINDER

The upstream cylinder is a polished aluminum pipe with outer diameter, D_o, of 40 mm, inner diameter, D_i, of 32 mm, and length, L_u, of 651 mm, producing a wall thickness of 4 mm and a length to diameter ratio, L_{wt}/D_o, of about 15.4, where L_{wt} is the distance between the parallel sides of the test section walls. A longitudinal slit of width, h, 0.75 mm was cut along part of the length of the cylinder to provide the exit nozzle for the synthetic jet. Two different cylinders with two different slit lengths were used, the short slit cylinder, with a slit length, l, of 205 mm providing an aspect ratio, l/h, of 273 and a long slit cylinder, with a slit length of 580 mm providing an aspect ratio of 773.

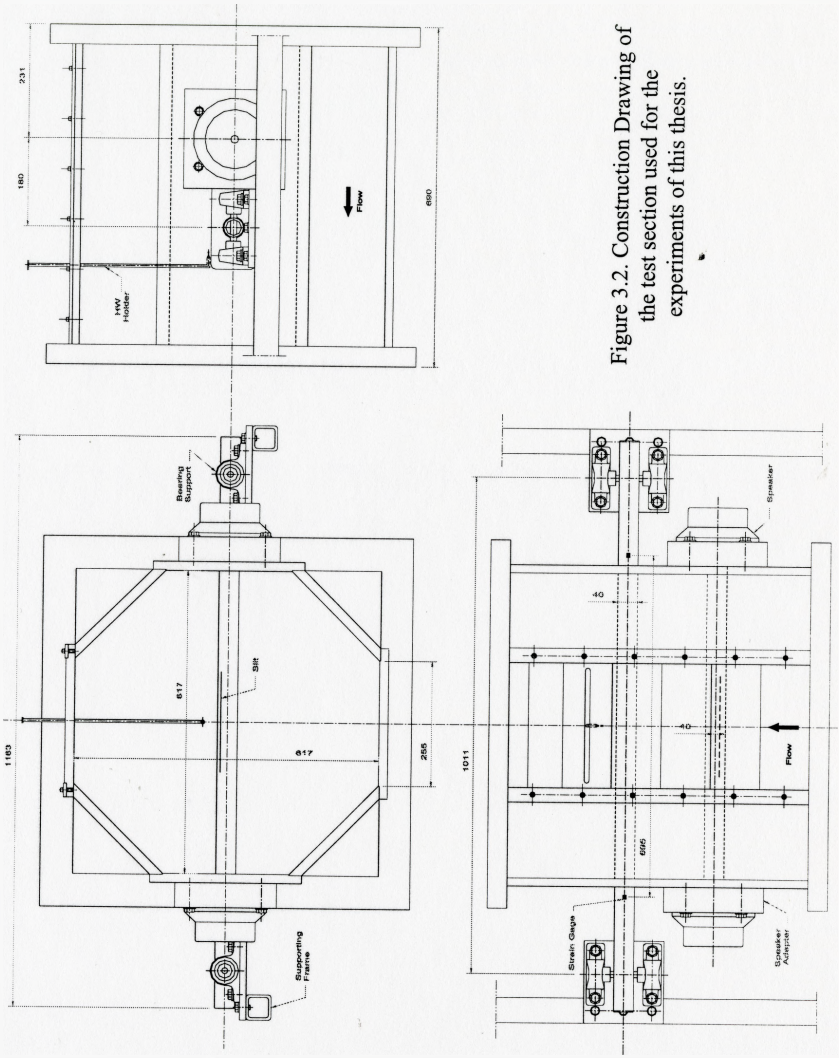

Figure 3.2. Construction Drawing of the test section used for the experiments of this thesis.

The cylinder is rigidly mounted to the sides of the test section as shown in Figure 3.3. It passes through 40 mm holes in the side-plates of the test section, with one side fitted with a collar to allow easy mounting of the cylinders. Moreover, the collar is fitted with a setscrew to prevent any cylinder rotation.

3.3.1. LOUDSPEAKERS

A pair of Rockford Fosgard FNQ2405 speakers are used to produce the excitation needed to produce the synthetic jet through the slit in the upstream cylinder. The speakers are rated at 200 Watts peak power, which is more than enough to produce the desired excitation. The speakers have a nominal diameter of 133 mm and are connected to the cavity of the upstream cylinder with a diameter of 32 mm through adapters as shown in Figure 3.3. The adapters are bell-mouth shaped and are created into hardwood blocks. As

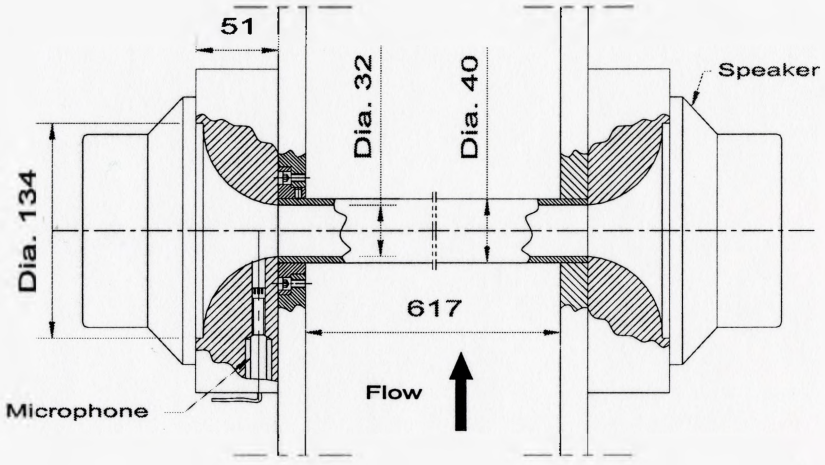

Figure 3.3. Upstream Cylinder Mounting.

the reduction in diameter is significant, from 133 mm to 32 mm, the design of the adapters is quite difficult. The adapters are designed to provide the minimum volume and length possible with the least steep angles possible to minimize acoustic power loss.

Speakers with a nominal diameter of 32 mm would have been ideally used without adapters, but obtaining speakers with this diameter with an acceptable response at the low frequencies used, down to about 70 Hz, is not possible. Moreover, the best available speakers for this range of low frequencies would have much larger diameters than the ones used, and would have been very troublesome to install. Therefore, the used speakers provide the best combination of acceptable low frequency response and size for the current application. Full specifications of the speakers used are listed in Appendix A.

A RAMSA WP-1200 400 Watts, two-channel power amplifier powers the speakers. The two speakers are connected in parallel and the amplifier is provided with analog gain knobs, which are set at two for the jet characterization experiments, and at the maximum value of 10 for the control experiments.

3.3.2. MICROPHONE

A G.R.A.S Type 40BP Microphone is mounted in the speaker adapter block at one side of the upstream cylinder as shown in Figure 3.3. The microphone is located about 40 mm away from the speaker and is used to measure the sound pressure level inside the cylinder. Ideally, a microphone situated further away from speaker or even more than one microphone would be desired, but such arrangement would be very difficult to install and would affect the sound field inside the cylinder or the flow field around it. This is the reason for choosing such an arrangement, as it is the furthest

distance the microphone can be located without causing problems. The microphone is installed through a 7 mm diameter hole and is located at about 37 mm away from the centerline of the adapter, thus forming a small cavity whose characteristic length is very small and therefore does not affect the produced sound field.

3.4. DOWNSTREAM CYLINDER

The downstream cylinder is a polished aluminum pipe, identical in diameters to the upstream one. It has an outer diameter, D_o, of 40 mm, inner diameter, D_i, of 32 mm, and length, L_d, of 1163 mm, producing a wall thickness of 4 mm and a length to diameter ratio, L_{wt}/D_o, of about 15.4, where L_{wt} is the distance between the parallel sides of the test section walls. The cylinder is centered horizontally in the test section and extends outside of the wind tunnel through 44 mm holes in the side panels of the test section as shown in Figure 3.4. These holes provide a 2 mm circumferential clearance to allow the cylinder to vibrate without hitting the side-plates as well as to prevent the transmission of the wind tunnel vibrations to the cylinder.

The cylinder is mounted on an external steel frame isolated from the wind tunnel body. Two ball bearing mountings on each end of the cylinder provide pivoted supports. A pin is fixed to each end of the cylinder and in turn is mounted in the bearings. This construction is shown in details in Figure 3.4.

The choice of diameter for both cylinders was to provide the desired range of Reynolds number, L/D ratio and vortex shedding frequency. Moreover the choice of the material and length of the downstream cylinder was to provide a resonance frequency

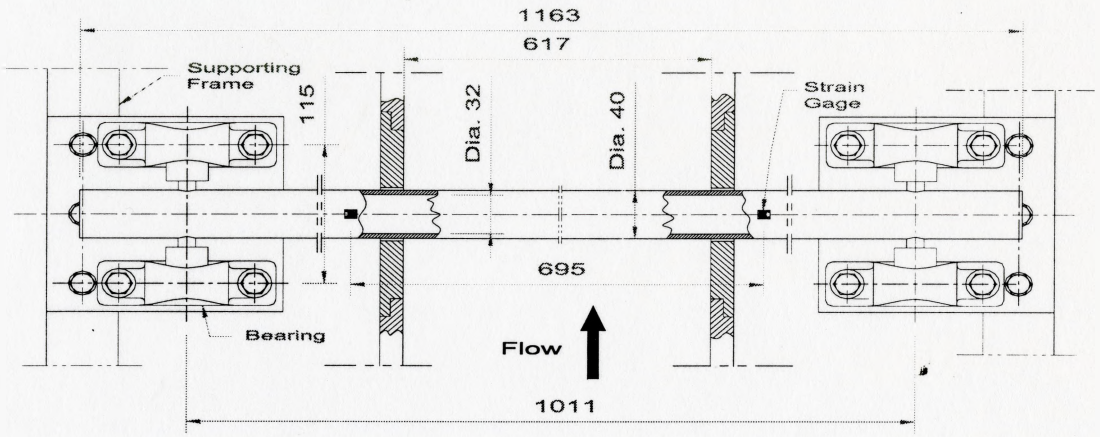

Figure 3.4. Downstream Cylinder Mounting.

within the desired range. As will be discussed in later sections the resonance frequency of the cylinder was chosen to be 72 Hz.

3.4.1. Strain Gages

3.4.1Four M-M CEA-13-125UW-350 strain gages are mounted on the surface of the downstream cylinder to measure the fluctuating lift force acting on it. As shown in Figure 3.4, they are mounted, two on each side of the cylinder, just outside of the test section and are connected together to form a full bridge. The gages are aligned to respond to the lift force and be least sensitive to the drag force. Calibration data provided in Appendix C and discussed in section 4.3.3 provide more insight into the sensitivity of the strain gages to both the lift and drag forces.

3.5. VELOCITY MEASUREMENTS

A Dantec Socket-type single-wire hotwire probe is used to measure velocity fluctuations in the flow. The hotwire is mounted on a Dantec holder, which in turn is mounted to the traversing mechanism. A single channel Dantec Type 55M01 bridge is used to power the hotwire probe with an overheat ratio of 1.8.

The traversing mechanism used is a Valmex NF90 Series, three-axis, computer controlled traversing mechanism capable of moving in steps of 0.005 mm/step. The traversing mechanism is controlled through a serial port connection and the software used is National Instrument's Labview. It is mounted on the external frame of the wind tunnel to separate it from the tunnel vibrations and allow the mechanism to be horizontally and vertically balanced. The mechanism is installed to allow movements of the hotwire probe in the streamwise, spanwise and transverse directions. The top wall of the test section is modified to allow for the introduction of the hotwire into the test section. This is done by sectioning the tope part into interchangeable pieces of different widths to allow for inserting the probe in any streamwise position as shown in Figure 3.2. One of the pieces has a longitudinal hole through which the probe passes and it allows for the transverse and spanwise movements of the probe.

Hotwire measurement for the synthetic jet characterization part required the calibration of the hotwires. The calibration was performed inside the wind tunnel with the test cylinder removed. A pitot tube was used to calibrate the hotwires. The calibration data obtained were used in labview to obtain a velocity value output directly from the measurement program. This is done through the Measurement & Automation tool of

Labview, which controls the data acquisition from the different channels. This tool allows for the use of a calibration table or equation to directly calibrate the data before being used by the acquisition program. Calibration curves obtained from the hotwires are shown in Appendix B.

3.6. PC EQUIPMENT

The monitoring, analysis, and storage of the data collected, as well as the control process and signal generation require the use of different hardware equipment for the different tasks. Online monitoring of different signals, including the signal generation (signals used for the jet characterization part of the experiments) are realized using a 4-channel spectrum analyzer type Hewlett-Packard 35670A.

3.6.1. DATA ACQUISITION

Storage and analysis of the data is done on a Dell Optiplex GX1 PC with an Intel Pentium III 500 MHz processor. The PC is equipped with an 8-channel PCI-6024E National Instruments data acquisition board and the interface to the board is through National Instrument's Labview program. A program was developed for the purpose of storing the time series along with performing online analysis and the storage of this data as well.

Data collected was sampled at 4 kHz with a sample of 2 seconds averaged over 75 averages. A flat top window was used as it provides the highest accuracy in measuring signal amplitudes over other windowing functions. The utilized data acquisition program was first tested using harmonic signals of different amplitudes and frequencies to

measure errors in measuring the spectral amplitudes of acquired signals. It was found that the maximum error measured in the power spectra of the signals was about 3%.

3.6.2. CONTROLLER

The controller used for the active control experiments is a software based controller, where the controlled signal is fed into a PC using an A/D card and is altered using the control software, and is then fed back to the controller output port through a D/A card.

The data acquisition card used for this task is a Quanser Multi-Q3 data acquisition system. It is equipped with eight analog input channels and eight analog output ones. The card is connected to a Dell Optiplex GX1p PC with an Intel Pentium III 450 MHz processor. This data acquisition system is capable of sampling a single signal at about 30 kHz, while adding additional signals decreases this limit. The card is controlled via a software supplied by Quanser called Wincon. Wincon controls the card by running a program created and compiled in Simulink, a toolbox of Matlab, independently of Matlab. This provides the necessary speed for processing the signal at such high sampling frequencies.

CHAPTER 4

EXPERIMENTAL SETUP CHARACTERISTICS

4.1. INTRODUCTION

The first step in performing the experiments of interest in this thesis is to determine the dynamic characteristics of the different components involved in the experimental setup and their effect on the results. The setup consists of two main components, the upstream cylinder system including the synthetic jet production system and the downstream cylinder including the mounting and force transducer. Each component will be dealt with separately starting with the upstream cylinder, where the characteristics of the jet production system will be studied. Then, the downstream cylinder system will be discussed starting with the dynamic characteristics of the cylinder itself then the lift coefficient and finally with the response of the force transducer. This chapter will conclude by describing the response of the whole tandem cylinder arrangement to flow.

Each part will include a brief outline of the experimental procedure along with any comments or observations, and then the results will be presented followed by some discussion and analysis.

4.2. Upstream Cylinder Cavity Characteristics

The synthetic jet studied is produced by acoustical excitation from the pair of speakers mounted on both ends of the upstream cylinder through the cylinder's internal cavity. The characteristics of this system, e.g. its resonance frequency and frequency response, must be investigated.

To identify the response of the system, a white noise signal up to 1.6 kHz is sent to the speakers and the response of the microphone mounted in one of the speaker adapter blocks is measured. The white noise signal was chosen as it excites the system equally at the whole frequency range of interest, thus enabling to get most of the information required in one test. The frequency response of the system is then calculated for both cylinder cases, the long slit cylinder and the short slit cylinder, and is shown in Figure 4.1. From the figure, it can be seen that for the long slit cylinder the resonance frequency is at 350 Hz, while that for the short slit case it is at 280 Hz. Moreover, it can be observed that the frequency range of interest, from 70 to 115 Hz, is well below the natural frequency of the cavity system as well as it exhibits a rather flat response.

4.3. Downstream Cylinder Characteristics

The downstream cylinder is supported to the external frame of the wind tunnel as a simply supported beam, hence when flow is introduced the cylinder will be subject to vibrations due to excitation from the vortex shedding process as well as the broadband turbulence in the flow. The resonance frequency of the cylinder is within the frequency range of flow excitation, so the effect of the resonant response of the cylinder must be

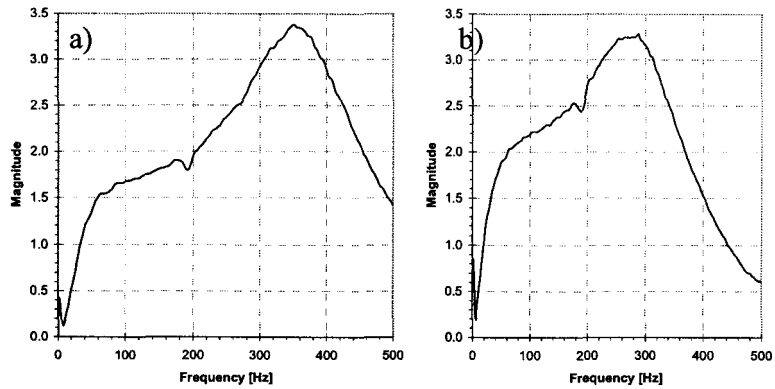

Figure 4.1. Frequency response of upstream cylinder cavity.
a)Long slit cylinder. b) Short slit cylinder.

taken into consideration. The following sections deal with the characteristics of this resonant response as well as its effect on the total response of the system.

4.3.1. DAMPING AND RESONANCE FREQUENCY

In order to account for the resonance effect of the downstream cylinder when estimating the lift signal, the damping of the cylinder system has to be measured as well as the natural frequency of the cylinder. The resonance frequency can be calculated as that of a simply supported beam as well as it can be measured from the frequency response of the cylinder when it is subjected to flow. From calculations as well as the measurements, the resonance frequency was found to be 72 Hz.

The damping ratio can be determined using two methods; one is the logarithmic decrement method and involves the impulse response of the cylinder, while the other is the half-power method.

The damping ratio is determined using the logarithmic decrement from the impulse response by determining the amplitude of the signal after a number of

consecutive cycles and then calculating the logarithmic decrement from which the damping ratio can be found. A typical time trace of the impulse response for the downstream cylinder is shown in Figure 4.2. The logarithmic decrement is the determined from

$$\delta = \frac{1}{n} \ln\left(\frac{y_1}{y_{n+1}}\right)$$

where δ is the logarithmic decrement, n is the number of cycles between amplitudes y_1 and y_{n+1}. After calculating the logarithmic decrement, the damping ratio can then be calculated using

$$\zeta = \frac{\delta}{2\pi}$$

where ζ is the damping ratio. For the calculation of the damping coefficient using this method, the impulse test was repeated 15 times. Each acquired signal was divided into 2 different segments, each consisting of 15 cycles, representing high and low vibration amplitudes in order to see whether the damping is amplitude dependent. The damping was then calculated for each segment and average values for the 15 trails were obtained. The obtained results do not show any significant dependence of the damping on the amplitude of vibration where a value of 0.61% was obtained for higher signal values and a value of 0.63% for low amplitudes of vibration.

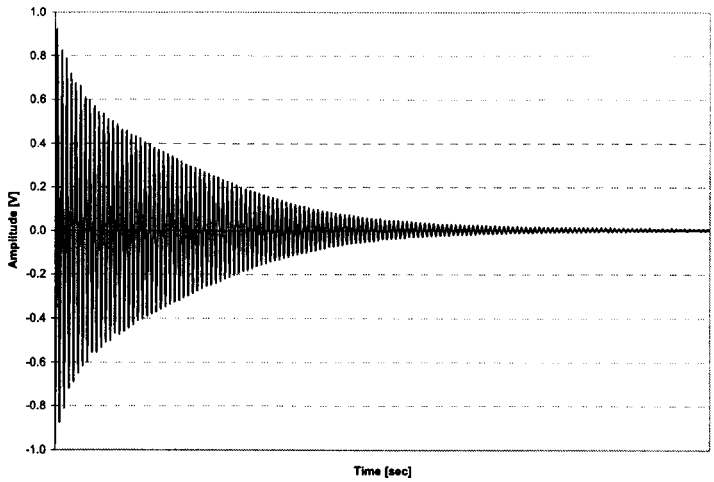

Figure 4.2. A typical time trace of an impulse response of the downstream cylinder.

For the half-power method, the damping ratio is calculated from the power spectra of the response of the cylinder. In this case, the spectra at maximum tunnel flow velocity are used in order to achieve the maximum separation between the vortex shedding peak and the resonant peak. This separation is necessary to insure that the resonance response is triggered only by broadband turbulence. At this flow velocity of 23 m/s, vortex shedding is at 108 Hz while the resonance frequency is at 72 Hz, i.e. the vortex shedding frequency is 1.5 times higher than the resonance frequency. The damping ratio is calculated from

$$\zeta = \frac{f_2 - f_1}{2f_r}$$

where ζ is the damping ratio, f_r is the resonance frequency and f_2 and f_1 are the frequencies at half the power at resonance.

A sample of the spectra used to calculate the damping ratio using the half-power method is shown in Figure 4.3.a. along with the spectra of the hotwire signal indicating that the resonant peak is only excited by turbulence. The damping ratio calculated by this method was found to be 1.16%. This value of damping is obtained by measuring the damping ratio using 10 different power spectra at the same flow velocity. A magnified plot of the resonant peak is shown in Figure 4.3.b. As mentioned earlier, adequate separation is necessary between the resonant frequency and the vortex shedding frequency; hence, damping ratio values for all flow velocities were not attainable. However, preliminary measurements showed that for a flow velocity of about 7 m/s the difference in the measured value of damping ratio was about 10%.

As seen from the above discussion, the values obtained for the damping ratio

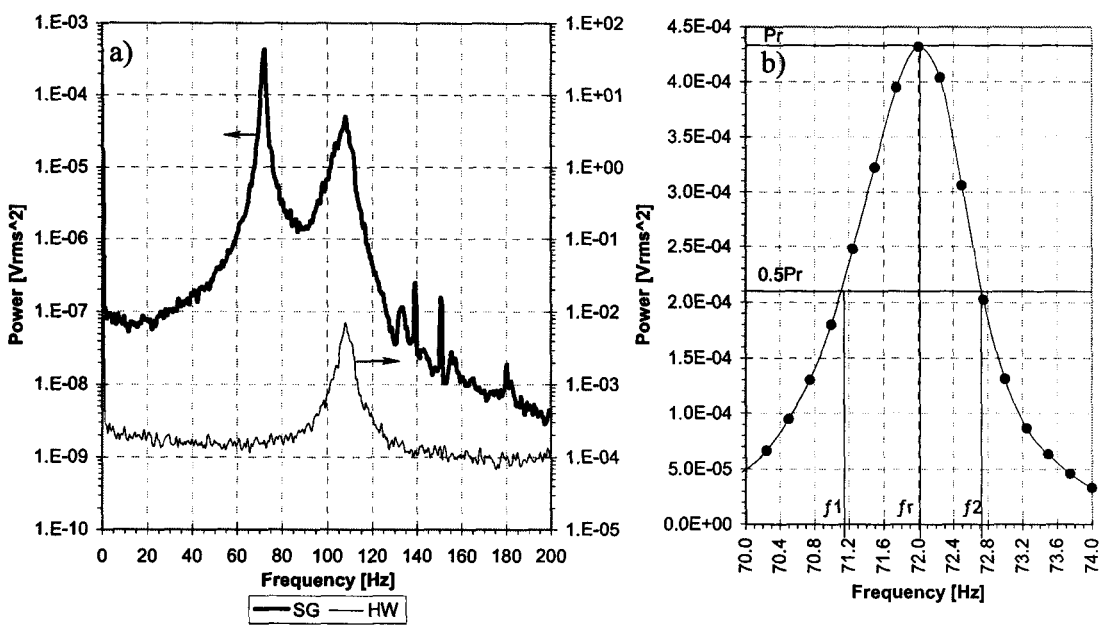

Figure 4.3. Typical power spectra used in the half-power method.
a) Power spectra. b) Magnified view of resonance peak.

using both methods are different. The increase in the value of damping with flow can be attributed to the fact that with the logarithmic decrement method we only account for the structural damping and the damping of supports as there is no flow, while with the half-power method the effect of the viscous damping of the flow is also considered. This can be further elaborated considering the fact that flow dissipates energy away from the cylinder by the vortices being shed thus increasing the overall damping of the system. Blevins (1994) shows that fluid damping increases with increasing the flow velocity for a cylinder in cross flow. Although the damping ratio calculated with the half-power method introduces and error for low flow velocity measurements, it will be used in the analysis of the data for two reasons. The first is that it better represents the actual damping of the system than the value obtained by the logarithmic decrement method, while the second is that experiments carried out in this thesis are around the same velocity of 23 m/s and this value represents the actual damping at that velocity.

4.3.2. Lift Coefficient

One of the important factors that need to be investigated is the lift coefficient. It is a dimensionless parameter that gives an insight into the effect of the cylinder vibration on the lift exerted on the cylinder. The lift coefficient is calculated from the total RMS lift force exerted on the cylinder and measured by the strain gages. The first step in calculating the RMS lift force is to correct the lift spectra of the downstream cylinder vibration signal for the resonant response of the downstream cylinder. This is achieved by considering the downstream cylinder as a single degree of freedom system whereby the

lift spectra are multiplied by the inverse of the magnification factor of the single degree of freedom system response.

The magnification factor M is calculated, using measured values of damping, from

$$M = \frac{1}{\sqrt{\left(1-(f/f_r)^2\right)^2 + 4\zeta^2 (f/f_r)^2}}$$

where M is the magnification factor, f is the frequency of vibration of interest, f_r is the resonance frequency of the system and ζ is the damping ratio, previously measured in the previous section. Figure 4.4 shows an example of the raw and corrected lift spectra for the system.

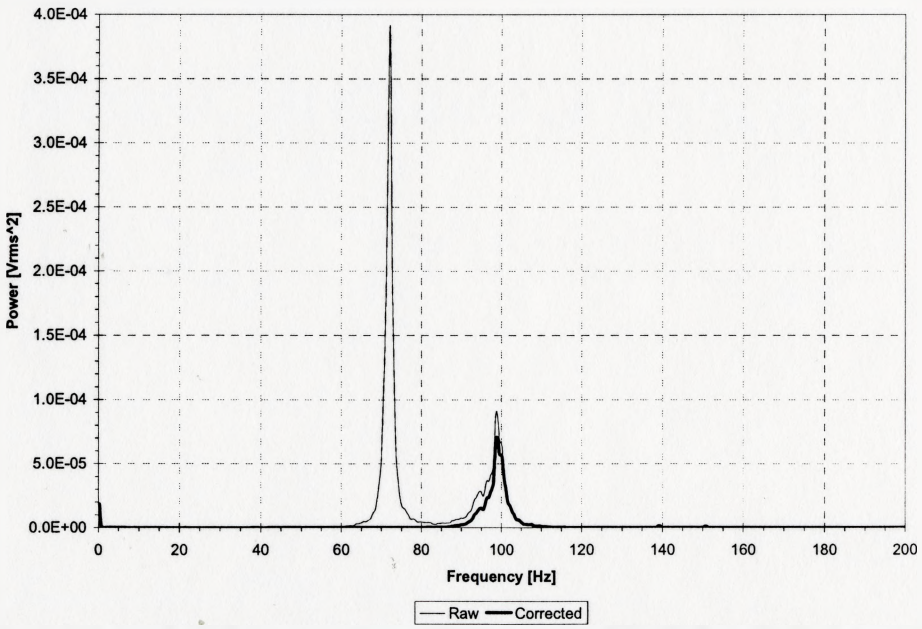

Figure 4.4. A sample of the raw and corrected power spectra of the lift force for the downstream cylinder. The shown spectra are for a flow velocity of 21 m/s.

The lift coefficient is then calculated from

$$C_L = \frac{F_L}{\frac{1}{2}\rho U^2 A}$$

where C_L is the lift coefficient, F_L is the total corrected RMS lift force, ρ is the fluid density, U is the free stream flow velocity and A is the projected surface area where the lift force acts.

Lift force measurements are discussed in the following section where the force transducer is discussed in more details. The RMS lift force is calculated by obtaining the square root of the sum of the corrected RMS power spectra of the lift force for frequencies from 20 Hz to 130 Hz. The high frequency limit, 130 Hz, was chosen as 1.8 times the resonance frequency to exclude any non-linear effects like the higher harmonics of the resonant peak.

Figure 4.5 shows the lift coefficient values measured for different flow velocities. It can be seen that the values of lift coefficient range from about 0.7 to 1, except in the lock-in range, where the vortex shedding coincides with the resonance frequency of the cylinder. For this case, the lift coefficient increases to about 1.5. The variations in the lift coefficient seen in Figure 4.5, except in the lock-in region, are to be expected as the lift coefficient depends on many flow-related variables such as the Reynolds number and the turbulence intensity in approaching flow.

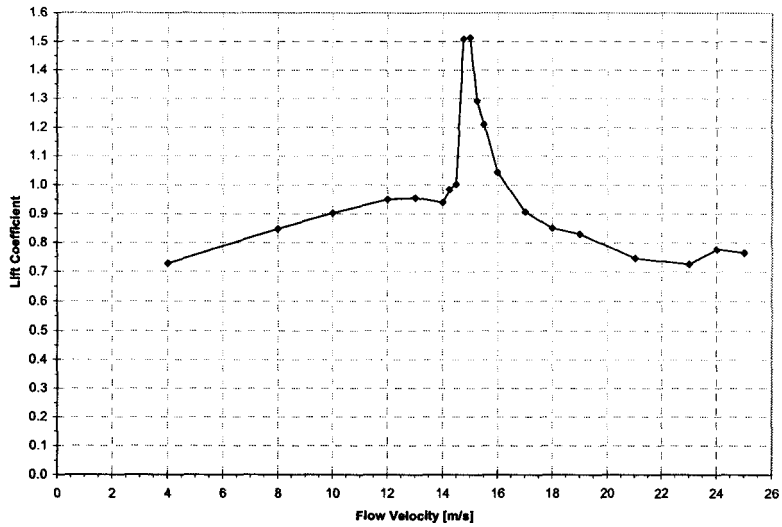

Figure 4.5. Lift coefficient measured for the downstream cylinder for different flow velocities. (Lines are only for visual aid)

The increase in the value of the lift coefficient for the lock-in part, which is about 50% from that just before the lock-in, can be attributed to the natural feedback effect occurring at the frequency coincidence. The large amplitude of vibration of the downstream cylinder at its resonance frequency causes a feedback effect to be transmitted back to the upstream cylinder, which results in an enhanced and more coherent vortex shedding process.

Comparable values of lift coefficient for the same cylinder spacing, 4.5D, were reported in the literature by Arie et al. (1983), Figure 4.6.a, for a slightly higher Reynolds number than the maximum obtained in the present experiments. The same applies for values obtained by Mahbub Alam et al (2003), Figure 4.6.b, for a Reynolds number of the same order as that of the current study.

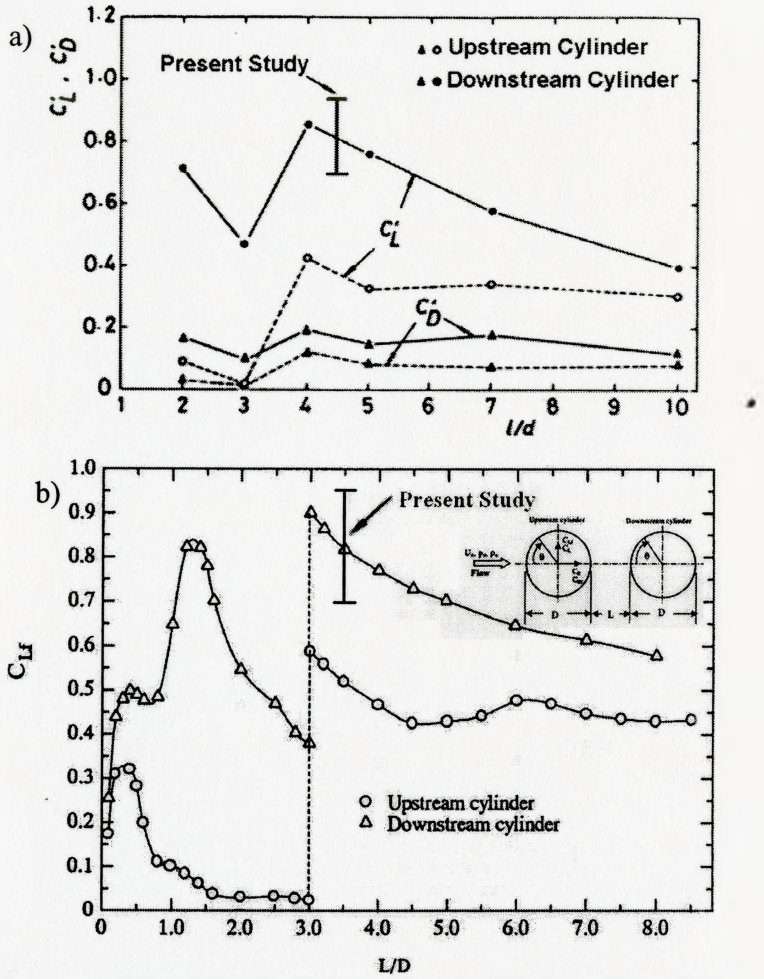

Figure 4.6. Lift and drag coefficients values for different cylinder spacing.
a) Arie et al. (1983). b) Mahbub Alam et al. (2003).
[I] represents the range of C_L measured over the *Re* range covered in the current study.

4.3.3. FORCE TRANSDUCER

For the measurement of the lift force on the downstream cylinder, four strain gages are used, two of which are placed on each side as described in section 3.4.1. The gages measure the strain produced by the vibrations of the cylinder and are calibrated to measure the lift force. The calibration is performed by static loading of the cylinder at its midspan. This method of calibration gives the same effect as the total distributed load of

the lift force on the cylinder as the gages are placed outside of the lift affected part of the cylinder and no further correction is required. The gages give a sensitivity of 6.72 mV/N. The cylinder vibration is also affected by the fluctuating drag force and care must be taken to insure that the strain gages are not affected by this drag force. A simple test was conducted to address this issue, where the cylinder was loaded with static weights to simulate the drag force and the response of the strain gages was recorded. It was found that the response to the lift force is about 100 times larger than that of the drag force. This result along with the fact that fluctuating drag forces are of the order of 2.5 to 10 times weaker than lift, as reported by King (1977), and that fluctuating drag forces are at twice the frequency of fluctuating lift forces assures that the response of the strain gages to the drag force is negligible. Calibration data of the strain gages are provided in Appendix C.

4.4. TANDEM CYLINDER ARRANGEMENT CHARACTERISTICS

To determine the response of the tandem arrangement at different flow velocities, the upstream cylinder was replaced with a cylinder having no slit. Hotwire measurements were perforemed with the hotwire placed between the cylinders, 2.75 D upstream of the downstream cylinder and 0.5 D in the vertical direction. The wind tunnel flow velocity was changed from no flow to the maximum velocity of 25 m/s. For each velocity chosen, the hotwire and the strain gage signals are recorded. The frequencies of the vortex shedding peak and the resonant peak are then plotted as shown in Figure 4.7. From the figure, it can be seen that the arrangement provides a Strouhal number of 0.188.

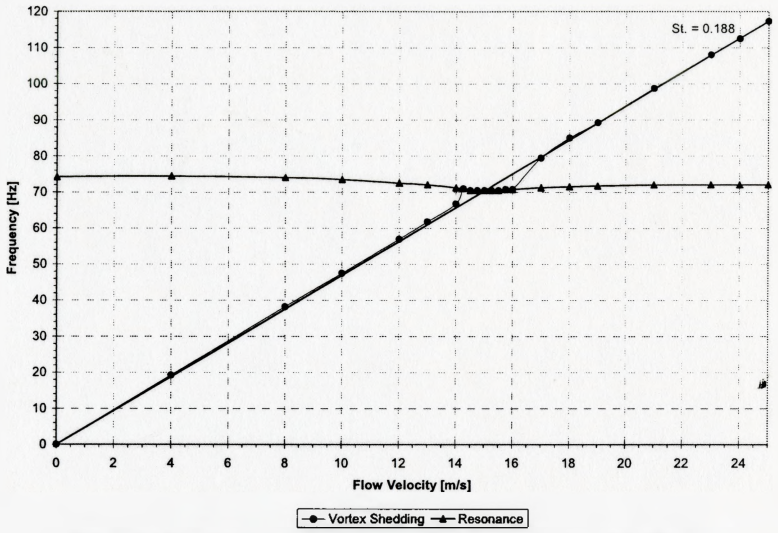

Figure 4.7. Response of tandem cylinder arrangement to flow.
(Lines are only for visual aid)

Values of Strouhal number for a tandem cylinder arrangement reported in the literature are in agreement with the value measured here. Figure 4.8. shows values of Strouhal number reported by Zdravkovich (1977 & 1987) for different cylinder spacing. The lift signal was then corrected for the resonant response as discussed in section 4.3.2. The amplitudes of the vortex shedding peak and the resonant peak were then plotted as

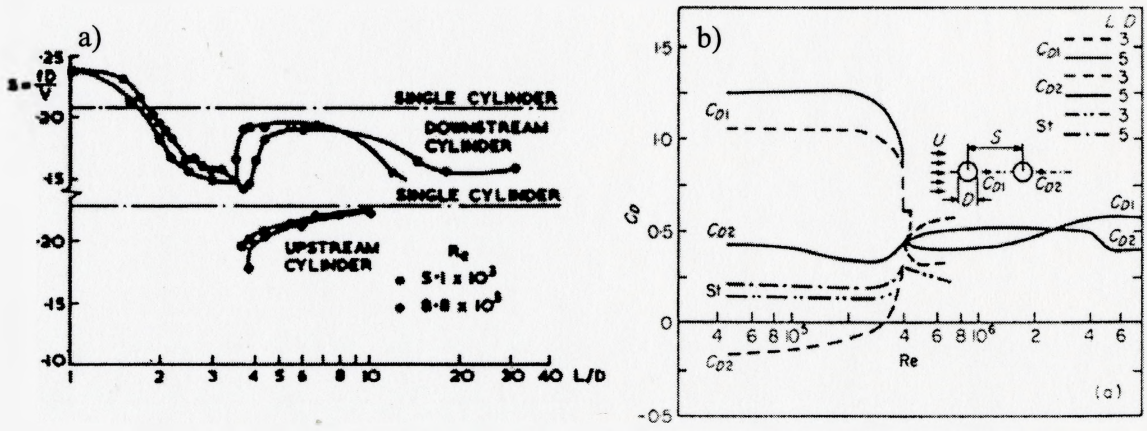

Figure 4.8. Strouhal number and drag coefficient values for tandem cylinder arrangements.
a) Zdravkovich (1977). b) Zdravkovich (1987).

shown in Figure 4.9. The figure shows clearly the effect of the feedback in the lock-in region where the vortex shedding frequency locks-in with the resonance frequency. This feedback effect enhances the vibration of the downstream cylinder.

4.5. SUMMARY

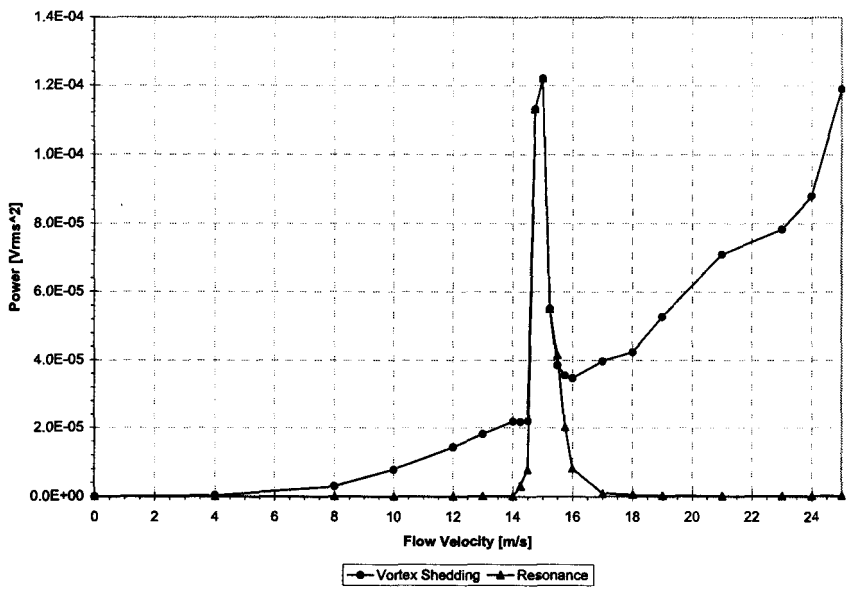

Figure 4.9. Modified vortex shedding and resonance peak amplitudes for different flow velocities.

The dynamic characteristics of the setup components were studied. The upstream cylinder cavity characteristics were investigated where it was found that the resonance frequencies of the two cavities, the short slit and the long slit cavities, were at least two times higher than the maximum frequency of interest in the forthcoming experiments. The dynamic characteristics of the downstream cylinder were then presented. The resonant frequency of the cylinder was found to be 72 Hz and the damping was measured

using both the logarithmic decrement method and the half-power method. The damping was found to increase with flow as indicated with the half-power method and was 1.16%. This value was chosen to represent the damping of the system and was used thereafter to correct the lift spectra of the strain gages for the resonant response.

In order to investigate the effect of the cylinder resonance on the dynamics of the vortex shedding process, the lift coefficient was measured for the range of flow velocities available. The values obtained were found to agree with those reported in the literature. The lift coefficient values indicate that the lock-in occurring at the frequency coincidence enhances the vortex shedding process and increases the lift coefficient by about 50%.

Finally, the response of the whole tandem cylinder arrangement to flow was discussed. A Strouhal number of 0.188 was measured which agrees with that reported for tandem arrangements for comparable values of Reynolds number.

CHAPTER 5

SYNTHETIC JET CHARACTERIZATION

5.1. INTRODUCTION

This chapter deals with the synthetic jet characterization. A synthetic jet, as discussed in Section 2.4, is a zero mass-flux jet formed by the successive blowing and suction of a fluid from a closed cavity through a narrow hole or slit. The synthetic jet studied in this chapter is produced through an axial slit along part of the length of a cylinder. The inner cavity of the cylinder is connected, at both of its ends, to two loudspeakers, as described in Chapter 3. The acoustic pulsations produced by the speakers are channeled through the inner cavity of the cylinder and produce the necessary excitation to produce the jet through the slit.

The objective of the experiment is to investigate the response of the jet to the excitation supplied to the speakers and to determine the characteristics of the jet along the span of the cylinder. Two cylinders with two different slit lengths are investigated. One cylinder, the long slit cylinder, has a slit along almost the whole length of the cylinder and the other, the short slit cylinder, has a slit extending about one third of the length of the cylinder. The two cases are compared to investigate their use as control actuators for active flow control.

5.2. MEASUREMENT SETUP

The experiment is carried out inside the wind tunnel test section with the downstream cylinder removed and the upstream cylinder rotated to position the slit horizontally facing the downstream side of the tunnel. A hotwire, mounted on the three axis computer controlled traversing mechanism, is traversed in the spanwise, the vertical and the downstream directions. The whole experiment is performed with no flow in the wind tunnel.

The characterization process involved exciting the pair of speakers in phase with harmonic signals at different frequencies and amplitudes and measuring the response of the jet to the different excitations. The quantities of interest are the mean centerline jet velocity and the phase between the jet velocity fluctuations and the exciting signal.

The following sections discuss the different experiment related parameters, their properties and settings.

5.2.1. EXCITATION SIGNAL

The exciting signal supplied to the speakers was generated using the HP spectrum analyzer discussed in Section 3.6. Three different frequencies were chosen for the excitation. They were chosen to represent the range of frequencies of interest, i.e. within the range from the natural frequency of the downstream cylinder to the maximum vortex shedding frequency attainable for this tandem cylinder configuration in the wind tunnel. The tested values of frequencies were 80, 100 and 120 Hz.

The amplitudes of the exciting signal were chosen to be 2, 4 and 6 Volts. These values include the gain of the speakers' amplifier. The 2 Volts value was chosen as it represents the lowest value of amplitude that produced a measurable velocity signal at the mid-span of the long slit cylinder.

5.2.2. COORDINATE SYSTEM

A hotwire was used for velocity measurements of the issuing jet. A system of axes was chosen to describe the position of the hotwire as shown in Figure 5.1; the *Z*-direction being the spanwise direction, the *Y*-direction being the vertical one and the *X*-direction being the downstream direction. The origin of the axes is the midspan of the cylinder, the mid-width of the slit and at the exit plane of the slit.

5.2.3. HOTWIRE PLACEMENT

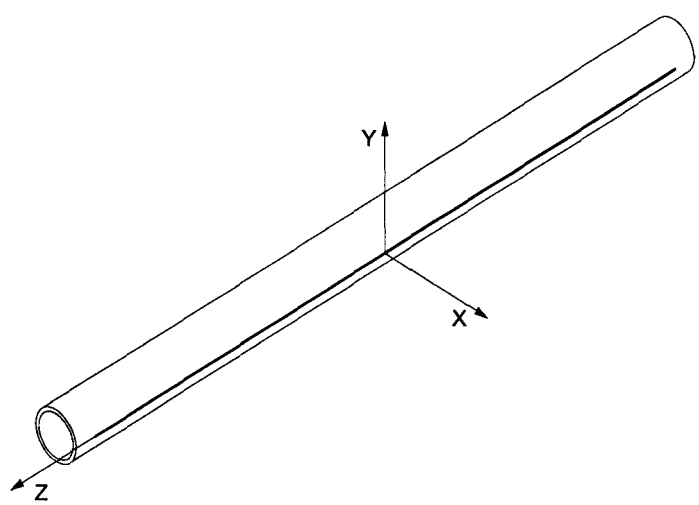

Figure 5.1. A sketch of the coordinate system set for the synthetic jet characterization.

Velocity measurements were performed using a single hotwire, discussed in chapter 3, whose position is defined according to the coordinate system mentioned above. Choosing the positions where measurements were to be made is discussed in the following sections.

5.2.3.1. Spanwise Position

Nine spanwise measurement positions, in the Z-direction, were chosen for each cylinder. For the long slit cylinder, with a slit length of l = 580 mm providing an aspect ratio of l/h = 773, the positions were chosen as Z = 0, ±58, ±116, ±174 and ±232 mm. These positions produce values of Z/h of 0, 77.33, 154.67, 232 and 364 respectively, where h is the slit width. In the short slit case, with a slit length of l = 205 mm providing an aspect ratio of l/h = 273, the positions were Z = 0, ±25, ±50, ±75 and ±90 mm. These positions produce values of Z/h of 0, 33.33, 66.67, 100 and 120 respectively.

5.2.3.2. Downstream position

The position of the hotwire in the jet was fixed and was chosen to be at X = 5 mm, i.e. at X/h = 6.67. The choice of this position was based on some preliminary measurements as well as consideration of the available literature discussing synthetic jet measurements. At this location, traces of the suction stroke of the excitation cycle seize to exist in the hotwire signal.

First, it should be noted that the focus of this study is the spanwise distribution of the jet. This feature of synthetic jets, to the author's knowledge, has not been addressed in

the literature. Hence, the downstream development of the jet was of minor importance for the current study and was made as a preliminary measurement at specific positions just for the determination of the suitable position for the forthcoming measurements.

The literature provides extensive research that addresses the downstream development of the synthetic jet, e.g. Smith and Glezer (1998), Smith et al. (2001), Smith and Swift (2003).

Secondly, since successive blowing and suction through the slit produce the synthetic jet, the hotwire signal near the slit exit plane contains traces of flow for both the blowing stroke as well as the reversed suction flow. This feature along with the fact that a single hotwire is not capable of distinguishing the direction of flow will produce a rectified harmonic hotwire signal that needs lengthy signal analysis to be de-rectified.

According to the above-mentioned considerations, some preliminary experiments were performed at three downstream positions of 0.5, 5 and 10 mm and at three spanwise positions of 0, 50 and 100 mm. Velocity profiles at these locations were obtained to investigate the shape of the jet and determine a suitable position for taking measurements. Figure 5.2 shows samples of the time traces of the hotwire signal of the issuing jet at its centerline and at the midspan location. It can be seen that at the exit plane the rectified suction stroke is evident in the time signal and disappears as the hotwire is progressively moved downstream. Furthermore, the 5 mm position was found to be the location after which the centerline velocity starts to decrease due to the widening of the jet. Similar

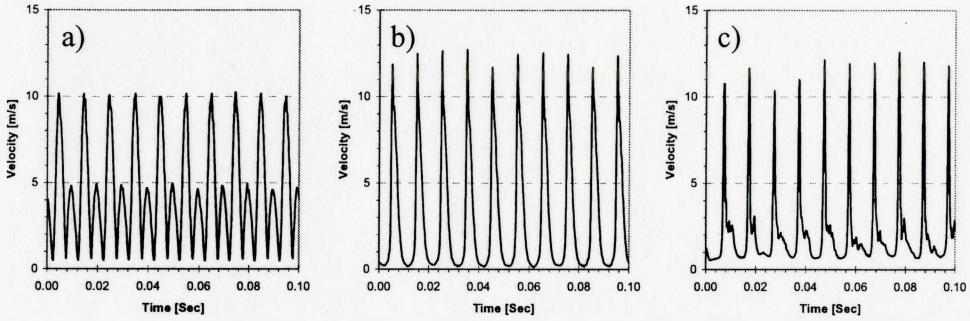

Figure 5.2. Time traces of the hotwire signal showing the downstream progression of the hotwire signal. The signals were recorded for the long slit cylinder at the jet centerline at Z=0 for an excitation of 100 Hz and 4 Volts. a) X=0.5 mm. b) X=5 mm. c) X=10 mm.

results were obtained for the other spanwise positions. The data obtained agrees with those reported by Smith and Glezer (1998), Smith et al. (2001), Smith and Swift (2003).

5.2.3.3. Vertical Position

In order to determine the centerline velocity and phase of the issuing jet accurately, the hotwire had to be traversed vertically across the centerline of the slit at each measurement position. This was made for two reasons; the first is to avoid any slight misalignments between the axis of the traversing mechanism and the cylinder axis that might cause the hotwire to be shifted from the jet centerline position when traversed in the spanwise direction. The second was to insure that any such misalignments would not cause subtantial errors in the hotwire measurement. This was achieved by insuring that there are no steep changes in neither the velocity nor the phase measurements near the centerline position.

Figure 5.3 shows a sample of the velocity profiles obtained for the different cases tested. Samples are shown for the short slit cylinder for the different frequencies and amplitudes tested and at two spanwise positions of Z/h = 0 and -100. The figure shows normalized velocity U/U_{cl} and phase of velocity fluctuations as functions of normalized

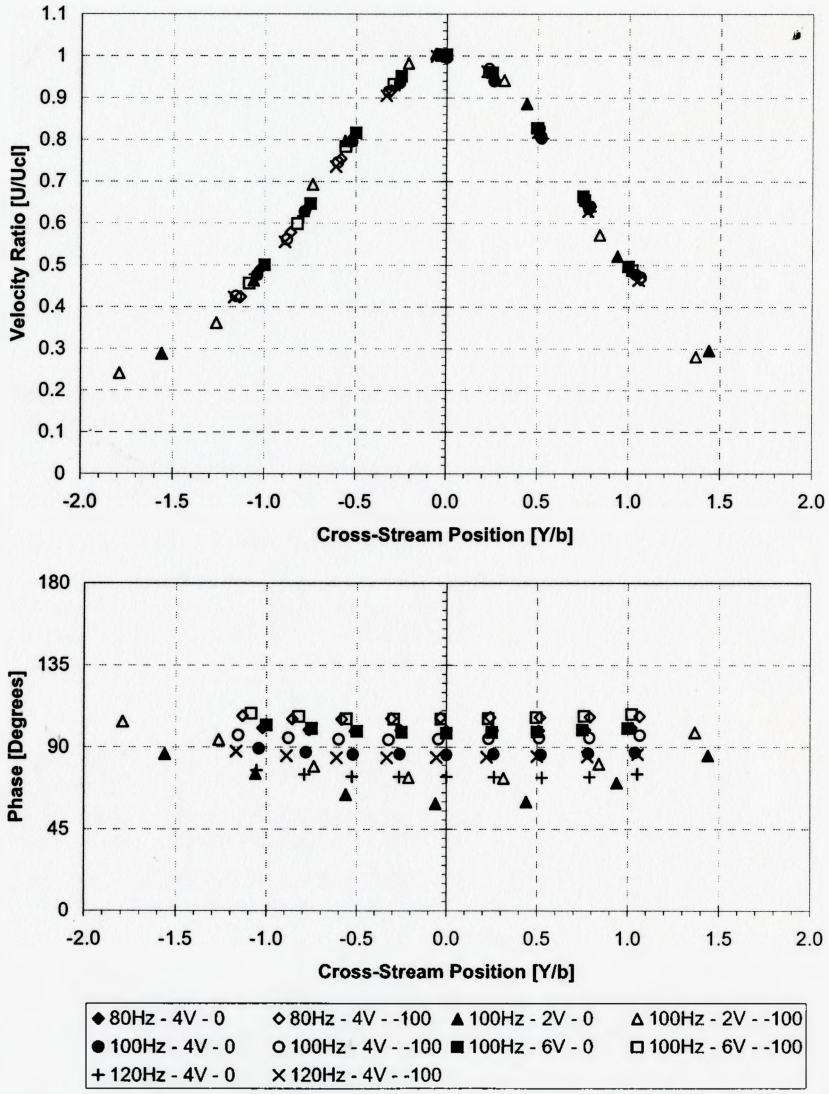

Figure 5.3. Sample velocity and phase profiles for the short slit cylinder plotted in similarity coordinates. [Figure legend shows frequency of exciting signal – amplitude of exciting signal – spanwise position (Z/h)]

vertical position Y/b, where b is the half width of the jet, i.e. the position where the flow velocity is half the centerline value. It can be seen, from the figure that all velocity profiles collapse together. This agrees with the findings of Smith and Swift (2001, 2003) discussed in Chapter 2. Moreover, errors involved in slight misalignments of the hotwire position produce small errors in the velocity and phase measurements. For example, a shift of about 20% of the jet width produces only about 4% error in the measurement of the velocity. In addition, the phase profiles are flat around the jet centerline, which minimizes any errors involved with hotwire misalignments.

5.3. Synthetic Jet Characterization

Having discussed the generation mechanism of the jet, the coordinate system established and the criteria for choosing where to carry out the measurements, the experimental results are now to be discussed. First, the spanwise characteristics of the issuing jet will be discussed with varying the excitation signal frequency, and then they will be studied with varying excitation amplitude. The characteristics of interest are the average centerline velocity and the average phase between the velocity fluctuations and the excitation signal.

5.3.1. Effect of Frequency Variation

For this experiment, the excitation signal amplitude was fixed at 4 Volts and the frequency was changed from 80 to 120 Hz as discussed before. Measurements were conducted as described above at $X = 5$ mm and at the nine spanwise positions described

for each cylinder above. The spanwise distribution of the averaged centerline velocity and averaged phase, between the velocity fluctuations and the excitation signal, is shown for the long slit cylinder in Figure 5.4 and for the short slit cylinder in Figure 5.5.

From Figure 5.4, for the long slit cylinder, it can be observed that the emanating jet is almost symmetric about the midspan position, which was to be expected as the excitation is supplied to the speakers in phase. Moreover, it can be seen that the velocity decreases as we progress towards the midspan of the cylinder from either end. Also, the velocity of the jet decreases and the deficit at the midspan increases with increasing the excitation frequency. The value of the velocity at the midspan decreases from about 3.8 m/s at 80 Hz to 3.3 m/s at 100 Hz (a reduction of about 14% from the value at 80 Hz) and to 2.65 m/s at 120 Hz (a reduction of about 30% from the value at 80 Hz). The deficit at the midspan on the other hand, increases from about 18% of the velocity at the slit terminations for the 80 Hz case to 28% for the 100 Hz case and to 41% for the 120 Hz case. This same trend exists for the phase change as it can be seen that large phase differences occur between the midspan and the ends of the slit. These deficits are about 70° for the 80Hz case, 89° for 100 Hz and 113° for 120 Hz.

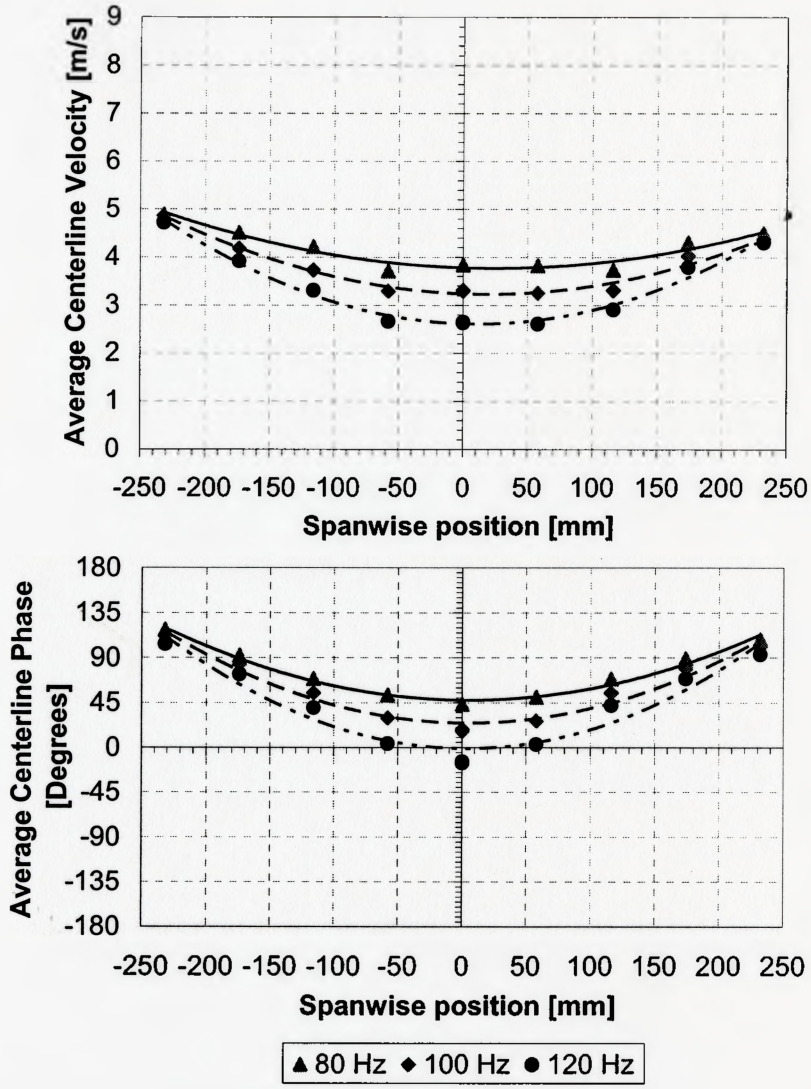

Figure 5.4. Spanwise distribution of the average centerline velocity and phase with varying excitation frequency. (Long slit cylinder) [Lines are for visual aid only]

The short slit cylinder case, however, clearly shows a much stronger and more uniform jet. For the same excitation, Figure 5.5 shows that the velocity of the jet at the midspan increases by an average value of about 79% from the value of the long slit jet. The jets are more uniform for the short slit, for which the values of the deficit drop to an

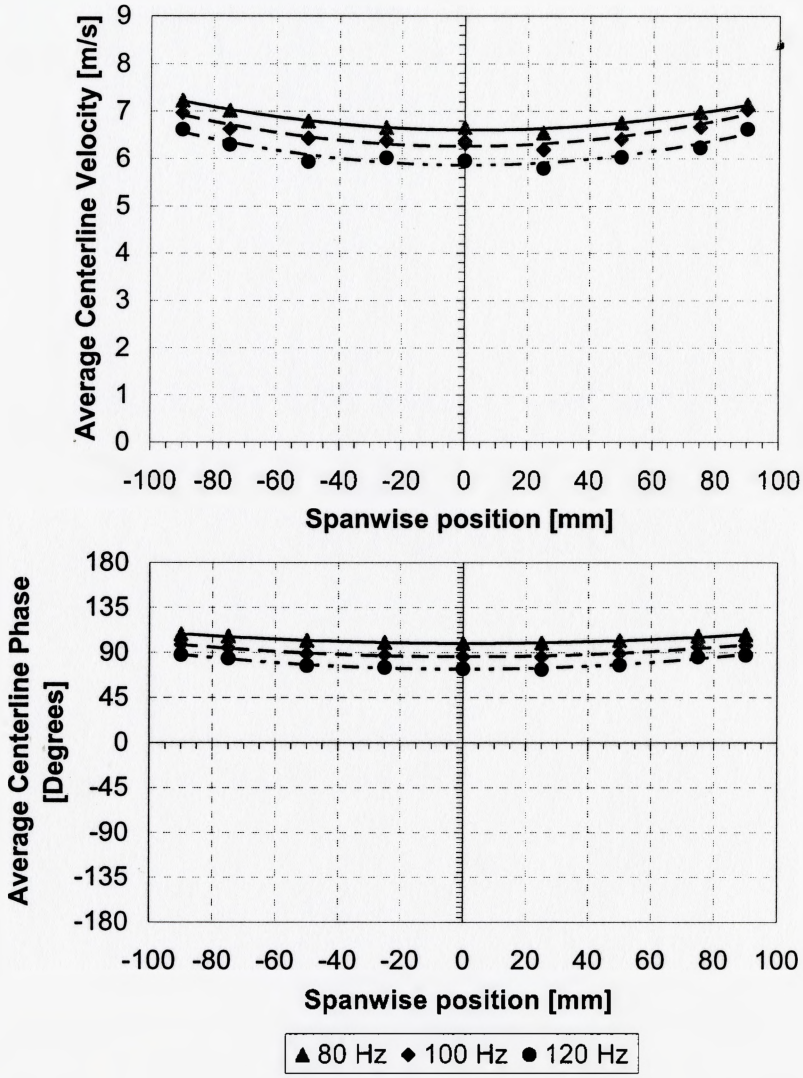

Figure 5.5. Spanwise distribution of the average centerline velocity and phase with varying excitation frequency. (Short slit cylinder) [Lines are for visual aid only]

average value of about 14% in comparison to an average of about 29% for the long slit cylinder. The phase, as well, is more uniform across the span of the slit where the values of the phase difference between the ends of the slit and its midspan drop substantially. Values of phase change for the short slit cylinder drop to 8° for 80Hz, 11° for 100 Hz and 13° for 120 Hz. It should be noted, however, that care should be taken when comparing the absolute values of phase as the velocity of the jets are different for the short slit than they are for the long slit, which would cause differences in the phase that are caused merely by the differences in the convection velocity.

5.3.2. Effect of Amplitude Variation

In this section, the effect of changing the amplitude of the excitation signal is studied. The frequency was set at 100 Hz and the amplitude was changed from 2 to 6 Volts as discussed before. As mentioned in the previous section, the average centerline velocity of the jet and the average phase between the fluctuating velocity and the excitation signal at each spanwise position is plotted against the spanwise position in Figure 5.6 for the long slit case and Figure 5.7 for the short slit one.

Figure 5.6 and Figure 5.7 show that in this case the same trends, as with varying the frequency, are observed for both the long and the short slit cases. All cases show a deficit in both the mean velocity and phase as the midspan of the jet is approached from either end. In this case, however, changing the amplitude produces higher changes in the mean velocity than changing the frequency, but the deficit value stays almost unchanged for different excitation amplitudes.

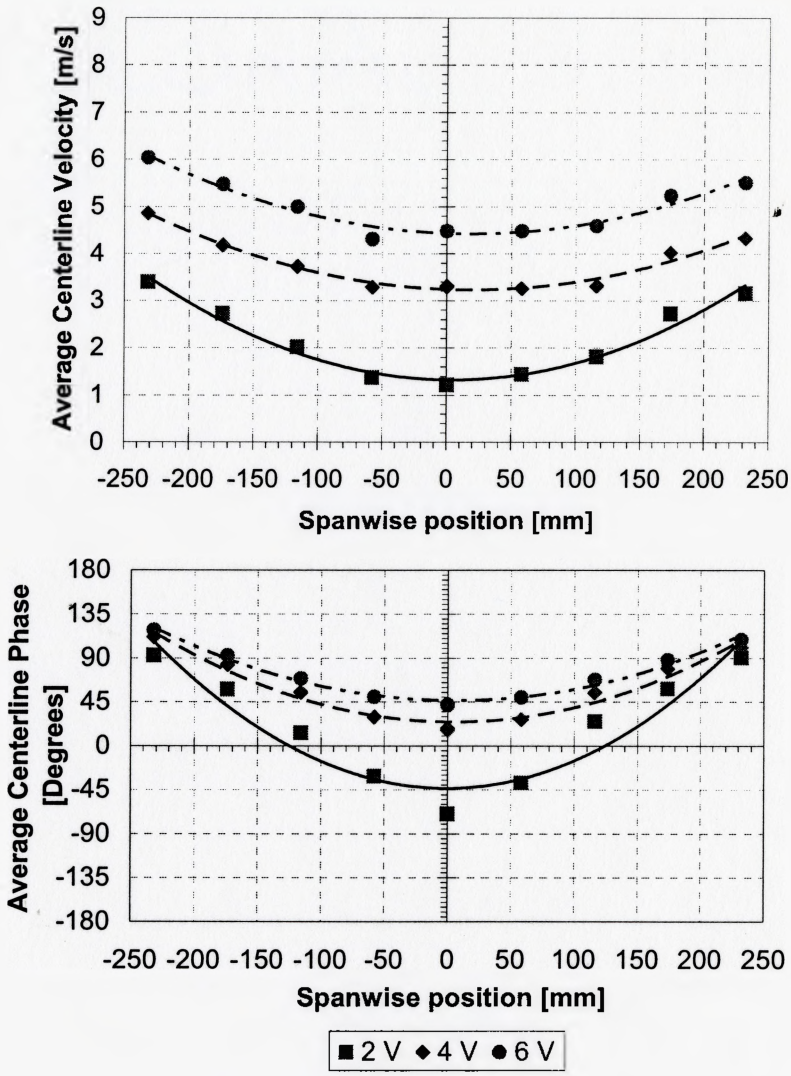

Figure 5.6. Spanwise distribution of the average centerline velocity and phase with varying excitation Amplitude. (Long slit cylinder) [Lines are for visual aid only]

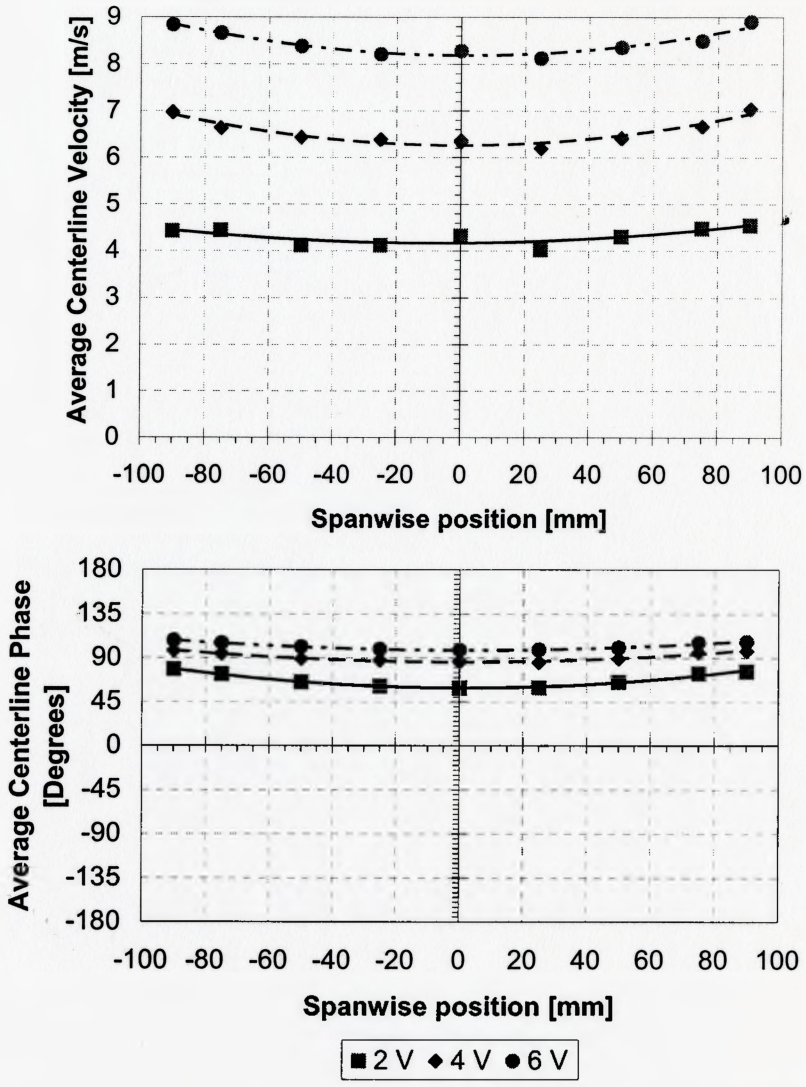

Figure 5.7. Spanwise distribution of the average centerline velocity and phase with varying excitation Amplitude. (Short slit cylinder) [Lines are for visual aid only]

The value of the velocity deficit for the long slit case is about 25% for both the 4 and the 6 Volt excitation and the value of the phase deficit is about 72°. It should be noted however that the 2 Volt case shows a slightly different trend as discussed later.

For the short slit cylinder, the same behavior exists as mentioned for the long slit cylinder where the deficit is about 7% for all the cases and the phase deficit is about 9.5°. The 2 Volt excitation for the short slit, however, does not show a different behavior than the other two cases.

The 2 Volt excitation case shows different trends for the distribution of velocity and phase than the other cases for the long slit case. For this case, the deficit in the velocity was 63% as compared to 25% for the other two amplitudes. For the phase, the deficit is about 161° for the 2 Volt case as compared to 72° for the other two. Moreover, the trend that the phase distribution follows appears to be different from the other two cases. These changes in the behavior of the jet for this case can be reasoned to the fact that this amplitude of 2 Volts represents the lowest excitation under test. According to other research done on synthetic jets, e.g. Smith and Glezer (1998), Smith et al. (2001), Glezer and Amitay (2002), Smith and Swift (2003), and Utturkar et al. (2003), a jet is not synthesized below a certain excitation level. It is expected that at this low excitation level, the jet is approaching this limit. This supposition is supported by the fact that the changes are more pronounced near the midspan of the long slit case where the jet is at its lowest mean velocity.

5.4. SUMMARY & CONCLUSIONS

In this chapter, the characteristics of a high aspect ratio synthetic jet are investigated experimentally in order to evaluate its use as an actuator for active flow control applications. The jet is generated through a 0.75mm wide axial slit on a cylinder (D_o=40mm D_i=34mm L=617mm) by acoustically exciting the fluid inside the cylinder using two speakers mounted at both ends of the cylinder. Two slits are investigated with lengths of 205 mm and 580 mm, giving aspect ratios, *l/h,* of 273 and 773 respectively. Velocity measurements are performed using a hotwire mounted on a three axis, computer controlled, traversing mechanism, and measurements are performed 5 mm downstream of the slit and at different locations in the spanwise and transverse directions. The loudspeakers are activated in phase with harmonic signals at three different amplitudes of 2, 4 and 6 Volts and three different frequencies of 80, 100 and 120 Hz. The characteristics of the jet are based on the spanwise distribution of the centerline velocity and the phase of jet fluctuations relative to the excitation signal.

In both cases, i.e. for the long and the short slits, the mean centerline velocity of the jet increases with increasing the amplitude of the exciting signal, but decreases with increasing its frequency. Moreover, the mean centerline velocity depends on the spanwise position along the slit where a velocity deficit is evident as the midspan of the cylinder is approached from either end. Similar trends are also observed for the centerline phase distributions of the velocity fluctuations. Thus, the jet characteristics depend on three

main parameters: the frequency and amplitude of excitation as well as the spanwise position.

The jet issuing from the long slit exhibits large variations in the spanwise direction, in both its mean velocity and phase. For example, a velocity deficit of up to 41% and phase changes up to 113° occur in the jet along its span. These variations are substantially smaller for the short slit, which exhibits a maximum velocity deficit of 10% and a maximum phase shift of 13°.

Due to its more uniform characteristics, i.e. uniform spanwise distributions of mean velocity and phase, the short slit constitutes a more favorable actuator for active flow control applications than the long slit. Nonetheless, since the long slit produces large phase variations in the spanwise direction, it may be useful in open-loop control applications to externally impose a strong phase gradient along the slit length.

CHAPTER 6

ACTIVE CONTROL EXPERIMENTS

6.1. INTRODUCTION

This chapter discusses the use of the synthetic jet studied in the previous chapter to control the vibrations of the downstream cylinder of a tandem cylinder arrangement using a feedback control mechanism. A PC-based controller is used to manipulate the vibration signal of the downstream cylinder by applying a gain and time lag to it and then feeding it back to the speakers exciting the synthetic jet.

The experiments discussed in the following sections can be divided into two main parts: first, the determination of the optimal controller settings for both cases; second, the study of the control effect on the flow. The first part involves the manipulation of the gain and time lag of the controller to determine their optimum values for each slit. In the second part, hotwire measurements will be performed in the wake of the upstream cylinder to investigate the effect of the synthetic jet on the flow.

The main objectives of the forthcoming experiments are to compare the performance of both slits in controlling the vibrations of the downstream cylinder as well as to investigate how the synthetic jet affects the flow and how the control effect propagates to the downstream cylinder.

The following sections describe how the test section was setup, how the experiments were conducted and finally a discussion of the results obtained.

6.2. EXPERIMENTAL SETUP

The description of the different components involved in the current experiments is discussed in details in Chapter 3. Drawings of the test section are shown in Figure 3.2. The cylinders are spaced 4.5 diameters apart and the synthetic jet is hosted in the upstream cylinder. The upstream cylinder is positioned so that the slit is at a position of 70° from the horizontal plane. A PC-based controller is designed and used to supply the excitation signal to the speakers. Hotwire measurements were realized in the wake of the upstream cylinder. Details of the above mentioned parameters are discussed in the following sections.

6.2.1. CYLINDER SPACING

As the active control experiments under test were conducted to study the effect of the synthetic jet actuator on the dynamic fluid loading of a cylinder placed in the wake of another, the spacing chosen was meant to maximize the fluid forces on the downstream cylinder. A spacing of 4.5 diameters was chosen based on the available literature by Arie et al. (1983), Mahbub Alam et al (2003) and the experiments conducted by Wolfe (2000) for a similar test section. According to Arie et al. (1983) and Mahbub Alam et al (2003), the maximum fluid forces are expected to occur at a spacing of about 4 diameters as

shown in Figure 4.6. Wolfe conducted an experiment to verify the spacing for maximum fluid forces and concluded that, for a similar setup, a spacing of 4.5 diameters achieves this goal. Figure 6.1, from Wolfe (2000), shows the RMS amplitude plots of the vortex shedding spectral peak in the lift spectra for different cylinder spacing. It can be seen that a spacing of 4.5 diameters produces the highest lift especially at frequencies higher than the resonance frequency, which is the case of importance for this study.

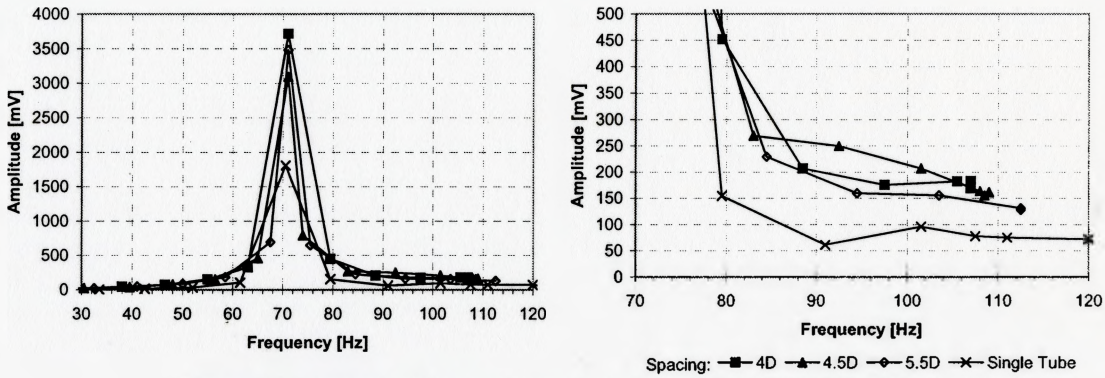

Figure 6.1. Vortex shedding peak amplitude in lift signal. [Wolfe (2000)]
a) Full frequency range. b) Zoomed view of frequencies above resonance.

6.2.2. SLIT POSITION

The angle at which the jet producing slit was positioned was chosen based on consulting the available literature. Huang (1995) reports that for the optimal suppression of vortex shedding the slit should be positioned near the flow separation point, i.e. $60° \leq \theta < 90°$ (where θ is measured from the stagnation point), and reported results for an angle of 80°. Hsiao and Shyu (1990) report an optimal position around the separation point, at an angle of 80°. Moreover, Wolfe (2000) reported using an angle of 60° for his control

experiments. Hence, an angle of 70° was chosen for both the long and the short slit cylinders.

6.2.3. HOTWIRE POSITION

A hotwire was used for velocity measurements in the wake of the upstream cylinder. For the first part of the experiments, i.e. the determination of the controller parameters, the hotwire was fixed at the midspan of the test section, 2.75 diameters upstream of the downstream cylinder and vertically at 0.5 diameters. The hotwire signal was not used in the control process and was just acquired to monitor the vortex shedding process; hence, its position was chosen to produce the strongest possible signal for the vortex shedding. The vertical position was based on measurements done by Wolfe (2000) for the determination of the optimal vertical position for the hotwire. Figure 6.2, after Wolfe (2000), shows the plots of the spectral RMS amplitude of the vortex shedding peak

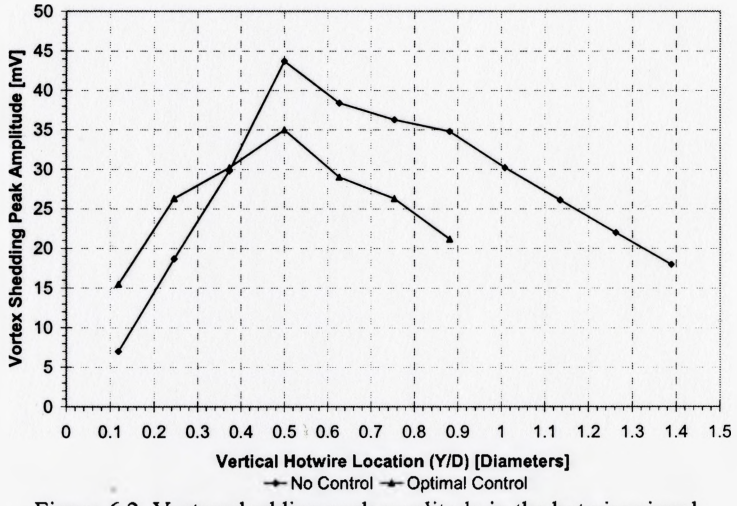

Figure 6.2. Vortex shedding peak amplitude in the hotwire signal at different vertical positions. [Wolfe (2000)].

for the nonresonant case, the case studied in this chapter, for different vertical positions.

For the second part of the experiments, i.e. studying the effect of the synthetic jet on the flow, the hotwire was traversed in the wake of the upstream cylinder at different positions along the span of the test section and at different downstream locations. The vertical position however was fixed at 0.55 diameters, i.e. 2 mm above the upper surface of the cylinder. This was necessary to achieve a strong measurable hotwire signal for the measurements performed directly above the upstream cylinder axis and to insure that the hotwire probe would not touch the cylinder. Hotwire measurements were realized downstream at four different positions in steps of 25 mm starting from the top of the upstream cylinder and at 0.625, 1.25 and 1.875 diameters downstream. The spanwise locations chosen for measurements will be discussed later for each slit separately.

6.2.4. Flow Velocity

The wind tunnel, for this setup, is able to produce flow velocities up to 25 m/s, producing vortex shedding frequencies up to about 118 Hz. This range of vortex shedding frequencies gives rise to two interesting cases of control to study. The first is the resonant case, i.e. when the vortex shedding frequency coincides with the resonance frequency of the downstream cylinder causing large amplitude resonant vibrations. The second is the case when the vortex shedding frequency is different from the resonance one.

The first case is a simple case of control where only one dominant frequency component is controlled, the resonance frequency. A simple time lag controller, as the

one used in this study, is expected to produce the optimal time lag necessary to achieve significant control. Wolfe (2000), for a similar test setup, reported significant reduction in the resonance spectral peak of up to 70% for the resonant case (71 Hz), for a Reynolds number of $Re = 4.1x10^4$. He used a similar active control mechanism using a long slit, extending over most of the length of the cylinder, for the synthetic jet actuator.

On the other hand, for the second case, two spectral peaks are present in the downstream cylinder vibration spectra, those of the natural frequency of the cylinder and the vortex shedding, which makes the control process quite complex. This is because adjusting the time lag to a value that is optimal for the control of one of the frequency components does not necessitate that this value corresponds to an optimal time lag for the other. Wolfe (2000) conducted an experiment at a Reynolds number of $Re = 5.8x10^4$ and reported reductions in the resonant peak (71 Hz) up to 75% and up to 47% for the vortex shedding one (97 Hz). However, the results reported by Wolfe introduce an interesting observation that makes this case interesting for further analysis. He found that in spite of the significant reduction in the resonant peak in the lift spectra of the downstream cylinder, the hotwire spectra between the cylinders do not show any significant peaks at the resonance frequency as it would be expected. These observations motivated choosing the non-resonant case for the analysis carried out in this study.

The non-resonant case, with a flow velocity of about 23 m/s, was chosen to perform the experiments described in this chapter. At this flow velocity, the Reynolds number is $Re = 6.3x10^4$ and the vortex shedding frequency is 100 Hz.

A flow velocity of about 23 m/s was chosen for the following reasons. First, choosing a flow velocity below that of resonance was not recommended as the response of the speakers exciting the jet deteriorates rapidly for frequencies below 70 Hz as discussed in section 3.3.1. Secondly, a large separation between both spectral peaks, the resonance and the vortex shedding, was desired so that the response of the downstream cylinder at its resonance frequency would only be caused by the turbulence in the flow and not be affected by the vortex shedding excitation. Thus, it was decided to produce vortex shedding at a frequency of 100 Hz, which is about 1.4 times higher than the resonance frequency. This frequency was achieved for a flow velocity of about 23 m/s. Additional discussion of the flow velocity and vortex shedding frequency choice can be found in section 6.3.1.

6.2.5. Feedback Control Mechanism

Due to the impingement of the vortices shed from the upstream cylinder on the downstream cylinder, it is expected that the vortex shedding process is accompanied by an upstream feedback effect. This feedback effect enhances the vibrations of the downstream cylinder especially close to the frequency coincidence where this feedback effect is further enhanced by the resonant vibrations of the downstream cylinder. As a result of this feedback effect, it is suggested that the reduction in vortex shedding excitation achieved by the controller is most likely due to the cancellation of this upstream feedback effect. Figure 6.3 shows a block diagram of the natural feedback

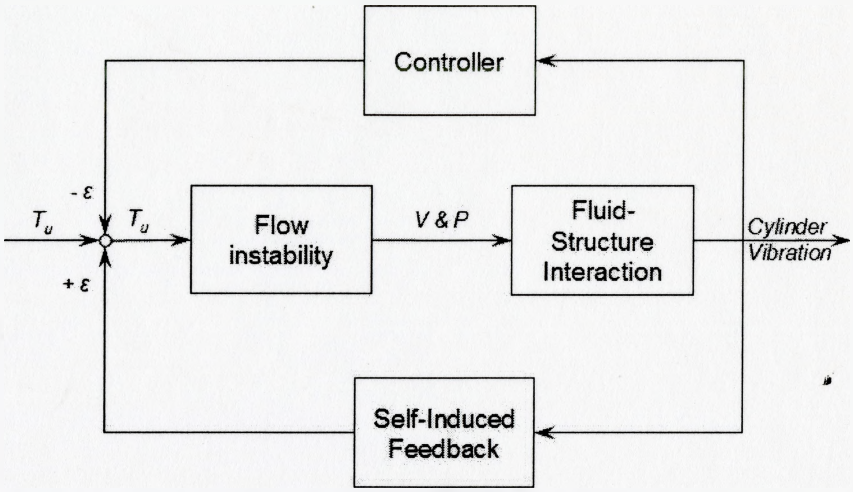

Figure 6.3. Block diagram of the feedback mechanism suggested to cause the self-excited oscillations of the downstream cylinder. T_u is the broadband flow turbulence, V & P are the velocity and pressure fluctuations, and ε is the upstream feedback. (After Ziada (1999))

effect, as proposed by Ziada (1999), along with the controller feedback used to counteract the self-generated upstream feedback.

6.2.6. CONTROLLER

The controller used in this experiment is a software based controller developed using Matlab and Simulink. The data acquisition system used for the control experiments, as discussed in chapter 3, uses software called Wincon that integrates itself within the Simulink toolbox of Matlab. The desired controller is designed in Simulink and is then compiled. When compiled the program runs in Wincon, independent from Simulink, providing the necessary speed the system is capable of achieving. Simulink provides an easy to use graphical programming environment where the program is created in a

diagram form with components wired together to form the desired functions. The controller used in the experiments of this chapter is shown in Figure 6.4. The controller consists of an input, the strain gage signal, which is time delayed by a set value, T_d, and then a gain is added, K_c, and finally the signal is sent to an output, which is used to activate the speakers. The switch supplied allows turning the controller on and off to take measurements. The values of T_d and K_c are manually set and can be changed to achieve the best control possible.

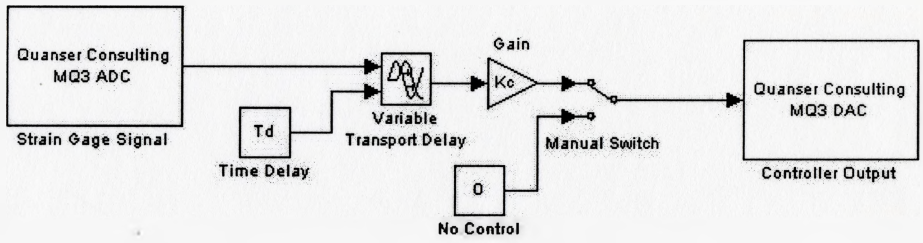

Figure 6.4. Block diagram of the Simulink program used.

6.3. RESULTS

The results can be divided into two main parts; the first deals with the controller parameters, gain and time lag, for both the long and the short slit cases. The second part deals with the hotwire measurements performed to analyze the effect of the jet on the flow between the cylinders. Before dealing with the experimental results, an uncontrolled reference for all cases must be chosen in order to compare the performance of the controller. This will be discussed in the following section followed by the discussion of the control results.

6.3.1. Uncontrolled Cylinder Reference

The comparison between the response of the controlled and the uncontrolled cases for each cylinder requires a no control reference case. The first thought was to simply use the cylinder with the slit, for each case separately, with no control signal sent to the speakers to represent the uncontrolled reference. However, it was observed that the presence of the slit, even with no control, alters the vortex shedding process. Figure 6.5 shows typical power spectra for three different upstream cylinders; a solid (or no slit) cylinder, the long slit cylinder, and the short slit cylinder. Typically, the spectra of the

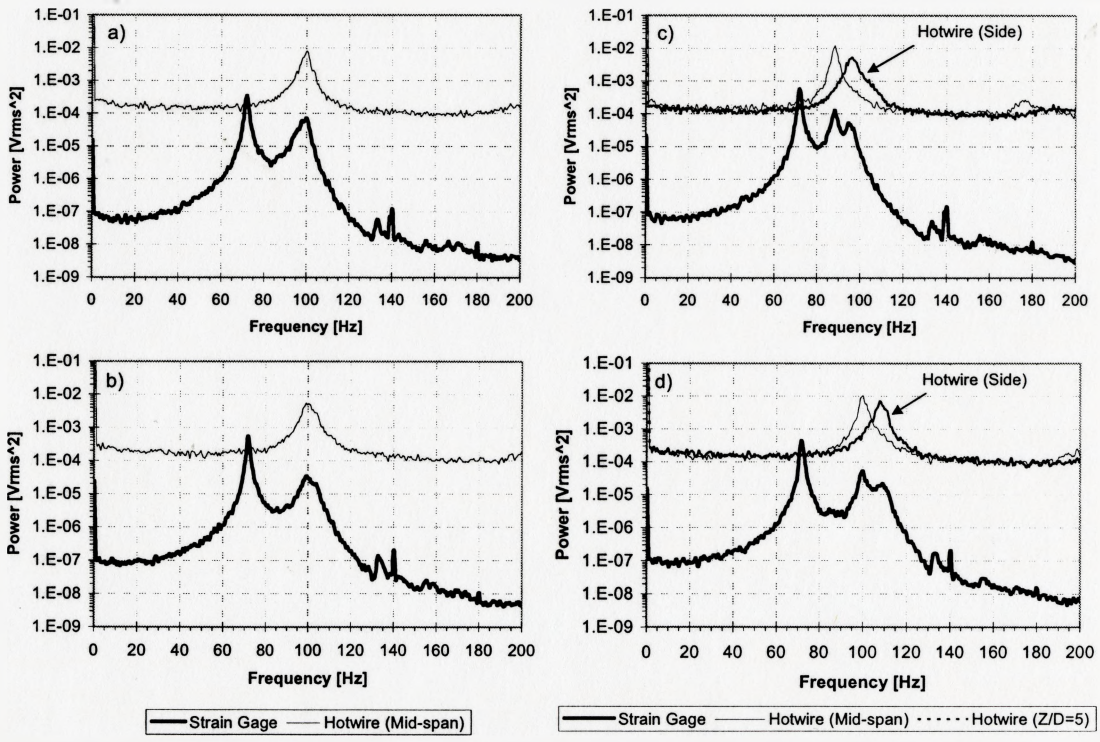

Figure 6.5. Power Spectra of the strain gage & the hotwire signals for the three cylinders used showing the effect of the presence of the slit on the vortex shedding phenomenon.
a) No slit cylinder at 22 m/s. b) Long slit cylinder at 23 m/s.
c) Short slit cylinder at 21.2 m/s. d) Short slit cylinder at 24 m/s.

vibration signal of the downstream cylinder (the strain gage signal) contain two dominant frequency components. One component corresponds to the vortex shedding frequency (around 100 Hz), and the other corresponds to the response of the cylinder at its resonance frequency, excited by the turbulence in the flow (at 72 Hz). From the figure, a flow velocity of 22 m/s was needed to achieve vortex shedding at 100 Hz for the no slit cylinder. For the long slit cylinder, a flow velocity of 23 m/s was required to obtain the same vortex shedding frequency. In the short slit cylinder case, two peaks were observed in the strain gage spectra and a flow velocity of 24 m/s was needed to produce a minimum vortex shedding frequency of 100 Hz.

In order to investigate the presence of the two vortex shedding peaks for the short slit cylinder, hotwire measurements were obtained at the midspan of the cylinder, where the slit is present, and at Z = 200 mm (Z/D = 5), which is 100 mm beyond the slit end. From Figure 6.5.(c) & (d), it can be observed that one peak, the lower frequency peak, corresponds to vortex shedding from the cylinder in the presence of the slit and the other corresponds to shedding from the part without the slit. . The shift in the vortex shedding frequency caused by the slit is quite substantial and amounts to about 10%.This phenomenon deserves further investigation and analysis, however this is beyond the scope of this thesis.

As a result of the above mentioned observation, it was decided that a vortex shedding frequency of 100 Hz would be selected for both the long and the short slit cylinders regardless of the velocity at which this frequency is obtained. The uncontrolled

reference for each case was chosen to be the no slit cylinder case tested at the same velocity as the cylinder with slit, regardless of the vortex shedding frequency it produces.

6.3.2. CONTROLLER PARAMETERS

The controller used in the experiments, as discussed earlier, is a simple gain and time lag controller. Those two parameters are set manually and hence it was necessary to determine the optimal settings for each to achieve the best control possible. The controller gain, based on some preliminary measurements, was initially set at a value of 2 and then the time lag was changed from 1 ms to 25 ms in steps of 1 ms. The optimal time lag was then chosen and was fixed and the gain was changed from 1 to 6. It should be noted, however, that these values of gain are arbitrary and only represent the value of K_c adjusted for the controller program. This is because the overall gain would have to include values of the gain of the strain gage bridge as well as the speakers' amplifier.

The following sections will discuss the results obtained for each of the two cylinder cases.

6.3.2.1. Long Slit Cylinder

The cylinder with the long slit was the first to investigate. The cylinder was set up in the wind tunnel and the flow velocity was set so that the vortex shedding frequency was 100 Hz. This vortex shedding frequency is achieved at a flow velocity of 23 m/s. The controller was then switched on with a gain of 2 and a time lag of 1 ms as discussed

above. The lift signal from the strain gages along with the hotwire signal and the controller output were recorded for further analysis as will be discussed.

The effect of changing the time lag from 1 to 25 ms for a constant gain of 2 was first investigated. Figure 6.6 summarizes the ratio of the controlled to the uncontrolled total RMS amplitude of the lift signal versus the time lag in milliseconds. The uncontrolled reference is the no slit cylinder as discussed above; thus, a value of 1 represents the value of the total RMS amplitude of the signal for the no slit cylinder, i.e. the controller is neither enhancing nor attenuating the signal. The total RMS amplitude is calculated by obtaining the square root of the sum of the power spectra of the Strain gage signal from the downstream cylinder for frequencies between 20 Hz and 130 Hz. The frequency limits chosen are discussed in section 4.3.2.

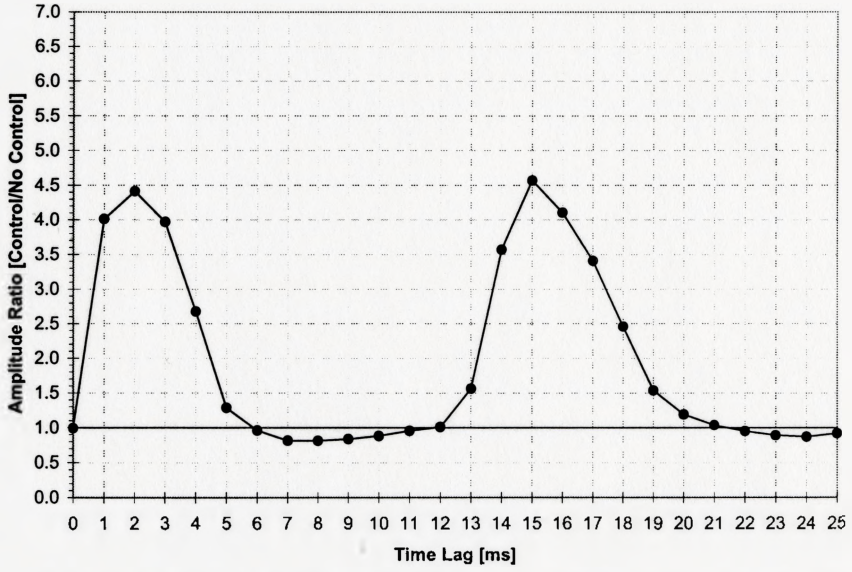

Figure 6.6. The effect of changing the controller time lag for a gain of 2 on the total RMS amplitude of the downstream cylinder vibration for the long slit cylinder case. (An amplitude ratio of 1 represents no amplification or attenuation) [Lines are for visual aid only]

The figure shows that the cylinder vibration goes through cycles of reduction and amplification and that the maximum reduction possible reduces the RMS amplitude to about 80% of the no control amplitude. Further insight can be obtained by considering the effect of the controller time lag on the two dominant peaks in the downstream cylinder vibration spectra.

Figure 6.7 shows the amplitude ratio of the controlled to the uncontrolled spectral peak amplitudes for each of the two dominant frequency components versus the controller time lag. Care should be taken for all the following figures that the value corresponding to a time lag of zero represents the uncontrolled slit case, i.e. the slit is present but no control signal was supplied to the speakers. This point is provided just for

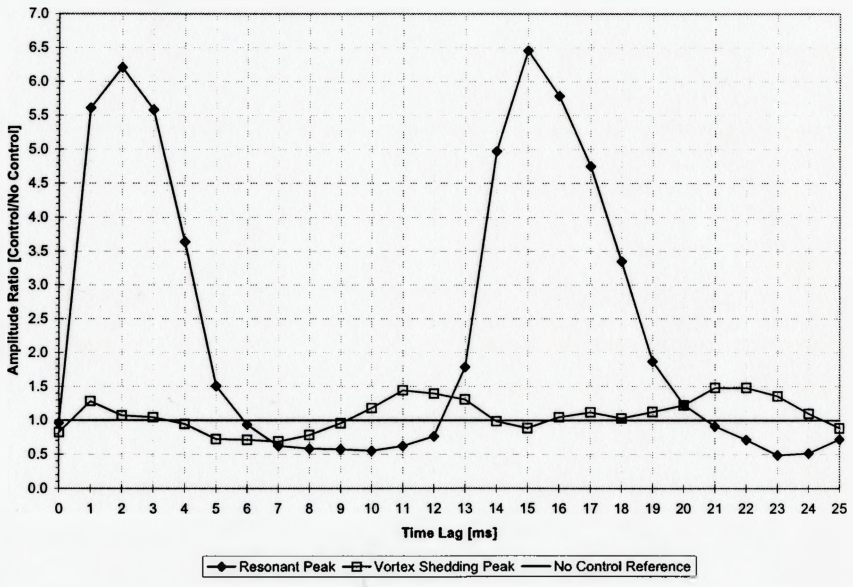

Figure 6.7. The effect of changing the controller time lag for a gain of 2 on the spectral peak amplitudes at the resonance and the vortex shedding frequencies for the long slit cylinder case. (An amplitude ratio of 1 represents no amplification or attenuation) [Lines are for visual aid only]

comparison with the no slit case, a value of 1. The figure shows that both peaks undergo cycles of amplification and reduction by changing the controller lag. The resonant peak shows a maximum reduction of about 50% at a time lag of 9 ms and 23 ms. This 14 ms period between the two values corresponds to the period of oscillation at a frequency of roughly 72 Hz, which is the resonance frequency. This indicates that a time lag of 23 ms produces a control signal that is delayed by a full cycle. The vortex shedding peak shows the same periodic amplification and reduction trend as the resonant peak, but with a period of roughly 10 ms, i.e. corresponding to an oscillation of 100 Hz, which is the vortex shedding frequency. The vortex shedding peak, however, does not show the same large amplification as the resonant peak, while the reduction is still at around the same order with a minimum amplitude of about 68% of the uncontrolled value at a lag of 7 ms.

When seeking the optimal controller gain, the time lag producing the maximum reduction in the vibration signal, i.e. 8 ms, was set and the controller gain was changed in steps of 1 from 1 to 6. Figure 6.8 shows the variation in the total RMS amplitude of the strain gage signal for the different gains tested. The figure shows that a gain of 3 produces the maximum reduction where the signal is reduced to 80% of its reference amplitude.

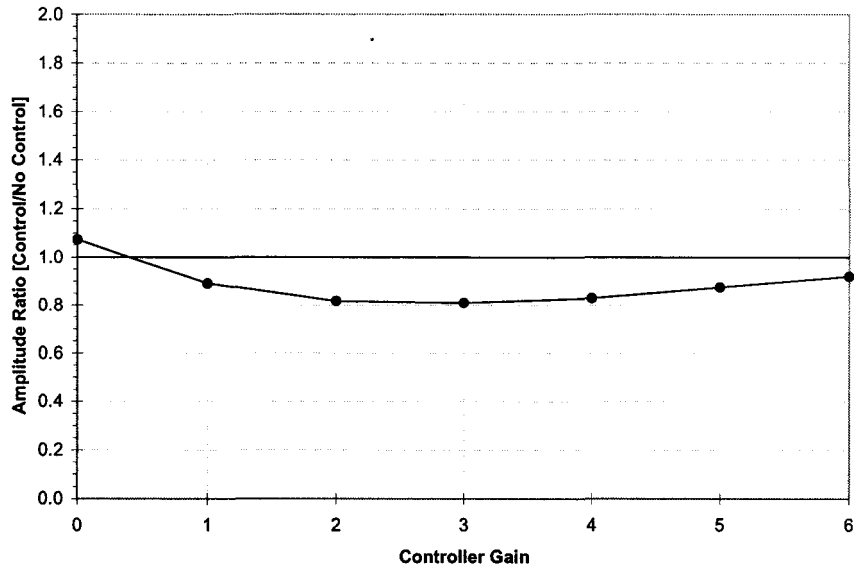

Figure 6.8. The effect of changing the controller gain for a time lag of 8 ms on the total RMS amplitude of the downstream cylinder vibration for the long slit cylinder case. (An amplitude ratio of 1 represents no amplification or attenuation) [Lines are for visual aid only]

A closer look at both frequency components is provided in Figure 6.9. The figure shows that the optimal gain setting for the resonant peak is 4 with an amplitude that is 40% of the uncontrolled reference, while that for the vortex shedding peak is at 1 with a value that is about 90% of the uncontrolled one. A controller gain of 3 was chosen to represent the optimal setting of the controller to be used in further analysis as will be detailed later. This choice, although does not represent the optimal reduction in either peak, gives an optimal overall reduction in the vibration of the cylinder as shown with the total RMS amplitude, Figure 6.8. Nonetheless, a significant reduction of the resonant peak was still achieved to with a value that is about 48% of the uncontrolled reference and the vortex shedding peak showed almost no change.

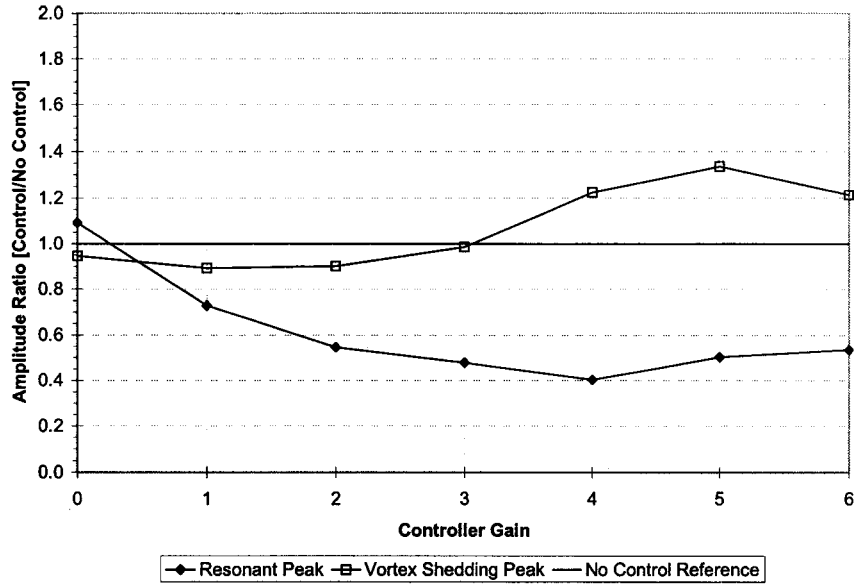

Figure 6.9. The effect of changing the controller gain for a time lag of 8 ms on the spectral peak amplitudes at the resonance and the vortex shedding frequencies for the long slit cylinder case. (An amplitude ratio of 1 represents no amplification or attenuation) [Lines are for visual aid only]

Power spectra of the optimally controlled and uncontrolled cases along with the no slit reference are shown in Figure 6.10. The significant reduction in the amplitude of the resonant peak is evident in the spectra. This peak is excited by the flow turbulence. Moreover, it can be seen that for the no slit case vortex shedding occurs at a frequency of 106 Hz, while this frequency drops to 100 Hz when the slit is introduced with no control. For the optimal control, a shift in the shedding frequency is observed, where the frequency increases slightly to 102 Hz.

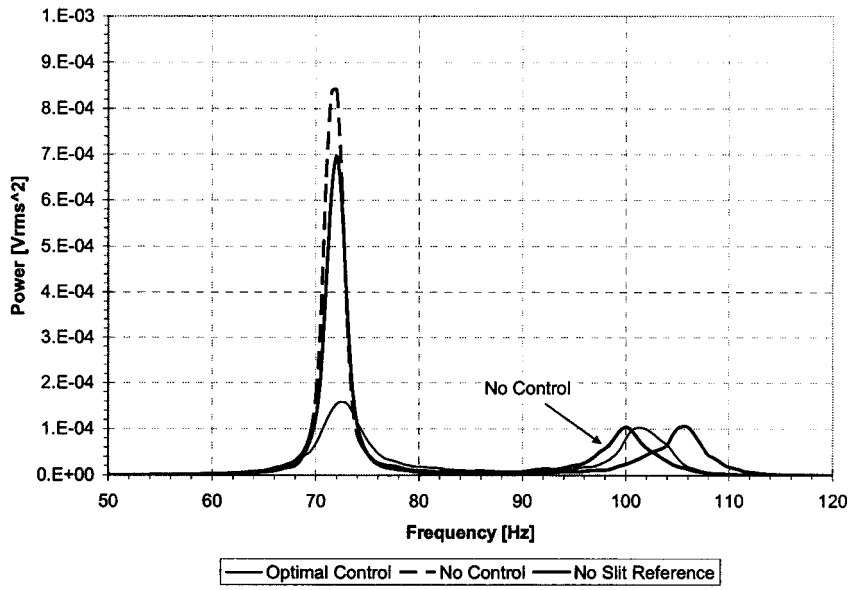

Figure 6.10. Power spectra of the optimally controlled case (K_c=3, T_d=8 ms), the no control case and the no slit reference for the long slit cylinder.

6.3.2.2. Short slit Cylinder

A similar group of experiments was performed for the short slit cylinder. The flow velocity in this case was 24 m/s. Figure 6.11 and Figure 6.12 summarize the results obtained for the short slit cylinder. All the data show similar trends as those observed for the long slit case. Figure 6.11 shows the variation of the total RMS amplitude of the vibration signal with changing time lag. The maximum reduction achieved for this case is slightly lower than that reported for the other case as the RMS amplitude is reduced to about 87% of the no control amplitude. This maximum reduction occurs for a time lag of 9 ms which is chosen as the optimal time lag. Care should be taken that although the cycles of attenuation and reduction have the same periods as those for the long slit case, the values of time lag for which maximum attenuation or reduction occur will be slightly

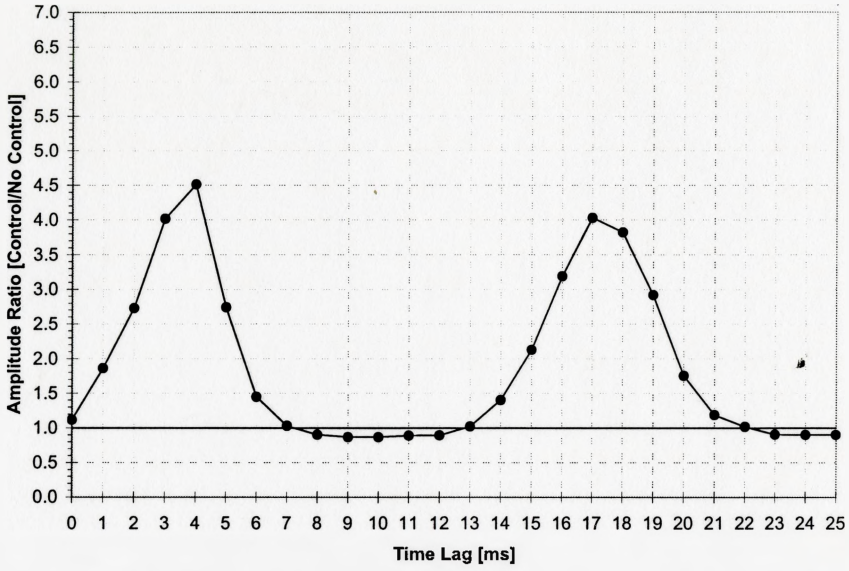

Figure 6.11. The effect of changing the controller time lag for a gain of 2 on the total RMS amplitude of the downstream cylinder vibration for the short slit cylinder case. (An amplitude ratio of 1 represents no amplification or attenuation) [Lines are for visual aid only]

different as the flow velocity is different for both cases. The periods of oscillation are the same as both cases have spectral components that are at equal frequencies, i.e. the resonance frequency and the vortex shedding frequencies are equal.

Figure 6.12 shows the variation of the spectral peak amplitudes for the resonance and the vortex shedding frequencies versus the controller time lag. The resonant peak shows a maximum reduction of about 42 % at a time lag of 10 ms. It should be noted here, that for the short slit case, two vortex shedding peaks appear in the spectra of the vibration signal. Both peaks exhibit the same periodic trend with a period corresponding to the vortex shedding frequency. The peaks show a reduction of about 45%

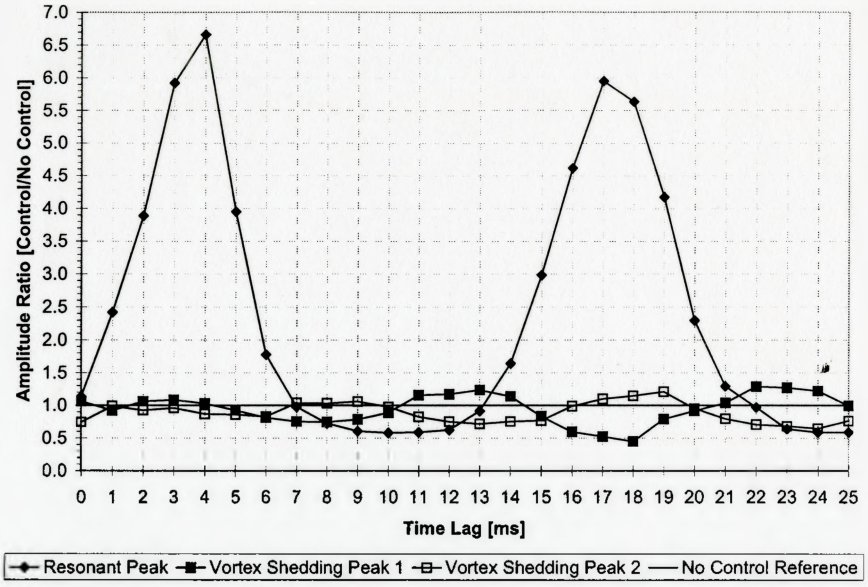

Figure 6.12. The effect of changing the controller time lag for a gain of 2 on the spectral peak amplitudes at the resonance and the vortex shedding frequencies for the short slit cylinder case. (An amplitude ratio of 1 represents no amplification or attenuation) [Lines are for visual aid only]

The effect of changing the controller gain for a constant time lag of 9 ms is shown in Figure 6.13 and Figure 6.14. The variation of the total RMS amplitude of the cylinder vibration signal for the different gains tested is shown in Figure 6.13. The figure shows that a gain of 3 produces the maximum reduction in the total RMS amplitude to an amplitude that is 82% of its reference value. In Figure 6.14, which shows the effect of changing the controller gain on the spectral peaks, the optimal gain setting for the resonant peak is 3 with an amplitude that is 43 % of the uncontrolled reference. For the vortex shedding peaks, it can be seen that the higher frequency peak does not show any reduction with increasing the gain while the other has a minimum value at a gain of 3 with a value that is 75% of the reference value.

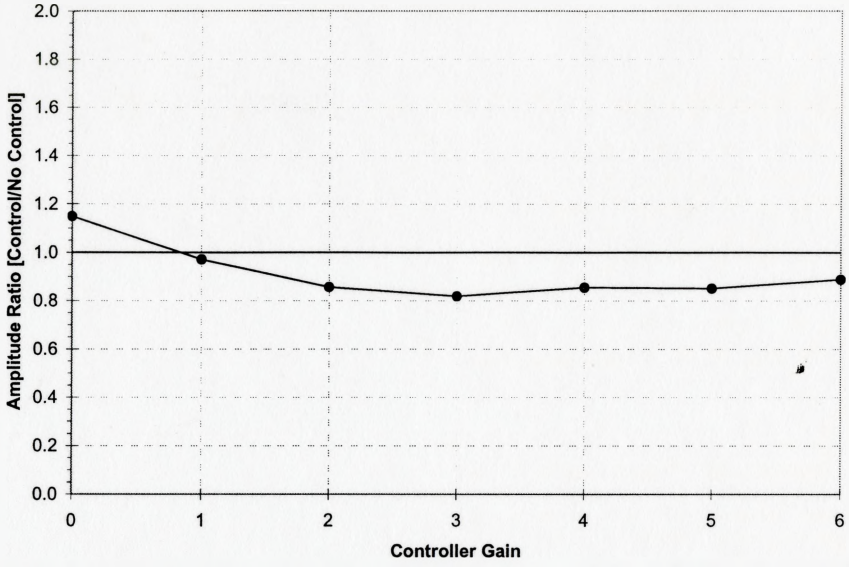

Figure 6.13. The effect of changing the controller gain for a time lag of 9 ms on the total RMS amplitude of the downstream cylinder vibration for the short slit cylinder case. (An amplitude ratio of 1 represents no amplification or attenuation) [Lines are for visual aid only]

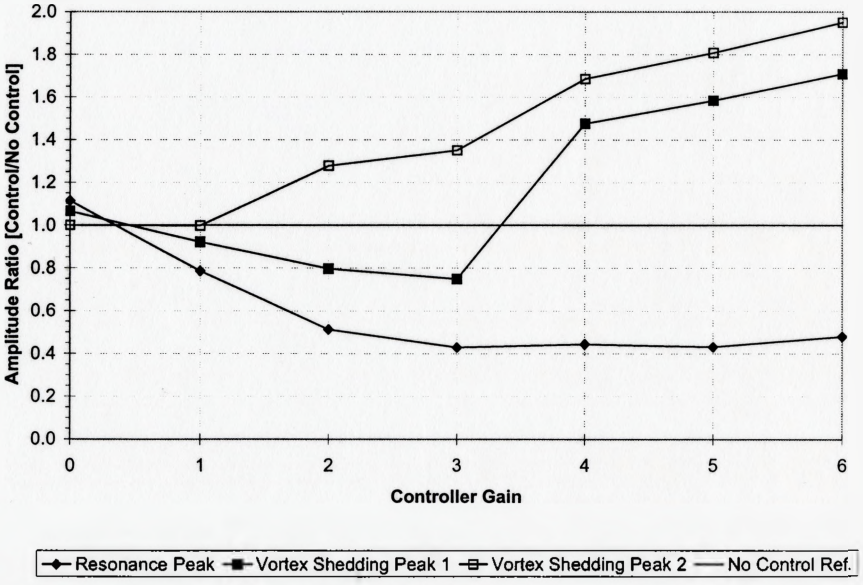

Figure 6.14. The effect of changing the controller gain for a time lag of 9 ms on the spectral peak amplitudes at the resonance and the vortex shedding frequencies for the short slit cylinder case. (An amplitude ratio of 1 represents no amplification or attenuation) [Lines are for visual aid only]

The optimal setting for the short slit cylinder were thus chosen as a gain of 3 and a time lag of 9 ms. These values produce an optimal overall reduction in the vibration of the cylinder as shown with the total RMS amplitude.

Power spectra of the optimally controlled and uncontrolled cases along with the no slit reference are shown in Figure 6.15. The significant reduction in the amplitude of the resonant peak is evident in the spectra. Moreover, it can be seen that for the no slit case the vortex shedding occurs at a frequency of 113 Hz, while the frequency drops to about 100 Hz when the slit is introduced with no control. For the optimal control, a shift in the shedding frequency is observed, where the frequency increases to 108 Hz.

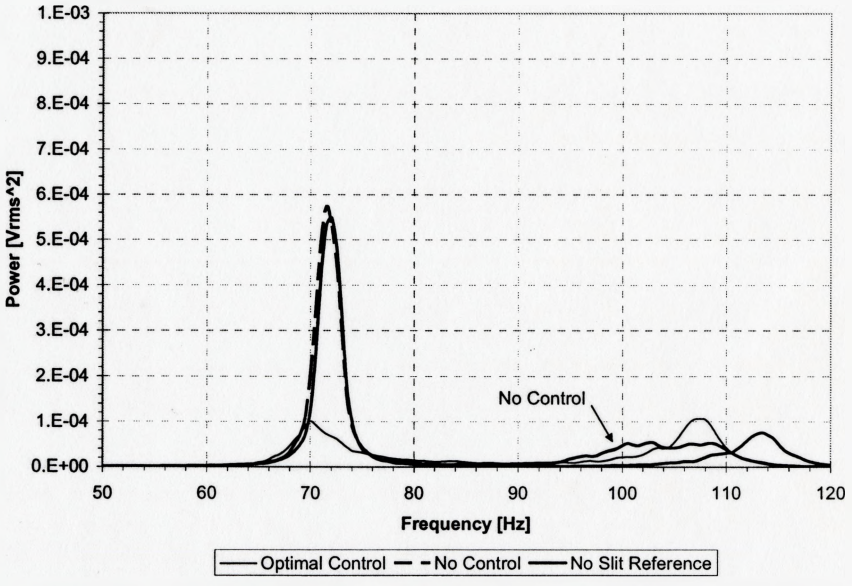

Figure 6.15. Power spectra of the optimally controlled case (K_c=3, T_d=8 ms), the no control case and the no slit reference for the short slit cylinder.

6.3.3. Effect of Synthetic Jet on Flow

After determining the optimal controller settings for each cylinder, these settings were used to investigate the effect of the synthetic jet on the flow between the two cylinders. The controller was switched on for each case using the optimal gain and time lag and hotwire measurements were performed in the wake of the upstream cylinder. As discussed in section 6.2.3 the hotwire was positioned vertically at Y/D = 0.55, i.e. 2 mm above the cylinder surface. The hotwire was then traversed in the spanwise and the downstream directions. Initially, the hotwire was positioned just on top of the upstream cylinder axis (X/D = 0), then it was traversed downstream in steps of 25 mm, i.e. at X/D = 0.625, 1.25 and 1.875. For each of those downstream locations, the hotwire was moved in the spanwise direction starting at the midspan (Z/D = 0) and to one side of the cylinder only. Only one side of the jet was studied because the jet was found to be symmetrical about the midspan of the cylinder as discussed in the previous chapter.

The spanwise locations chosen were set for each cylinder differently. For the long slit cylinder, the hotwire was traversed in steps of 50 mm. The positions chosen were Z/D = 0, 1.25, 2.5 and 3.75. For the short slit cylinder, positions were 40 mm apart, at Z/D = 0, 1, 2, 3. It should be noted that at the position Z/D = 3 for the short slit cylinder, the hotwire is 20 mm beyond the end of the slit. Details of the cylinder and slit dimensions can be found in Chapter 3.

At each position, the hotwire signal along with the downstream cylinder's lift signal, the control signal and the signal of the microphone mounted in the adapter cones of the speakers are collected. As the synthetic jet is excited by the downstream cylinder vibration signal that contains the two main frequency components, i.e. the resonance frequency of the downstream cylinder and the vortex shedding frequency, it would be expected that spectra of the hotwire signal would show peaks at both frequencies. In order to identify the effect of the synthetic jet at those two frequencies, the coherence between the hotwire signal and the strain gage signal was obtained. The coherence is a measure of how correlated the two signals are to each other, with a value of 1 for two identical signals and zero for totally uncorrelated signals. For the uncontrolled case, a high coherence value would be expected around the vortex shedding frequency as this component will be present in both signals. On the other hand, the controlled case is expected to show a strong coherence around both the resonance and the vortex shedding frequencies. This is because the issuing jet is produced by the control signal, which is a modified version of the lift signal containing both frequency components. These expectations are discussed for each slit case in the following sections.

6.3.3.1. Short Slit Cylinder

The optimal controller gain and time lag for this case were discussed earlier and their values were 3 and 9 ms respectively. The controller was operated at these values and hotwire measurements were done as discussed above. Starting at X/D = 0, i.e. on top of the upstream cylinder's axis, Figure 6.16 shows the power spectra of the hotwire and the

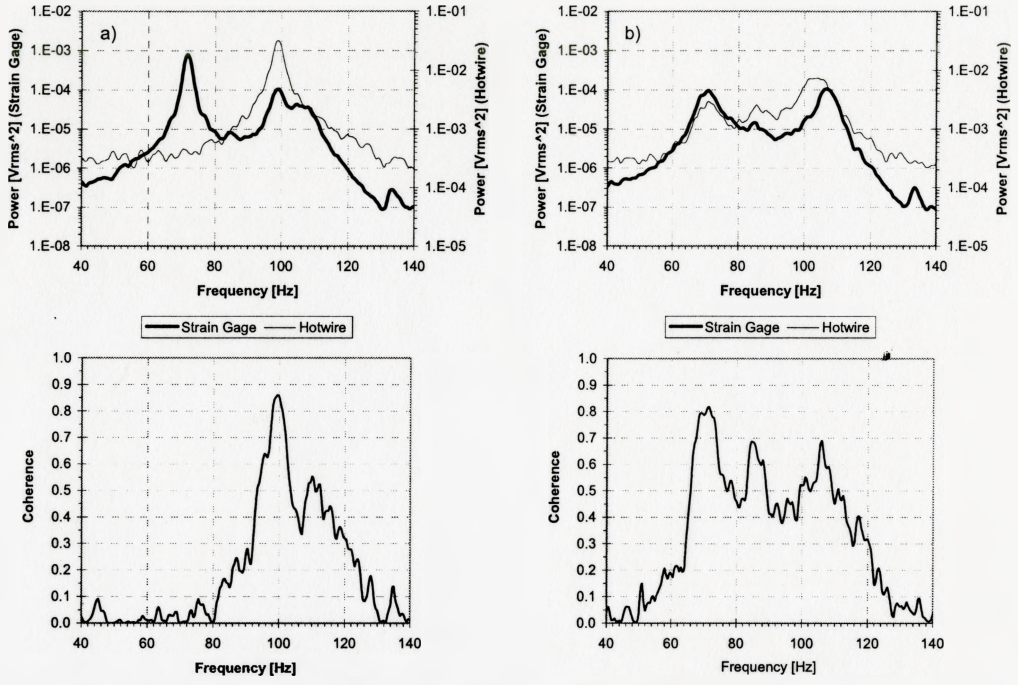

Figure 6.16. Power spectra of and coherence between the strain gage and hotwire signals at $X/D = 0$ and $Z/D = 0$ for the short slit case. a) No Control. b) Optimal Control.

strain gage signals at the midspan of the cylinder, $Z/D = 0$, along with the coherence between the two signals. It can be seen from the figure that for the no control case the coherence increases around the vortex shedding frequency as expected and has a maximum value of 0.85, with a negligible value of coherence at the resonance frequency. In the controlled case, the power spectra of the hotwire signal show a peak at the resonance frequency accompanied by an increase in the coherence between the two signals with a value of about 0.8. This increase in the coherence between the two signals around the resonance frequency for the controlled case is expected to prevail for all the measurement positions as the controller effect is propagated downstream.

Figure 6.17.(a) shows the spanwise variation of the coherence values between the strain gage and hotwire signals at the resonance frequency for the different downstream positions tested, and Figure 6.17.(b) shows the downstream progression of the coherence for the different spanwise positions. Emphasis was set on the resonance peak as it is the peak introduced by the controller action and its progression downstream was of interest.

Figure 6.17.(a) shows that coherence values start with a slight increase when

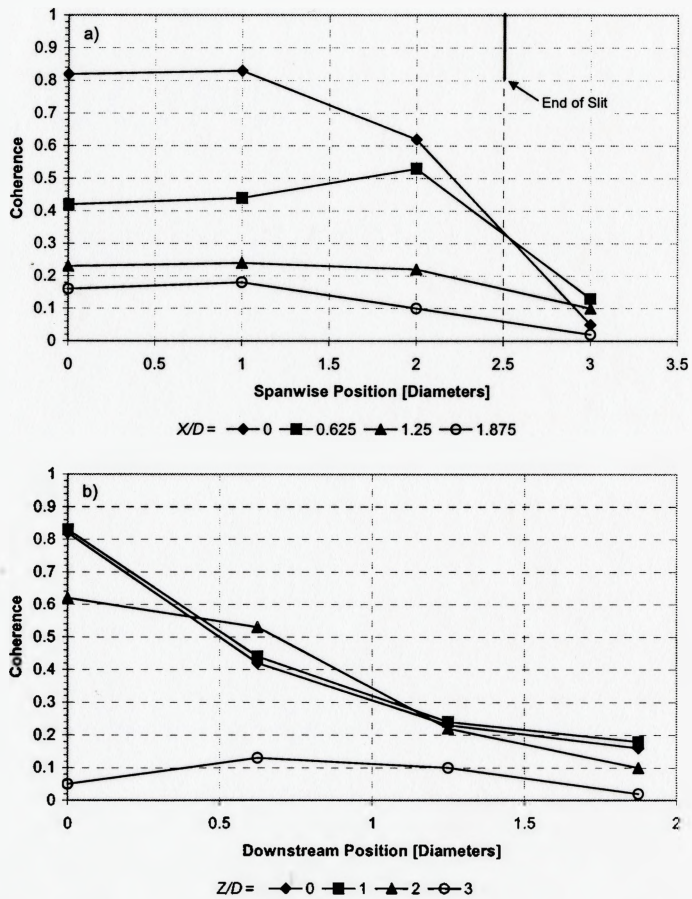

Figure 6.17. Variation of the coherence between the strain gage and hotwire signals at the resonance frequency for the short slit case. a) Spanwise distribution. b) Downstream variation. [Lines are for visual aid only]

progressing to one side of the slit, then drop rapidly when approaching the end of the slit. At Z/D = 3, i.e. 20 mm beyond the end of the slit, the coherence shows almost uncorrelated signals. The increase in the coherence can be attributed to an increase in the amplitude of the issuing jet as discussed in Chapter 5, while the drop at the end of the slit is due to the absence of the control effect once the slit ends.

Figure 6.17.(b) demonstrates that the correlation between both signals decreases dramatically as we progress downstream. It can also be seen that at a distance of X/D = 1.875, which is almost halfway between the two cylinders, the coherence drops to less than 0.2, indicating that the correlation between the hotwire signal and the vibration signal is very weak at this frequency. These findings are somewhat surprising as this implies that no control effect would be detectable at the resonance frequency at the downstream cylinder, while a significant reduction in the resonant peak was still achievable. It is suggested that although the flow oscillations at the resonance frequency become very weak when approaching the downstream cylinder they are at a favorable phase that causes the reduction in the magnitude of the vibrations at this frequency. It should be noted that without the control the vibrations at the resonance frequency are originally produced by the broadband turbulence in the flow as shown in the uncontrolled case spectra shown in Figure 6.16.

Details of the power spectra and coherence plots for the data shown in Figure 6.17 can be found in Appendix D.

6.3.3.2. Long Slit Cylinder

The optimal controller gain and time lag for this case, as discussed previously, were 3 and 9 ms respectively. Following the same procedure as with the short slit, Figure 6.18 shows the power spectra of the hotwire and the strain gage signals at the midspan of the cylinder, Z/D = 0, along with the coherence between the two signals. It can be seen that the hotwire peak at the resonance frequency for the controlled case is much weaker than that for the short slit case. Moreover, the value of the coherence shows a much weaker correlation between the two signals. This can be attributed to the weaker jet produced for the long slit case. The synthetic jet in both the short slit and the long slit

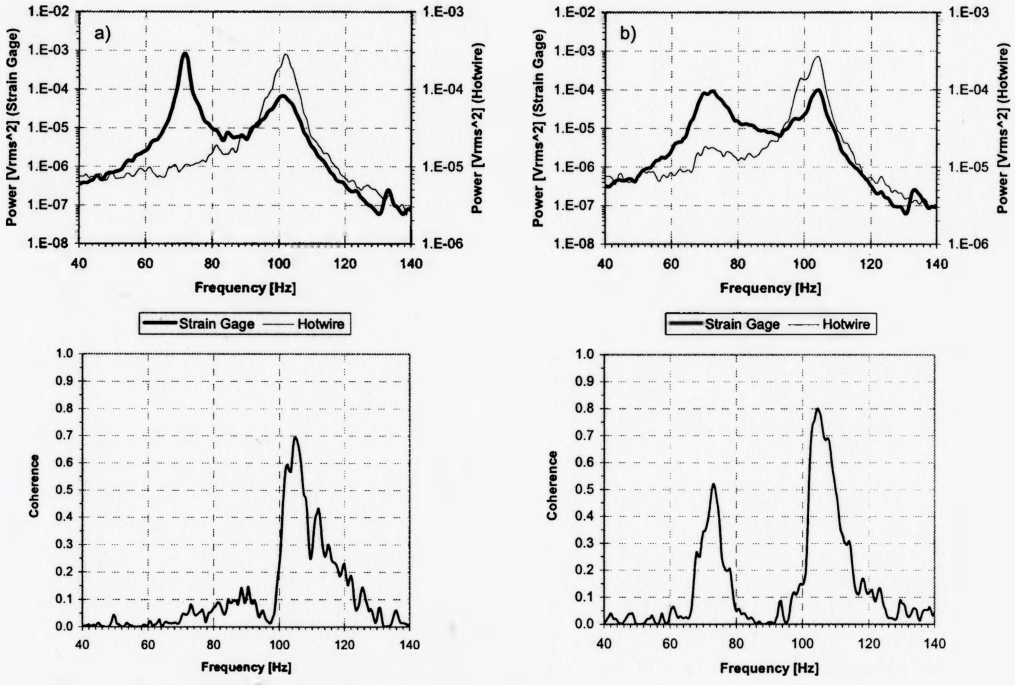

Figure 6.18. Power spectra of and coherence between the strain gage and hotwire signals at X/D = 0 and Z/D = 0 for the long slit case. a) No Control. b) Optimal Control.

cases is excited with almost the same signal and both cases are operating at the same gain value. This will lead to a weaker synthetic jet for the long slit case as discussed in Chapter 5.

Figure 6.19.(a) shows the spanwise variation of the coherence values between the strain gage and hotwire signals at the resonance frequency for the different downstream positions tested, and Figure 6.19.(b) shows the downstream progression of the coherence for the different spanwise positions. Details of the power spectra and coherence plots for the points shown in Figure 6.19 can be found in Appendix D.

Figure 6.19.(a) shows that for the $X/D = 0$ position, the synthetic jet exhibits an almost constant coherence value at this frequency. This is due to the fact that the slit in this case extends to a value of Z/D = 7.25, which is larger than the furthest position of measurement ($X/D = 3.75$). Moreover, the values of coherence are lower than those for the short slit jet which is due to the weaker jet as discussed earlier.

Figure 6.19.(b) shows that the imprint of the long slit on the flow is much weaker than that of the short slit. Values of the coherence drop dramatically almost as soon as the hotwire is moved downstream to values below 0.1, which shows almost no correlation between the two signals. The spectra of the hotwire signal also do not show any peaks around the resonance frequency as shown in the figures of Appendix D. These findings agree with what was reported by Wolfe (2000) where no significant peaks in the power spectra of a hotwire, positioned midway between the two cylinders, were observed at the resonance frequency.

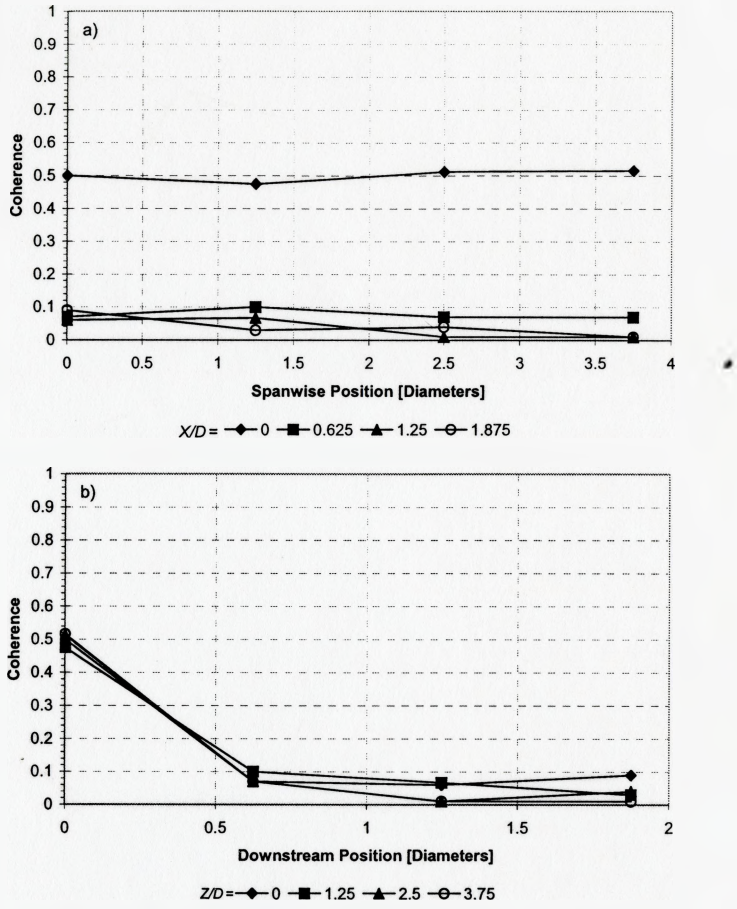

Figure 6.19. Variation of the coherence between the strain gage and hotwire signals at the resonance frequency for the long slit case. a) Spanwise distribution. b) Downstream variation. [Lines are for visual aid only]

The very low coherence values reported for this case along with the observations discussed for the short slit and the fact that the short slit jet is stronger support the already discussed supposition that although the flow oscillations at the resonance frequency are weak and undistinguishable from the broadband turbulence, they are at a favorable phase that produces a significant reductions in the resonant vibration amplitude.

6.4. SUMMARY

The synthetic jet studied earlier was used as a control actuator for the control of the vibrations of the downstream cylinder in a tandem cylinder arrangement. These experiments were performed in order to compare the performance of both the long and the short slit cases as active control actuators. Moreover, the effect of the two jets on the flow was studied to shed more light onto how the synthetic jet affects the flow between the cylinders.

Results show that although the short slit jet produced a potentially better controller as discussed in Chapter 5, it did not produce better reduction in the amplitude of the vibrations of the downstream cylinder when tested. Both jets produced comparable reductions in the vibration of the downstream cylinder. However, it should be noted that the short slit jet produced these results while affecting only one third the length of the cylinders, while for the long slit jet, the jet affects the whole length of the cylinder. A reduction of about 20% in the total RMS amplitude of the vibration signal was achieved and about 50% for the resonant peak and an average value of about 40% for the vortex shedding peak. These values were obtained at different values of gain and time lag for each case.

These optimal values of gain and time lag were then used to investigate the effect of the jet on the flow. It was found that the short slit jet produced an effect that was traced up to $X/D = 1.875$, while the effect of the long slit jet decayed rapidly very close to the

upstream cylinder. These findings endorse the suggestion that the mechanism by which the jet produces significant reduction in the vibration of the downstream cylinder involves the imposition of a favorable phase at the resonance frequency rather than a strong amplitude velocity fluctuation at the downstream cylidner.

CHAPTER 7

CONCLUSION, CONTRIBUTIONS AND FUTURE WORK

7.1. CONCLUSION AND CONTRIBUTIONS

Since their first use as an active flow control actuator in 1994 by smith and Glezer, synthetic jets have gained an increasing amount of interest. Owing to their unique property of being formed from the working medium and their wide range of scales, they have proven to be a successful control actuator. Their applications cover a wide range of flow control applications including active flow control, separation control, virtual aeroshaping of bodies, jet vectoring, cooling, and mixing enhancement.

Recently, Synthetic jets were introduced as a means to control vortex shedding from single and tandem cylinders (e.g. Hsiao and Shyu 1991; Huang 1995; and Wolfe and Ziada 2003). This application entails the production of synthetic jets from an axial slit along part of the length of a cylinder. The jet in this case is excited at the cylinder terminations providing non-uniform excitation along the length of the slit. Hence, the necessity to study the characteristics of the jet along the span of the slit arises. Moreover, the mechanism by which the synthetic jet manipulates the flow field is not fully understood. This investigation, to the author's knowledge, is the first to address the spanwise characteristics of a non-uniformly excited synthetic jet and its effect on the flow past two cylinders in tandem arrangement.

The current study investigates the characteristics of a long aspect ratio, acoustically excited, synthetic jet. The jet is produced through a narrow axial slit along part of the length of a cylinder and is excited at the cylinder terminations. Two slit lengths were compared, namely, a short slit with an aspect ratio of 273, and a long slit with an aspect ratio of 773. It was found that the characteristics of the jet not only depend on the actuating frequency and amplitude, but also on the spanwise position along the slit. Both slit cases exhibited deficits in the mean centerline velocity of the jet as the midspan of the slit was approached from either end. The phase between the velocity fluctuations of the jet and the exciting signal behaved similarly. Velocity deficits of up to 41% of the value at the slit termination and phase deficits of up to 113° were observed for the long slit case. The short slit case, on the other hand, showed a much more uniform jet along the span with a maximum velocity deficit of only 10% and a maximum phase deficit of 13°.

Due to the more uniform characteristics of the short slit jet, it constitutes a more favorable actuator for active flow control applications. Nonetheless, the long slit jet may be useful in open-loop control, to impose strong phase gradients along the length of the slit, due to the large spanwise phase variations observed. Experiments were then carried out to compare the performance of both slits to control the dynamic loading on the downstream cylinder of a tandem cylinder arrangement spaced 4.5 diameters apart. Another objective of these experiments was to better understand the mechanism by which the jet affects the flow.

It was observed that although the short slit jet produced a potentially better control actuator, it did not perform better than the long slit one. The reader must bear in mind that although similar reductions in the downstream cylinder vibration were obtained for both cases, the short slit jet affects only one third the length of the cylinder while the long slit jet affects almost the whole length. Both jets produced comparable reductions in the dynamic loading of the downstream cylinder with a reduction in the total RMS amplitude of the vibration signal of about 20%. The spectral component at the resonance frequency was reduced by about 50% and that at the vortex shedding frequency by about 40%. These values were obtained at different values of controller gain and time lag.

The effect of the synthetic jet on the flow past the cylinders was investigated using hotwire measurements in the wake of the upstream cylinder. Focus was set on the effect produced at the resonant frequency component of the downstream cylinder vibration signal. The vibration of the cylinder at this frequency is excited by broadband turbulence in the flow. Results show that the short slit jet produced effects that were traced up to $X/D = 1.875$, while the effect of the long slit jet decayed rapidly very close to the upstream cylinder. These findings endorse the suggestion that the mechanism by which the synthetic jet achieves control is through the imposition of a favorable phase at the resonant frequency component rather than strong amplitude velocity fluctuations at the downstream cylinder.

7.2. FUTURE WORK

The findings of the current study shed light into the spanwise characteristics of synthetic jets and produces valuable findings on how the jet performs when excited non-uniformly. Integrating this study with flow visualizations of the jet would be beneficial, as well as studying how the synthetic jet would be affected with the presence of flow in the absence of the downstream cylinder can provide more detailed analysis of the jet behavior. Moreover, the differences observed with using two different slit lengths introduce the possibility of using different slit configurations or geometries, such as using more than one slit segment along the length of the cylinder with similar or different excitations, or inducing a strong phase gradient along the length of the slit by introducing excitation at one end of the cylinder.

Investigating the possibility of developing a mathematical model for the synthetic jet actuator mechanism in the light of the obtained data as well as numerical simulations of the process can provide an insight to the physical phenomena involved in the production of the synthetic jet.

With respect to the controller used, this study applies a feedback controller whose parameters are manually set. This controller would not be useful for practical applications as any change in flow conditions would require adjustments to the controller settings. Development of an adaptive controller, such as that employed by Ziada (1999), would be of great benefit. Also, investigating the use of the long slit cylinder for open loop control need to be investigated owing to the large phase variations they exhibit.

For the investigation of the effect of the synthetic jet on the flow for the tandem cylinder control case, more investigation is required to test the feasibility of the proposed theory. Such investigation may include observing phase variations along the span of the cylinder in the wake of the upstream cylinder and how this phase is affected by the control action, as well as flow visualization in the gap between the cylinders to monitor the changes imposed by the control action.

REFERENCES

Amitay, M., Honohan, A. M., Trautman, M. and Glezer, A., (1997), '*Modification of the Aerodynamic Characteristics of Bluff Bodies Using Fluidic Actuators*', 28th AIAA Fluid Dynamics Conference, Snowmass, Colo., AIAA paper 19997-2004.

Arie, M., Kiya, M., Moriya, M. and Mori, H., (1983), *'Pressure Fluctuations on the Surface of Two Circular Cylinders in Tandem Arrangement'*, Journal of Fluids Engineering, Vol. 105, pp. 161 – 167.

Bearman, P.W., (1984), *'Vortex Shedding from Oscillating Bluff Bodies'*, Annual Review of Fluid Mechanics, Vol. 16, pp. 195-222.

Blevins, R. D., (1994), *'Flow-Induced Vibration'*, Second Edition, Krieger Publishing Company, Florida.

Blevins, R.D., (1985), *'The Effect of Sound on Vortex Shedding from Cylinders'*, Journal of Fluid Mechanics, Vol. 161, pp. 217 – 237.

Bloor, M.S., (1964), *'The Transition to Turbulence in the Wake of a Circular Cylinder'*, Journal of Fluid Mechanics, Vol. 19, pp. 290 – 309.

Coe, D. J., Allen, M. G., Smith, B. L., Glezer, A., (1995), *'Addressable Micromachined Jet Arrays'*, Technical Digest: TRANSDUCERS '95, Stockholm, Sweden.

Coe, D. J., Allen, M. G., Trautman, M., Glezer, A., (1994) *'Micromachined Jet Arrays for Manipulation of Macro Flows'*, Technical Digest: Solid-State Sensor and Actuator Workshop, pp. 243 – 247.

Collins, F. and Zelenevitz, J., (1975), *'Influence of Sound on Separated Flow over Wings'*, AIAA Journal, Vol. 13 no. 3, pp. 408 – 410.

Crook A. and Wood, N. J., (2001), *'Measurements and Visualizations of Synthetic Jets'*, 39th AIAA Aerospace Sciences Meeting and Exhibit, Reno, NV, January 2001, AIAA paper 2001-0145.

Davis, S. A., Glezer, A., (1999), '*Mixing Control of Fuel Jets Using Synthetic Jet Technology*', 37th Aerospace Science Meeting, Reno, NV, AIAA paper 1999-0447.

Every, M.J., King, R. and Weaver, D.S., (1982), *'Vortex-Excited Vibrations of Cylinders and Cables and their Suppression'*, Ocean Engineering, Vol. 9, pp. 135 – 157.

Ffowcs-Williams, J. and Zhao, B., (1989), *'The Active Control of Vortex Shedding'*, Journal of Fluids and Structures, Vol. 3, pp. 115 – 122.

Fitzpatrick, J. and Nitti, F., (1997), *'Flow/Acoustic Interactions for Two Cylinders in Cross Flow'*, ASME Fluid-Structure Interaction, Aeroelasticity, FIV and Noise, Vol. 1, pp. 463 – 470.

Fujisawa, N., Kawaji, Y. and Ikemoto, K., (2001), *'Feedback Control of Vortex Shedding from a Circular Cylinder by Rotational Oscillations'*, Journal of Fluids and Structures, Vol. 15, pp. 23 – 37.

Gad-el-Hak, M., (1996), *'Modern Developments in Flow Control'*, Applied Mechanics Reviews, Vol. 49, pp. 365 – 379.

Gallas, Q., Holman, R., Nishida, T., Carroll, B., Sheplak, M., and Cattafesta, L., (2003a), *'Lumped Element Modeling of Piezoelectric-Driven Synthetic Jet Actuators'*, AIAA Journal, Vol. 41 no. 2, February 2003, pp. 240 – 247. (See also AIAA paper 2002-0125).

Gallas, Q., Wang, G., Papila, M., Sheplak, M. and Cattafesta, L., (2003b) *'Optimization of synthetic jet actuators'*, 41st AIAA Aerospace Sciences Meeting & Exhibit, Reno, NV, January 2003, AIAA paper 2003-0635.

Gilarranz, J. L. and Rediniotis, O.K., (2001), *'Compact, High-Power Synthetic Jet Actuators for Flow Separation Control'*, 39th AIAA Aerospace Sciences Meeting and Exhibit, Reno, NV, January 2001, AIAA paper 2001-0737.

Glezer, A. and Amitay, M., (2002), *'Synthetic Jets'*, Annual Review of Fluid Mechanics, Vol. 34, pp. 503 – 529.

Glezer, A., Allen, M. G., Coe, D. J., Smith, B. L., Trautman, M. A., Wiltse, J. W., (1998), *'Synthetic Jet Actuators and Applications Thereof'*, US Patent no. 5,758,823, June 1998.

Glezer, A., Allen, M. G., Coe, D. J., Smith, B. L., Trautman, M. A., Wiltse, J. W., (1999a), *'Synthetic Jet Actuators and Applications Thereof'*, US Patent no. 5,894,990, April 1999.

Glezer, A., Smith, B. L., (1999), *'Synthetic jet actuators for modifying the direction of fluid flows'*, US Patent no. 5,988,522, November 1999.

Glezer, A., Smith, B. L., Trautman, M. A., (1999b), *'Modifications of fluid flow about bodies and surfaces with synthetic jet actuators'*, US Patent no. 5,957,413, September 1999.

Glezer, A., Wiltse, J. W., (2000), *'Synthetic jet actuators for mixing applications'*, US Patent no. 6,056,204, May 2000.

Ho, C.M. and Tai, Y.C., (1998), *'Micro-Electro-Mechanical-Systems (MEMS) and Fluid Flows'*, Annual Review of Fluid Mechanics, Vol. 30, pp. 579 – 612.

Hsiao, F., and Shyu, J., (1991), *'Influence of Internal Acoustic Excitation Upon Flow Passing a Circular Cylinder'*, Journal of Fluids and Structures, Vol. 5, pp. 427 – 442.

Hsiao, F., Liu, C. and Shyu, J., (1990), *'Control of Wall-Separated Flow by Internal Acoustic Excitation'*, AIAA Journal, Vol. 28 no. 8, August 1990, pp. 1440 – 1446.

Huang, L. S., Maestrello, L. and Bryant, T. D., (1987), *'Separation Control over an Airfoil at High Angles of Attack by Sounding Emanating from the Surface'*, AIAA paper 87-1261.

Huang, X. Y. and Weaver, D.S., (1991), *'On the Active Control of Shear Layer Oscillations Across a Cavity in the Presence of Pipeline Acoustic Resonance'*, Journal of Fluids and Structures, Vol. 5, pp. 207 – 219.

Huang, X. Y. and Weaver, D.S., (1994), *'Control of Flow-Induced Fin Vibration by Anti-Sound'*, Journal of Sound and Vibration, Vol. 169 no. 3, pp. 428 – 432.

Huang, X. Y., (1995), *'Suppression of Vortex Shedding from a Circular Cylinder by Internal Acoustic Excitation'*, Journal of Fluids and Structures, Vol. 9, pp. 563 – 570.

Huang, X. Y., (1996), *'Feedback Control of Vortex Shedding from a Circular Cylinder'*, Experiments in Fluids, Vol. 20, pp. 218 – 224.

Igarashi, T., (1981), *'Characteristics of the Flow around Two Circular Cylinders Arranged in Tandem (1st Report)'*, Bulletin of the JSME, Vol. 24 no. 188, February 1981, pp. 323 – 331.

Igarashi, T., (1984), *'Characteristics of the Flow around Two Circular Cylinders Arranged in Tandem (2nd Report)'*, Bulletin of the JSME, Vol. 27 no. 233, November 1984, pp. 2380 – 2387.

Ingrad, U. and Labate S., (1950), *'Acoustic Circulation Effects and the Nonlinear Impedance of Orifices'*, Journal of the Acoustic Society of America, Vol. 22 no. 2, March 1950, pp. 211 – 218.

King, R., (1977) *'A Review of Vortex Shedding Research and its Applications'*, Ocean Engineering, Vol. 4, pp. 141 – 171.

Kwon, K. and Choi, H., (1996), *'Control of Laminar Vortex Shedding Behind a Circular Cylinder Using Splitter Plates'*, Physics of Fluids, Vol. 8 no. 2, February 1996, pp. 479 – 485.

Lebedeva, I. V., (1988), *'Experimental Study of Acoustic Streaming in the Vicinity of Orifices'*, Sov. Phs. Acoust., Vol. 26, p. 331.

Lienhard, J., (1988), *'Synopsis of Lift, Drag and Vortex Frequency Data for Rigid Circular Cylinders'*, Washington State University, College of Engineering, Research Division Bulletin 300.

Lin, J. C., Yang, Y. and Rockwell, D., (2002), *'Flow Past Two Cylinders in Tandem: Instantaneous and Averaged Flow Structure'*, Journal of Fluids and Structures, Vol. 16 no. 8, pp. 1059 – 1071.

Mahbub Alam, Md., Moriya, M., Takai, K. and Sakamoto, H., (2003), *'Fluctuating Fluid Forces Acting on two Circular Cylinders in a Tandem Arrangement at a Subcritical Reynolds Number'*, Journal of Wind Engineering and Industrial Aerodynamics, Vol. 91, pp. 139 – 154.

Mallinson, S.G., Reizes, J.A., Hong, G. and Buttini, M., (1999), *'Synthetic Jets for Flow Control'*, In: Proceedings of the SPIE Asia/Pacific Symposium on Microelectronics and MEMS, Gold Coast, Australia, October 1999.

Matsumoto, M., (1999), 'Vortex Shedding of Bluff Bodies: A Review', Journal of Fluids and Structures, Vol. 13, pp. 791 – 811.

McCormick, D.C., (2000), *'Boundary Layer Separation Control with Directed Synthetic Jets'*, 38th Aerospace Sciences Meeting, Reno, NV, January 2000, AIAA paper 2000-0519.

Medinkov, E. P. and Novitskii B. G., (1975), *'Experimental Study of Intense Acoustic Streaming'*, Sov. Phys. Acoust., Vol. 21, p. 152.

Miller, R. M., Tunkel, R. N., (2000), *'Vibration-driven acoustic jet controlling boundary layer separation'*, US Patent no. 6,109,566, August 2000.

Mittal, R., Rampunggoon, P. and Udaykumar, H. S., (2001), *'Interaction of a synthetic Jet with a plate Boundary Layer'*, 31st AIAA Fluid Dynamics Conference & Exhibit, Anaheim, CA, June 2001, AIAA paper 2001-2773.

Mittal, R., Rampunggoon, P., (2002), *'Brief Communications: On the Virtual Aeroshaping Effect of Synthetic Jets'*, Physics of Fluids, Vol. 14 no. 4, pp. 1533 – 1536.

Okajima, A., (1979), *'Flows around Two Tandem Circular Cylinders at Very High Reynolds Numbers'*, Bulletin of the JSME, Vol. 22 no. 166, April 1979, pp. 504 – 511.

Peterka, J. and Richardson, P., (1969), *'Effects of Sound on Separated Flows'*, Journal of Fluid Mechanics, Vol. 37, pp. 265 – 287.

Rediniotis, O.K., Ko, J., Yue, X. and Kurdila, A. J., (1999), *'Synthetic Jets, their Reduced-Order Flow Modeling and Applications to Flow Control'*, 37th AIAA Aerospace Sciences Meeting and Exhibit, Reno, NV, January 1999, AIAA paper 99-1000.

Rogers, A. C., (1983), *'An Assessment of Vortex Shedding Suppression Devices for Production Risers and Towed Deep Ocean Pipe Strings'*, Paper 4594, 15th Annual Offshore Technology Conference, Huston, Texas.

Roussopoulos, K., (1993), *'Feedback Control of Vortex Shedding at Low Reynolds Numbers'*, Journal of Fluid Mechanics, Vol. 248, pp. 267 – 296.

Sarpkaya, T., (1979), *'Vortex-Induced Oscillations'*, Journal of Applied Mechanics, Vol. 46, pp. 241 – 257.

Schumm, M., Berger, E and Monkewitz, P., (1994), *'Self-Excited Oscillations in the Wake of Two-Dimensional Bluff Bodies and their Control'*, Journal of Fluid Mechanics, Vol. 271, pp. 17 – 53.

Smith, B. L. and Glezer, A., (1994), *'Vectoring a High Aspect Ratio Rectangular Air Jet Using a Zero-net-mass-flux Control Jet'*, Bull. Am. Phys. Soc., Vol. 39, p. 1894.

Smith, B. L. and Glezer, A., (1997), *'Vectoring and Small-Scale Motions Effected in Free Shear Flows Using Synthetic Jet Actuators'*, AIAA paper 97-0213.

Smith, B. L. and Glezer, A., (1998), *'The Formation and Evolution of Synthetic Jets'*, Physics of Fluids, Vol. 10 no. 9, pp. 2281 – 2297.

Smith, B. L. and Glezer, A., (2002), *'Jet Vectoring Using Synthetic Jets'*, Journal of Fluid Mechanics, Vol. 458, pp. 1 – 34.

Smith, B. L., Swift, G. W., (2001), *'Synthetic Jets at Large Reynolds Number and Comparison to Continuous Jets'*, 31st AIAA Fluid Dynamics Conference, AIAA paper 2001-3030.

Smith, B. L., Swift, G. W., (2003), *'A Comparison Between Synthetic Jets and Continuous Jets'*, Experiments in Fluids, Vol. 34 no. 4, April 2003, pp. 467 – 472.

Smith, D. R., Amitay, M., Kibens, V., Parekh, D. E. and Glezer, A., (1998), *'Modification of Lifting Body Aerodynamics Using Synthetic Jet Actuators'*, 36th AIAA Aerospace Science Meeting, Reno, NV, AIAA paper 19998-0209.

Tokumaru, P. and Dimotakis, P., (1991), *'Rotary Oscillation Control of a Cylinder Wake'*, Journal of Fluid Mechanics, Vol. 224, pp. 77 – 90.

Utturkar, Y., Holman, R., Mittal, R., Carroll, B., Sheplak, M., and Cattafesta, L., (2003), *'A Jet Formation Criterion for Synthetic Jet Actuators'*, 41st Aerospace Sciences Meeting & Exhibit, Reno, NV, January 2003, AIAA paper 2003-0636.

Utturkar, Y., Mittal, R., Rampunggoon, P. and Cattafesta, L., (2002), *'Sensitivity of Synthetic Jets to the Design of the Jet Cavity'*, 40th AIAA Aerospace Sciences Meeting & Exhibit, Reno, NV, January 2002, AIAA paper 2002-0124.

Warui, H. and Fujisawa, N., (1996), *'Feedback Control of Vortex Shedding from a Circular Cylinder by Cross-Flow Cylinder Oscillations'*, Experiments In Fluids, Vol. 21, pp. 49 – 56.

Wolfe, D., (2000), *'Feedback Control of Vortex Shedding From Two Tandem Cylinders'*, Master of Engineering Thesis, McMaster University, Hamilton, ON.

Wolfe, D., Ziada, S., (2003), *'Feedback Control of Vortex Shedding from Two Tandem Cylinders'*, Journal of Fluids and Structures, Vol. 17, pp. 579 – 592.

Zaman, K., Bar-Sever, A. and Mangalam, S., (1987), *'Effect of Acoustic Excitation on the Flow over a Low-Re Airfoil'*, Journal of Fluid Mechanics, Vol. 182, pp. 127 – 148.

Zdravkovich, M. M., (1977), *'Review of Flow Interference between Two Circular Cylinders in Various Arrangements'*, Transactions of the ASME: Journal of Fluids Engineering, Vol. 99, pp. 618 – 633.

Zdravkovich, M. M., (1981), *'Review and Classification of Various Aerodynamic and Hydrodynamic Means for Suppressing Vortex Shedding'*, Journal of Wind Engineering and Industrial Aerodynamics, Vol. 7, pp. 145 – 189.

Zdravkovich, M. M., (1985), *'Flow Induced Oscillations of Two Interfering Circular Cylinders'*, Journal of Sound and Vibration, Vol. 101 no. 4, pp. 511 – 521.

Zdravkovich, M. M., (1987), *'The Effects of Interference between Circular Cylinders in Cross Flow'*, Journal of Fluids and Structures, Vol. 1, pp. 239 – 261.

Zdravkovich, M. M., (1997), *'Flow around Circular Cylinders, Vol. 1: Fundamentals'*, Oxford University Press, New York.

Ziada, S., (1995), *'Feedback Control of Globally Unstable Flows: Impinging Shear Flows'*, Journal of Fluids and Structures, Vol. 9, pp. 907 – 923.

Ziada, S., (1999), *'Feedback Control of Global Flow Oscillations'*, Engineering Mechanics, Vol. 6 no. 4/5, pp. 337 – 354.

APPENDIX A

The manufacturer's data sheet for the speakers used is shown below.

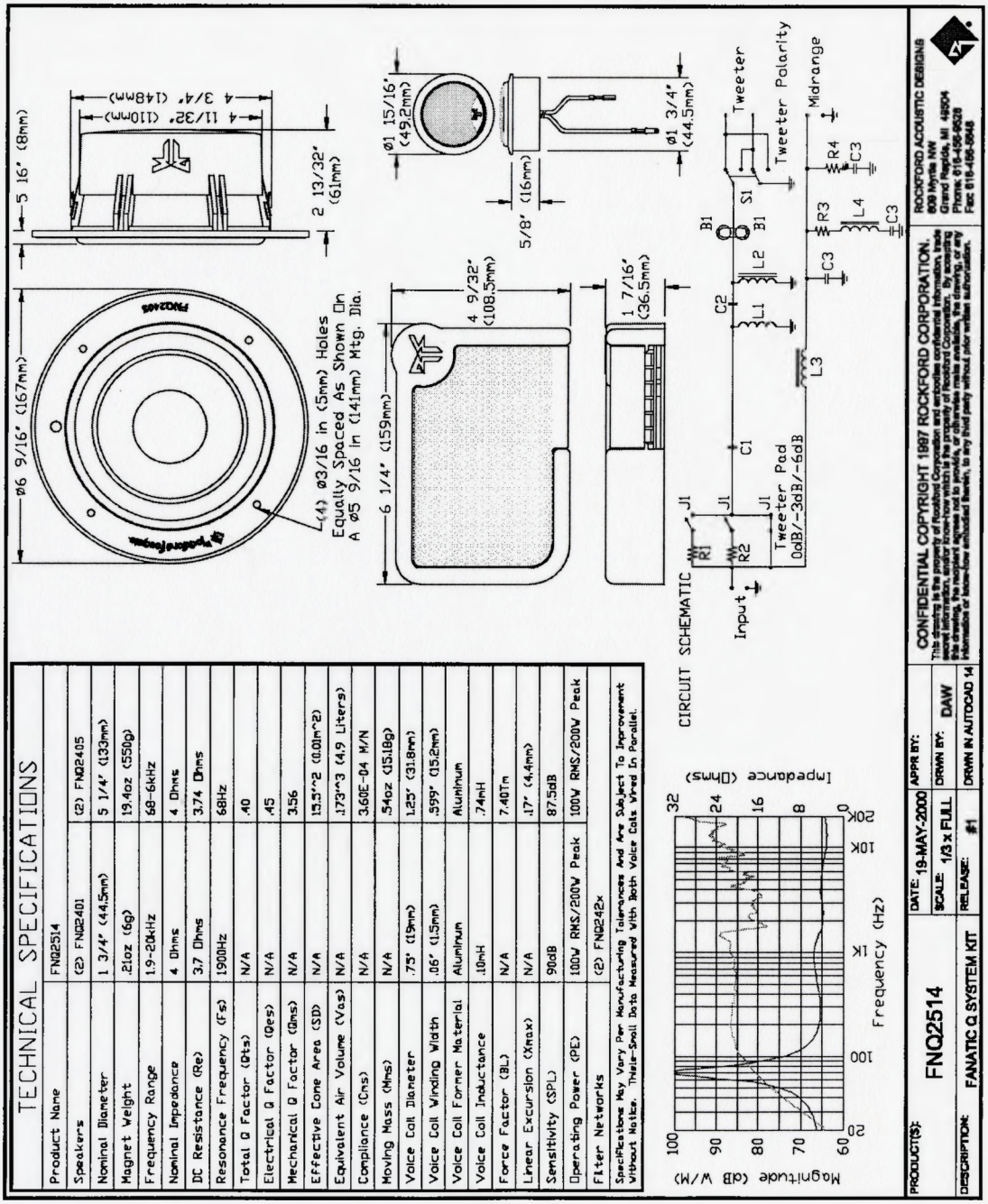

APPENDIX B

Calibration curves obtained for the hotwires used are provided in this appendix. The figure shows the calibration curves obtained for different calibration temperatures for the two hotwires used. During the time the experiments were performed, an air conditioning was installed in the room containing the wind tunnel and the temperature was fixed at 21 °C for the rest of the experiments.

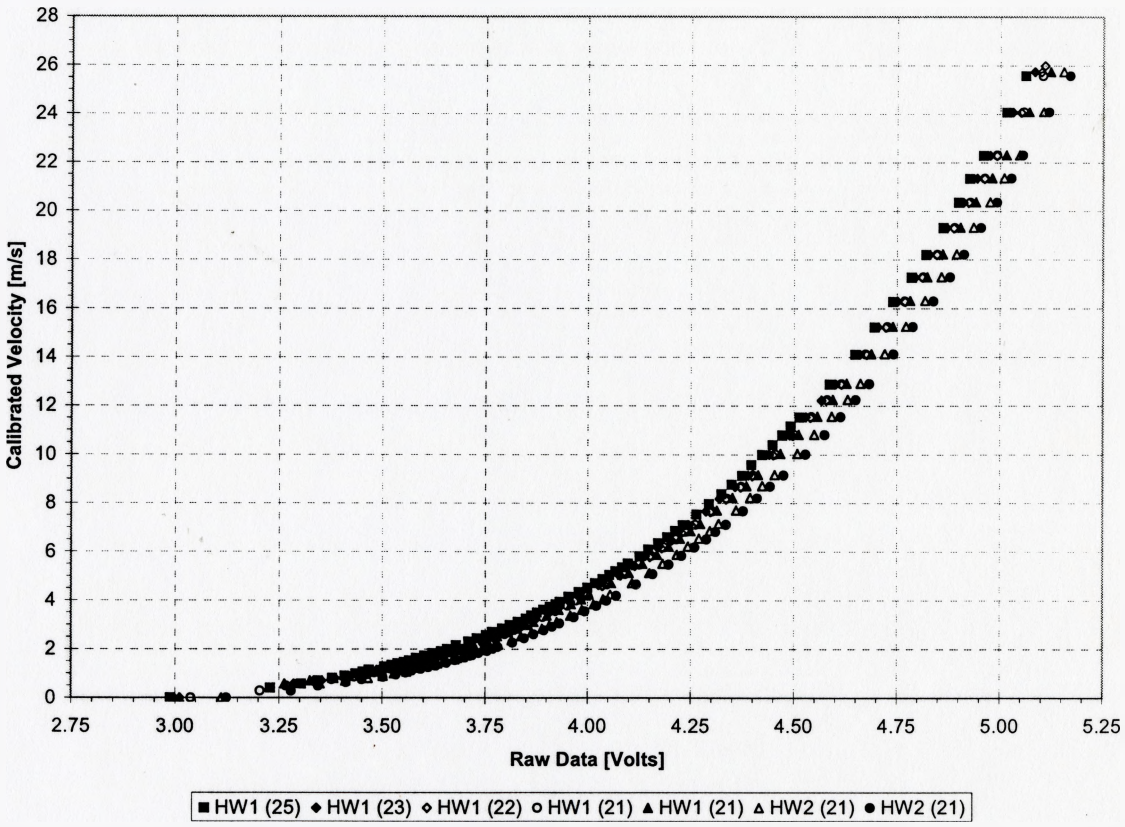

Figure B.1. Hotwire calibration data obtained for the two hotwires used in the experiments at different calibration temperatures. [Temperatures are shown between brackets]

APPENDIX C

This appendix shows the calibration data for the strain gages used to measure the vibration signal of the downstream cylinder. The calibration method is discussed in section 4.3.3. The figure shows the data obtained for the lift force calibration as well as the data obtained for the application of horizontal forces to simulate the drag on the cylinder.

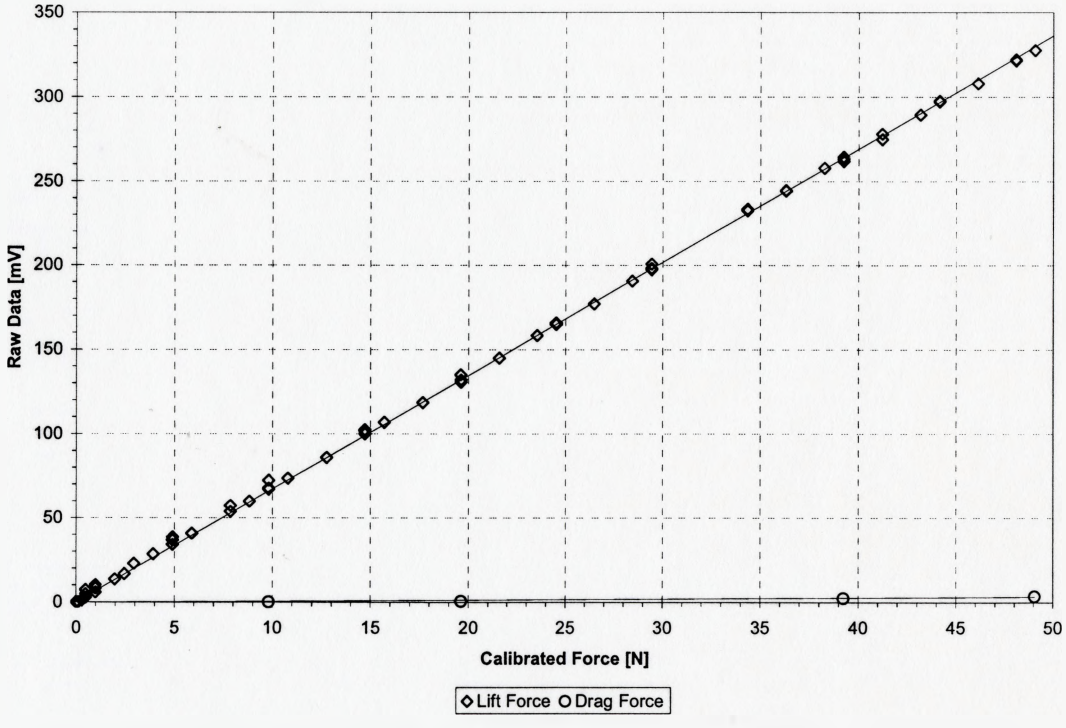

Figure C.1. Calibration data for the strain gages.

APPENDIX D

This appendix contains the power spectra of the hotwire signal and plots of the coherence between the hotwire and the strain gage signals used in Chapter 6 for the measurements concerning the effect of the synthetic jet on the flow in Section 6.3.3.

D.1. SHORT SLIT CYLINDER

Figures are shown for different spanwise positions for each downstream location. Measurement and positioning details are discussed in Section 6.3.3.

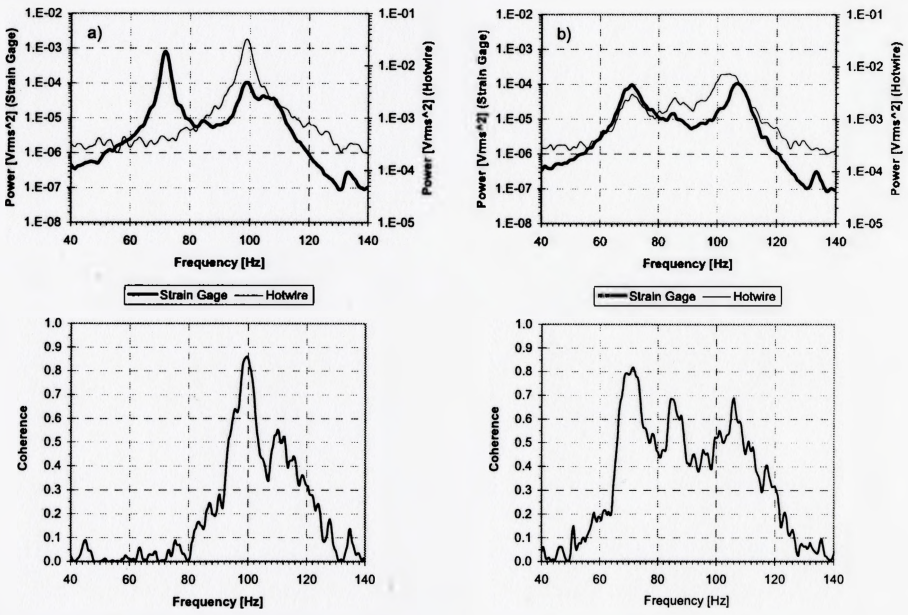

Figure D.1. Power spectra of and coherence between the strain gage and hotwire signals at X/D=0 and Z/D=0 for the short slit case. a) No Control. b) Optimal Control.

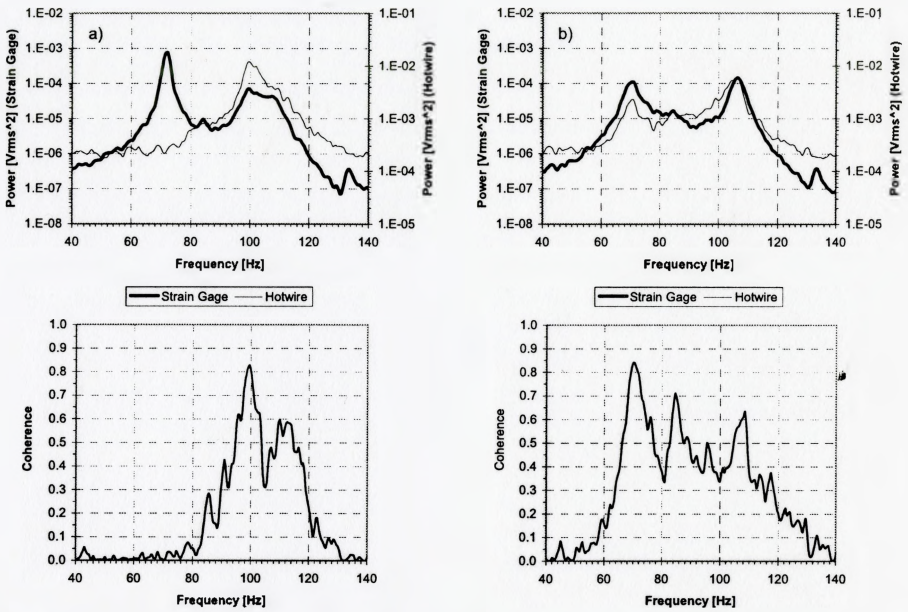

Figure D.2.Power spectra of and coherence between the strain gage and hotwire signals at X/D=0 and Z/D=1 for the short slit case. a) No Control. b) Optimal Control.

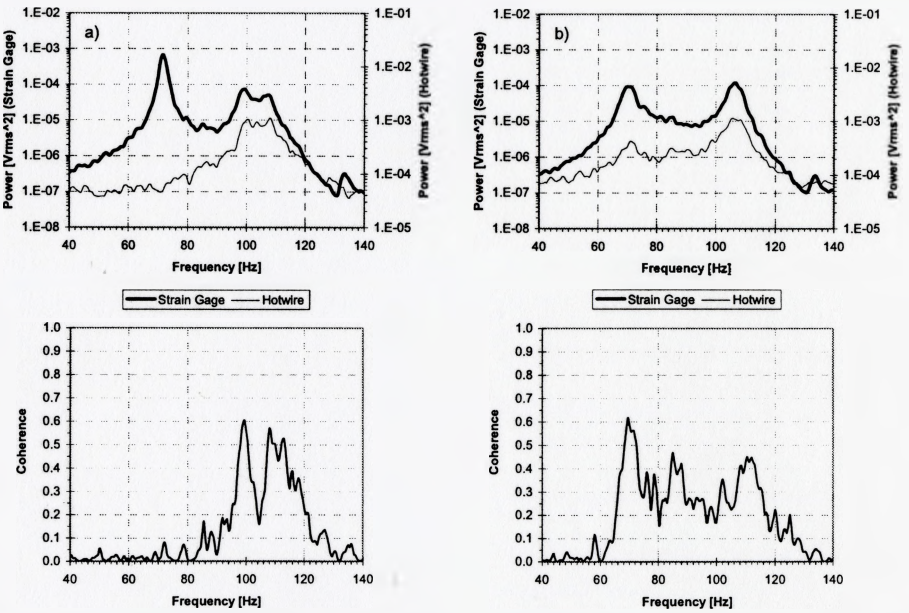

Figure D.3.Power spectra of and coherence between the strain gage and hotwire signals at X/D=0 and Z/D=2 for the short slit case. a) No Control. b) Optimal Control.

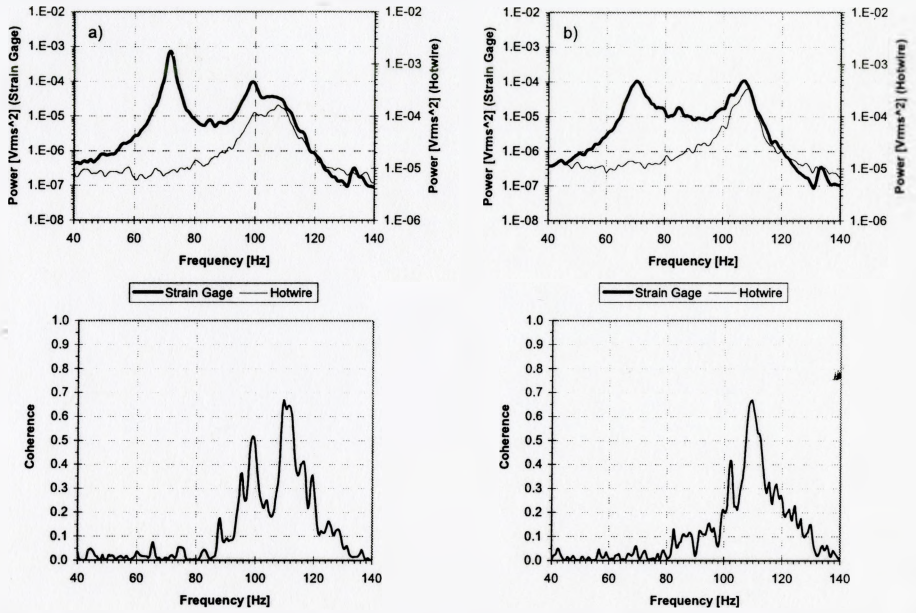

Figure D.4.Power spectra of and coherence between the strain gage and hotwire signals at X/D=0 and Z/D=3 for the short slit case. a) No Control. b) Optimal Control.

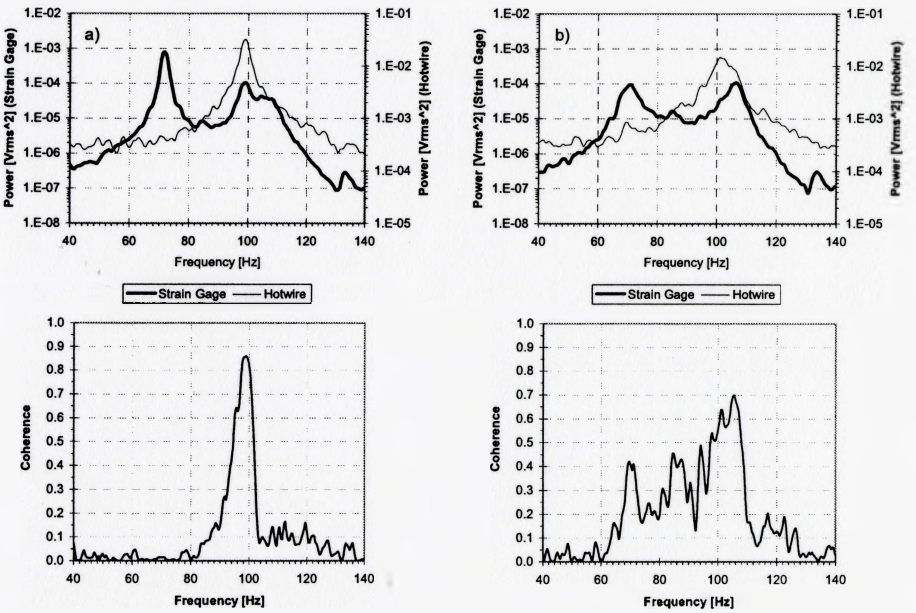

Figure D.5.Power spectra of and coherence between the strain gage and hotwire signals at X/D=0.625 and Z/D=0 for the short slit case. a) No Control. b) Optimal Control.

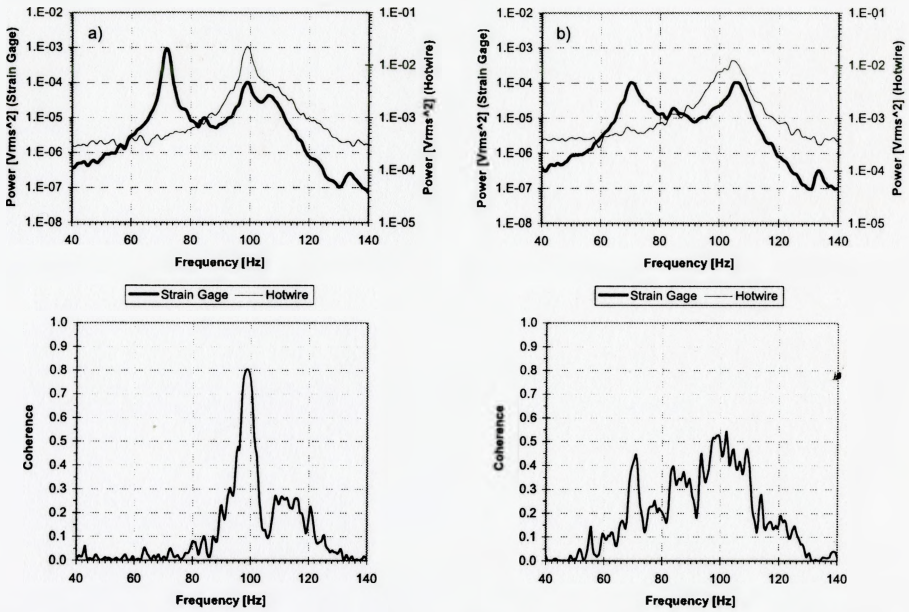

Figure D.6.Power spectra of and coherence between the strain gage and hotwire signals at X/D=0.625 and Z/D=1 for the short slit case. a) No Control. b) Optimal Control.

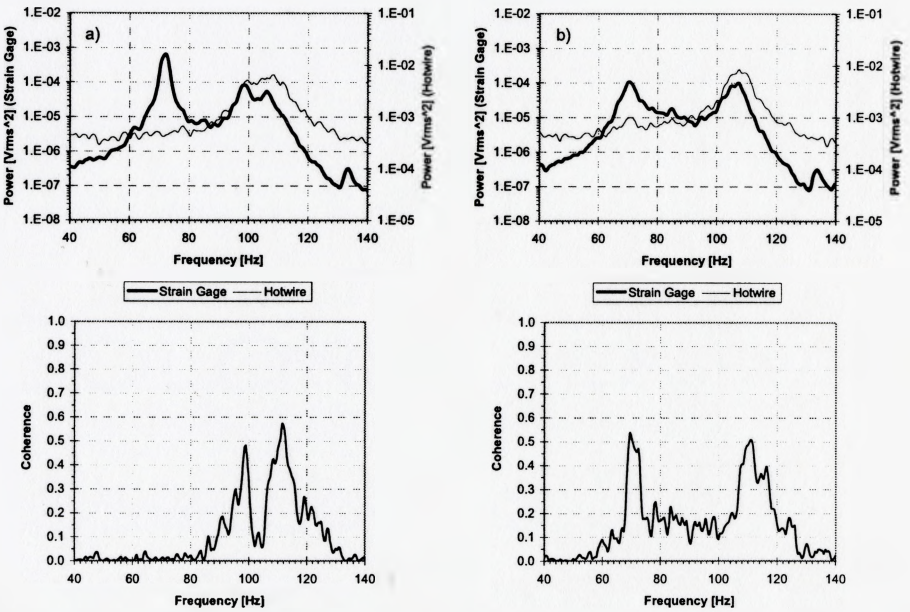

Figure D.7.Power spectra of and coherence between the strain gage and hotwire signals at X/D=0.625 and Z/D=2 for the short slit case. a) No Control. b) Optimal Control.

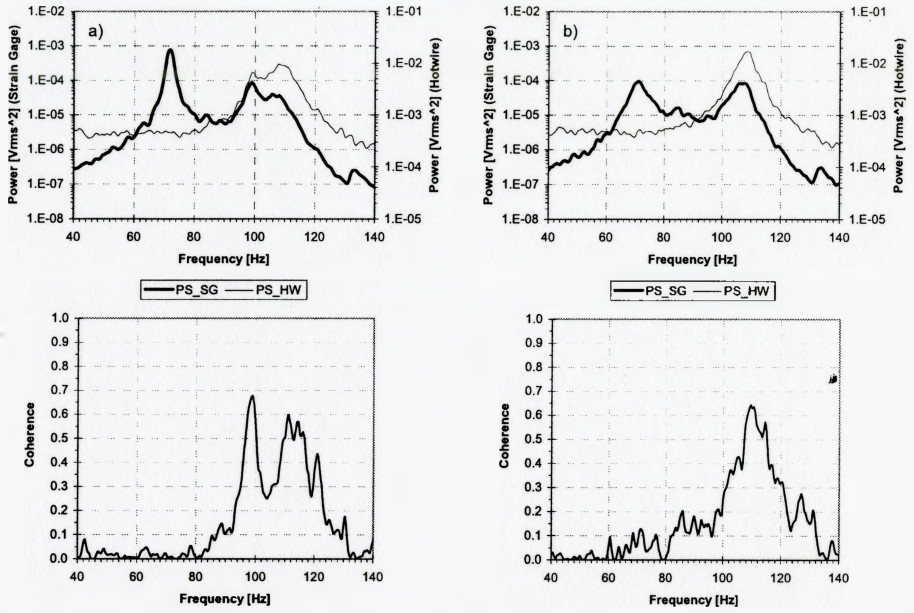

Figure D.8.Power spectra of and coherence between the strain gage and hotwire signals at X/D=0.625 and Z/D=3 for the short slit case. a) No Control. b) Optimal Control.

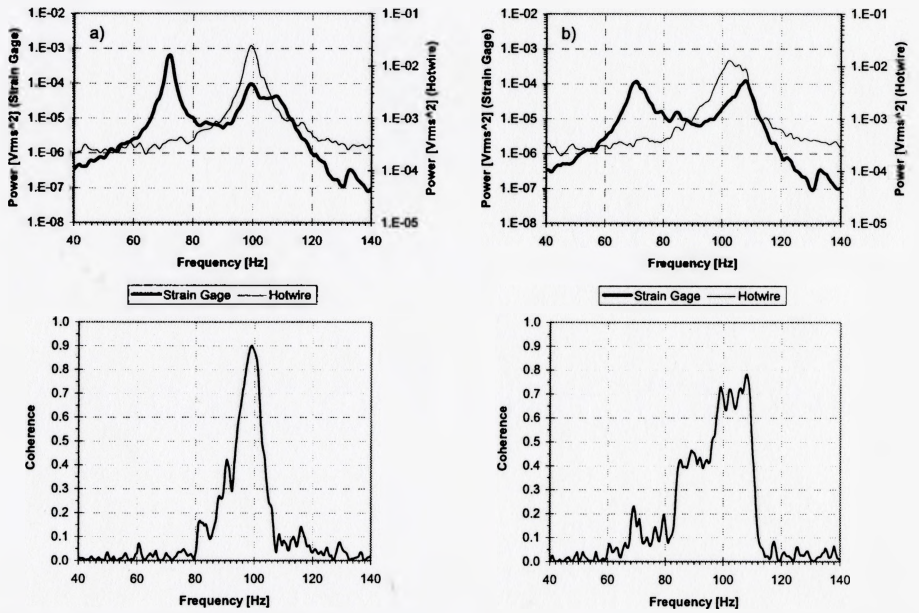

Figure D.9.Power spectra of and coherence between the strain gage and hotwire signals at X/D=0.1.25 and Z/D=0 for the short slit case. a) No Control. b) Optimal Control.

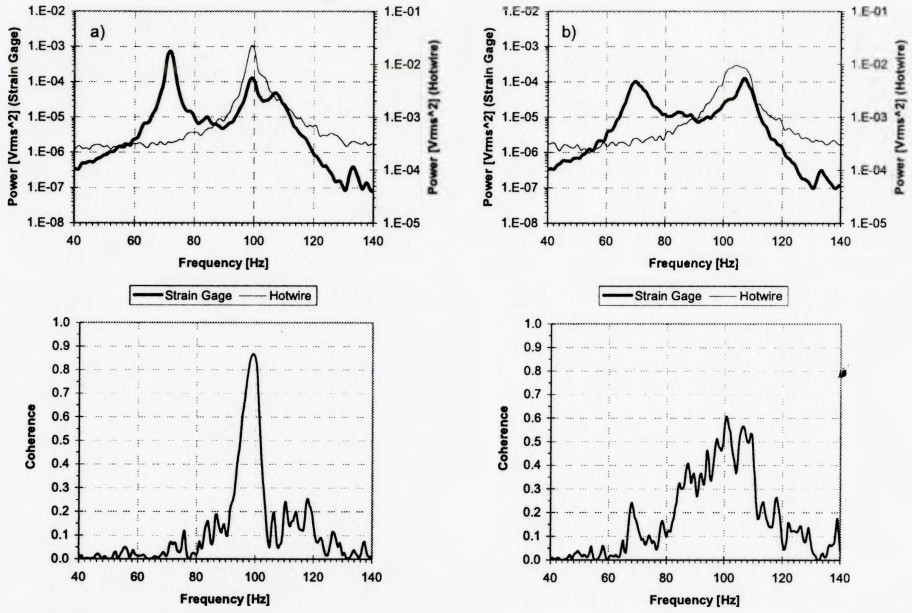

Figure D.10.Power spectra of and coherence between the strain gage and hotwire signals at X/D=1.25 and Z/D=1 for the short slit case. a) No Control. b) Optimal Control.

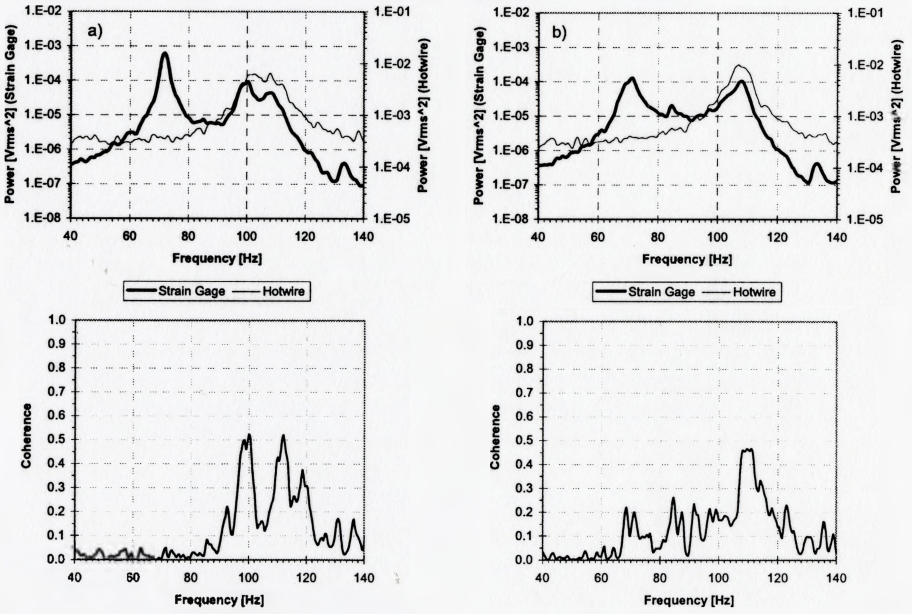

Figure D.11.Power spectra of and coherence between the strain gage and hotwire signals at X/D=1.25 and Z/D=2 for the short slit case. a) No Control. b) Optimal Control.

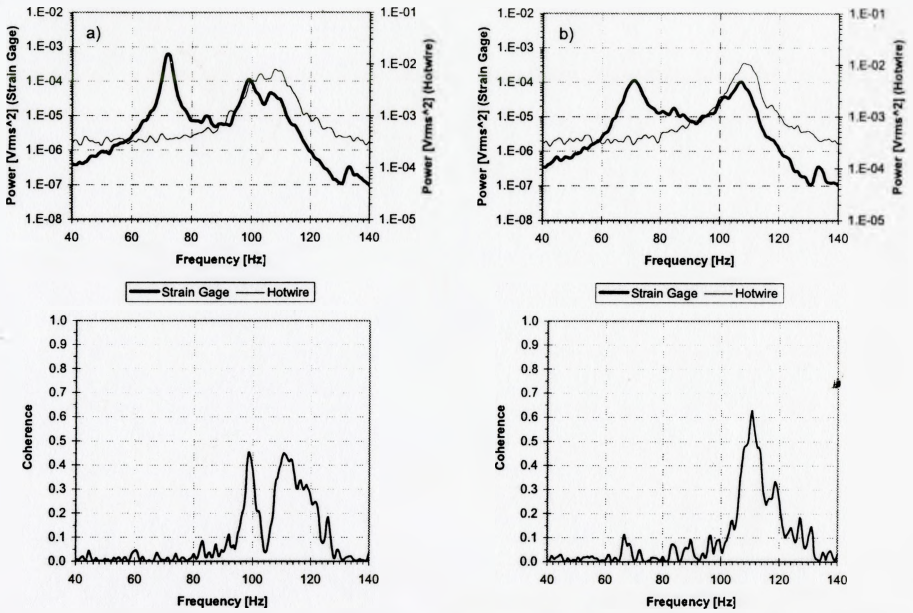

Figure D.12.Power spectra of and coherence between the strain gage and hotwire signals at *X/D*=1.25 and *Z/D*=3 for the short slit case. a) No Control. b) Optimal Control.

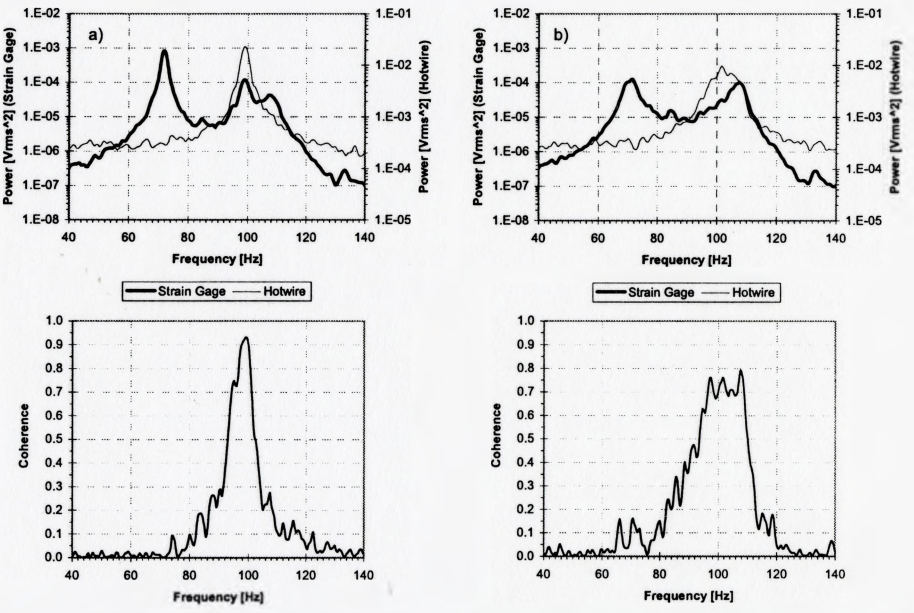

Figure D.13.Power spectra of and coherence between the strain gage and hotwire signals at *X/D*=1.875 and *Z/D*=0 for the short slit case. a) No Control. b) Optimal Control.

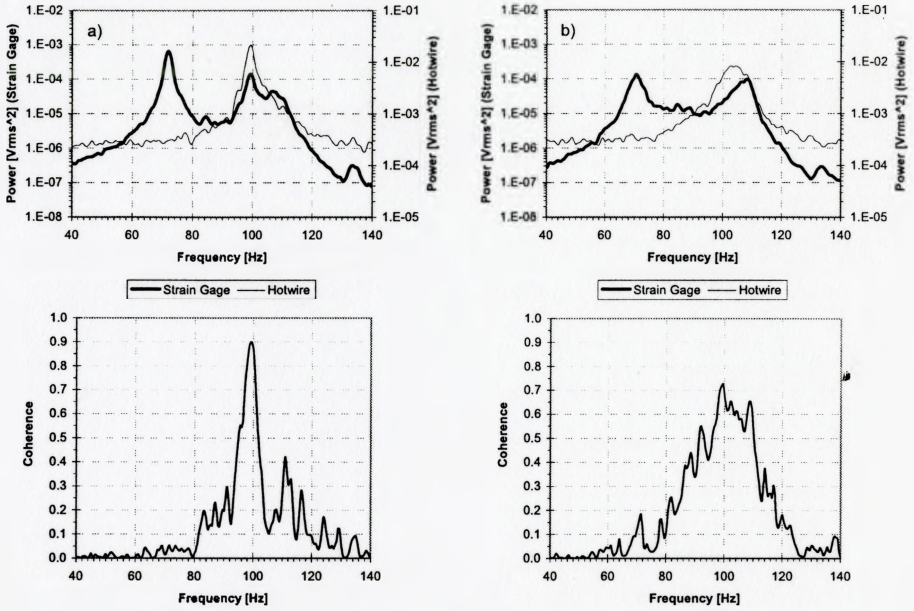

Figure D.14.Power spectra of and coherence between the strain gage and hotwire signals at X/D=1.875 and Z/D=1 for the short slit case. a) No Control. b) Optimal Control.

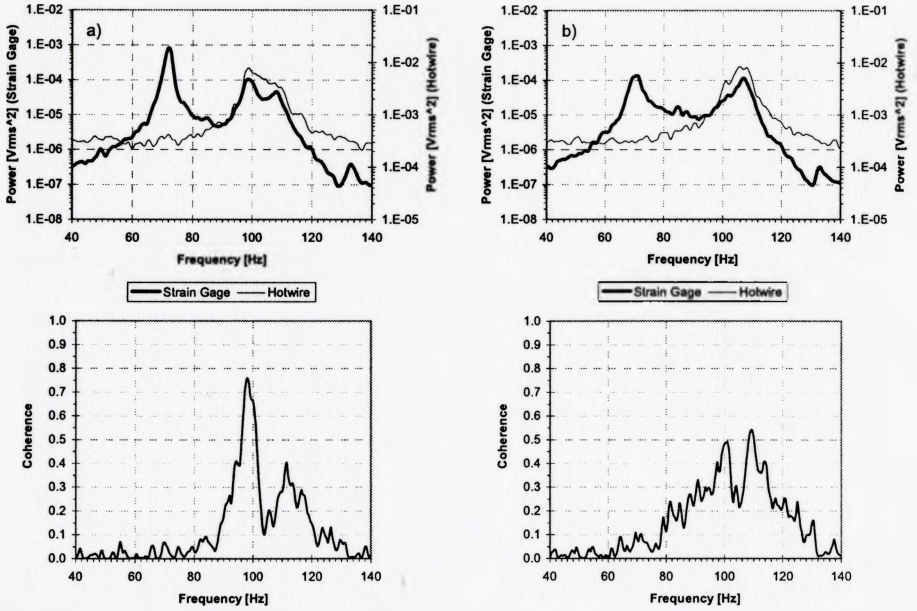

Figure D.15.Power spectra of and coherence between the strain gage and hotwire signals at X/D=1.875 and Z/D=2 for the short slit case. a) No Control. b) Optimal Control.

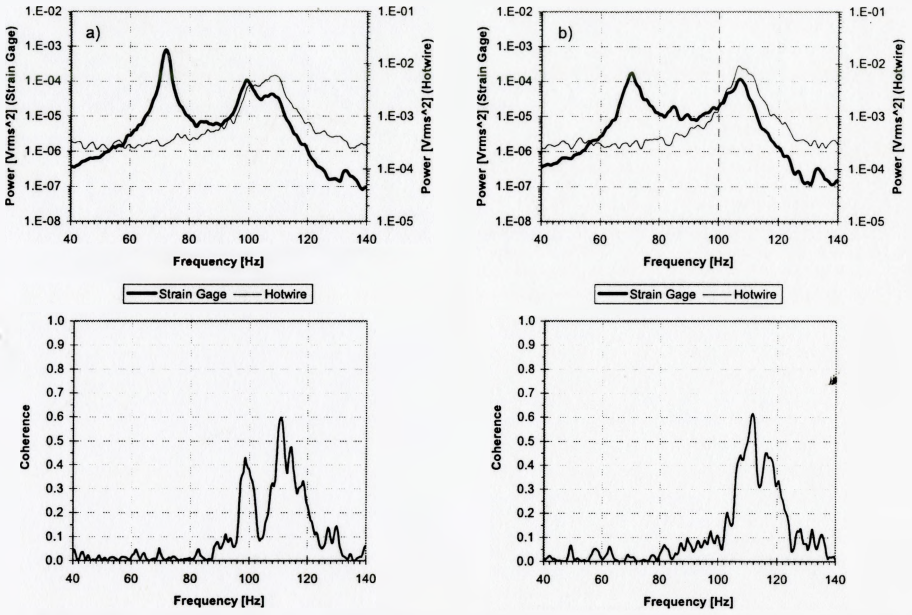

Figure D.16.Power spectra of and coherence between the strain gage and hotwire signals at X/D=1.875 and Z/D=3 for the short slit case. a) No Control. b) Optimal Control.

D.2. LONG SLIT CYLINDER

Figures are shown for different spanwise positions for each downstream location. Measurement and positioning details are discussed in Section 6.3.3.

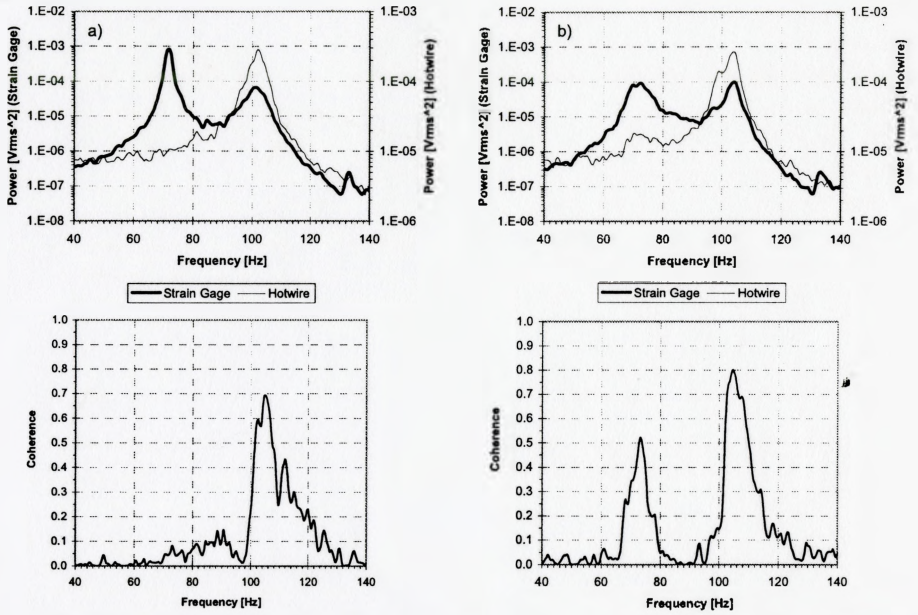

Figure D.17. Power spectra of and coherence between the strain gage and hotwire signals at X/D=0 and Z/D=0 for the long slit case. a) No Control. b) Optimal Control.

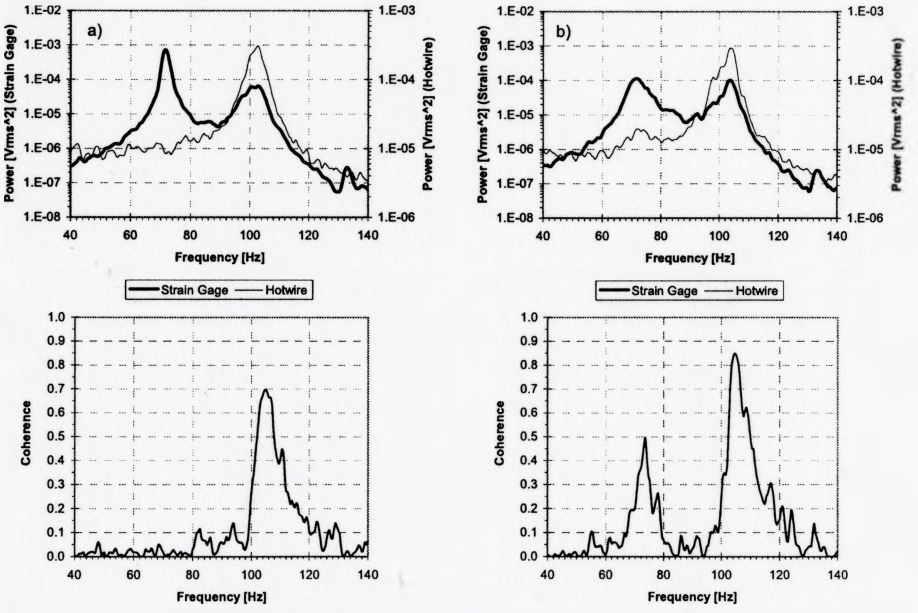

Figure D.18. Power spectra of and coherence between the strain gage and hotwire signals at X/D=0 and Z/D=1.25 for the long slit case. a) No Control. b) Optimal Control.

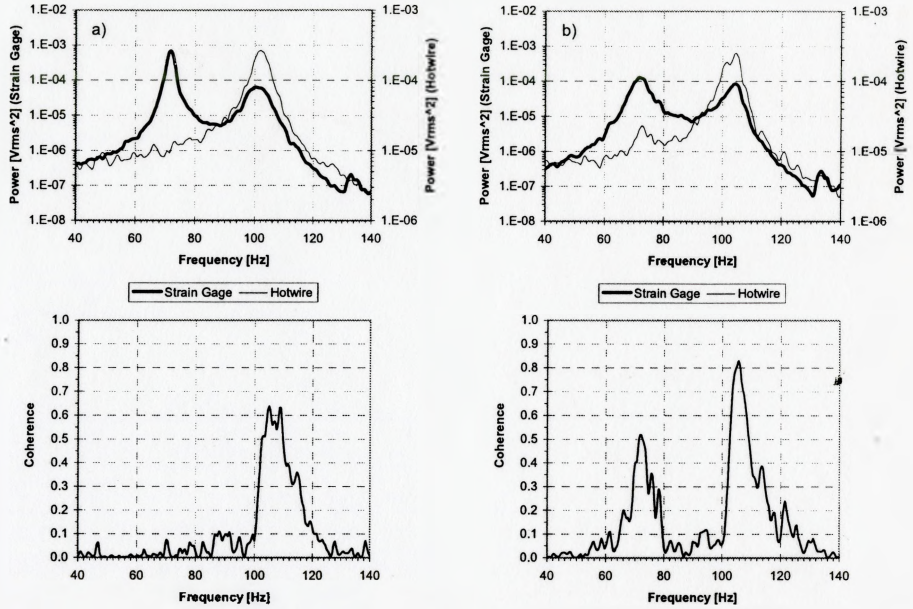

Figure D.19. Power spectra of and coherence between the strain gage and hotwire signals at X/D=0 and Z/D=2.5 for the long slit case. a) No Control. b) Optimal Control.

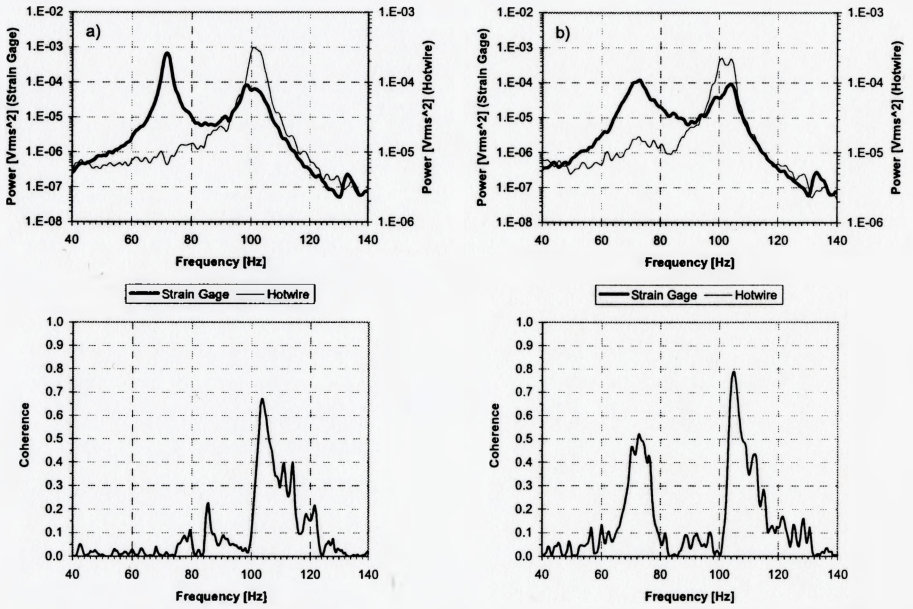

Figure D.20. Power spectra of and coherence between the strain gage and hotwire signals at X/D=0 and Z/D=3.75 for the long slit case. a) No Control. b) Optimal Control.

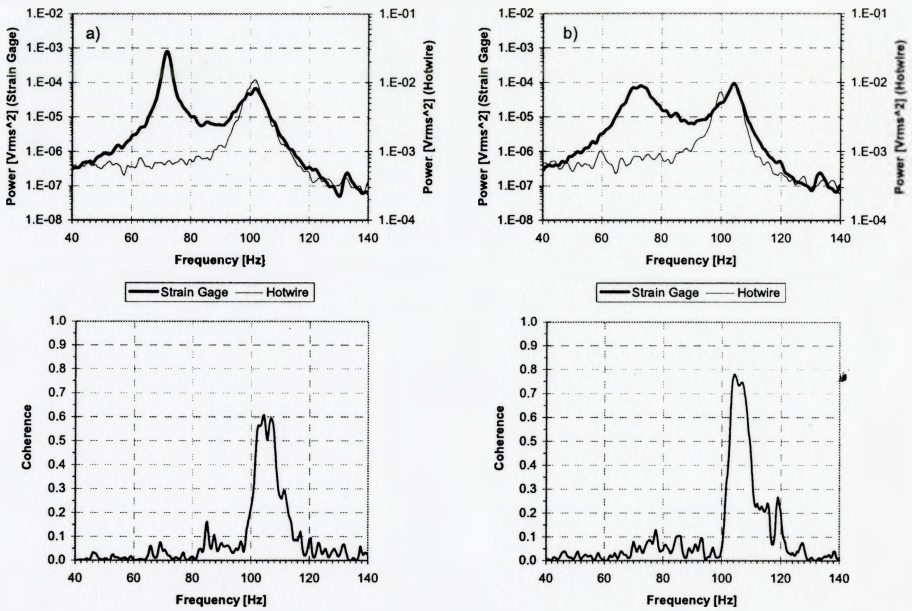

Figure D.21. Power spectra of and coherence between the strain gage and hotwire signals at X/D=0.625 and Z/D=0 for the long slit case. a) No Control. b) Optimal Control.

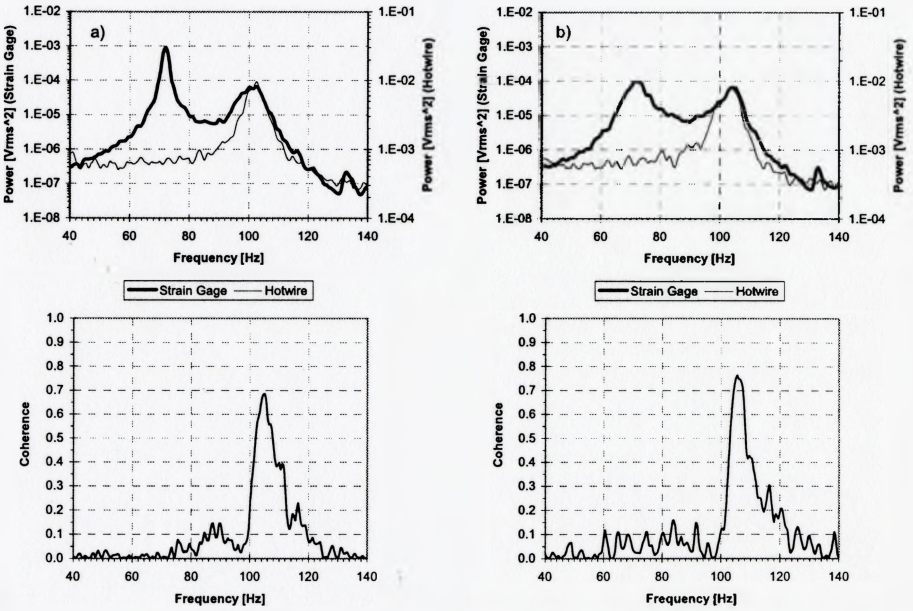

Figure D.22. Power spectra of and coherence between the strain gage and hotwire signals at X/D=0.625 and Z/D=1.25 for the long slit case. a) No Control. b) Optimal Control.

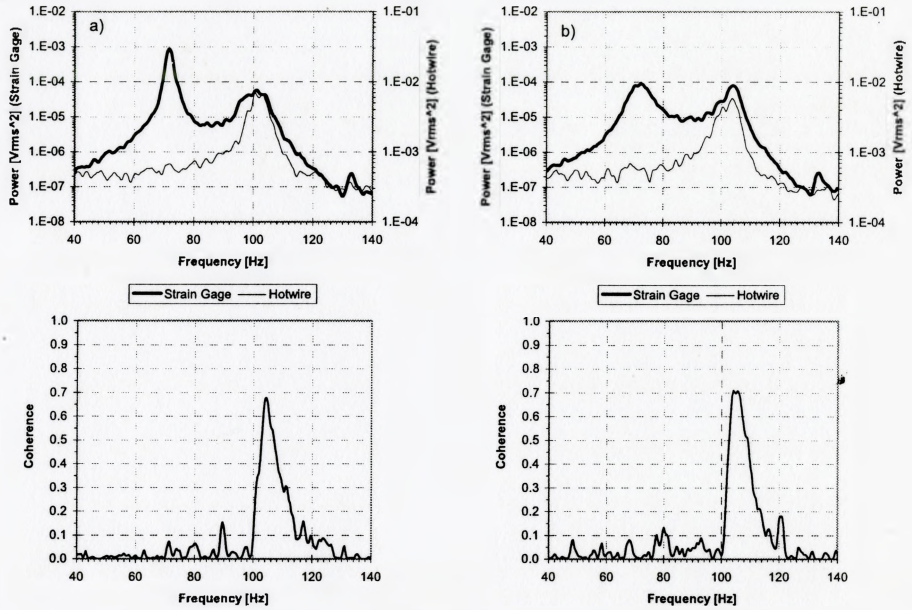

Figure D.23. Power spectra of and coherence between the strain gage and hotwire signals at X/D=0.625 and Z/D=2.5 for the long slit case. a) No Control. b) Optimal Control.

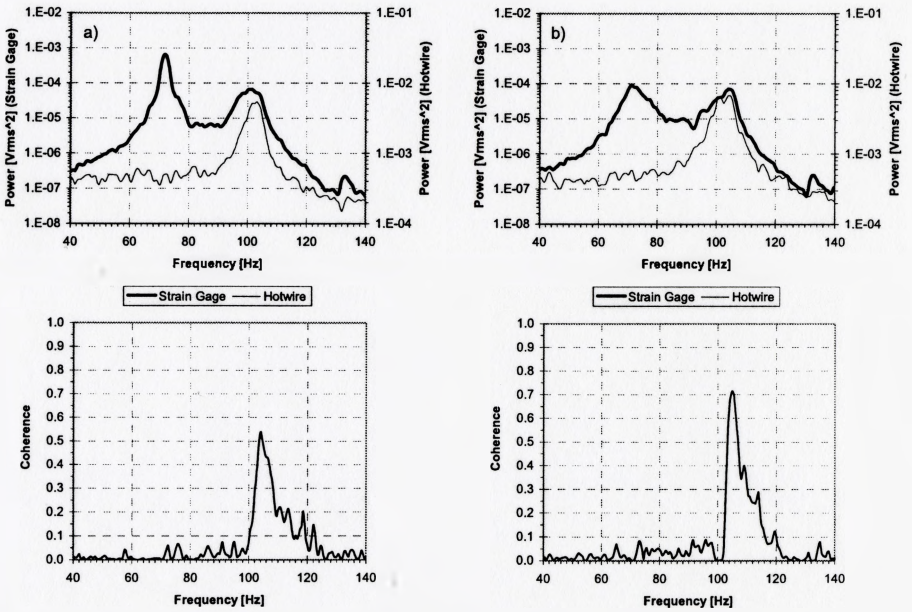

Figure D.24. Power spectra of and coherence between the strain gage and hotwire signals at X/D=0.625 and Z/D=3.75 for the long slit case. a) No Control. b) Optimal Control.

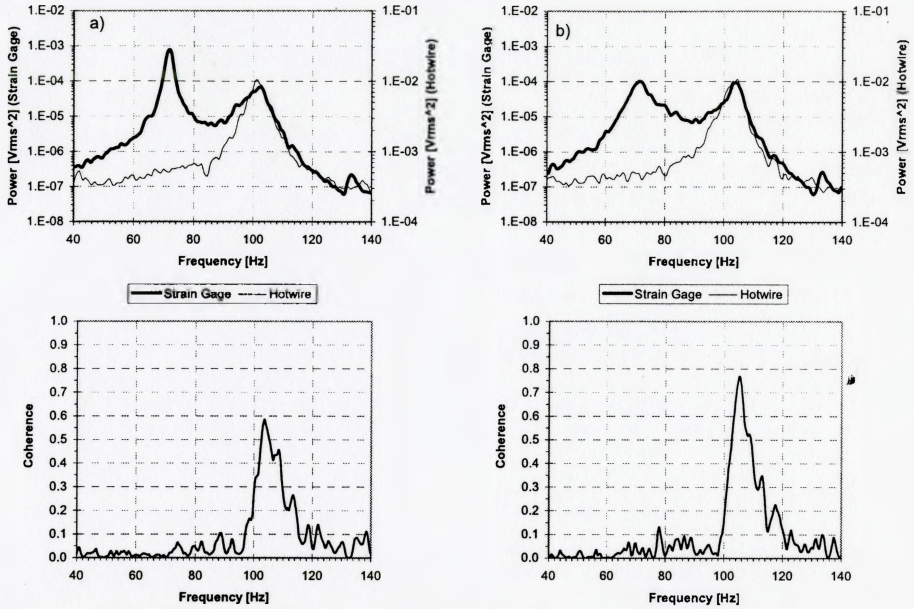

Figure D.25. Power spectra of and coherence between the strain gage and hotwire signals at X/D=1.25 and Z/D=0 for the long slit case. a) No Control. b) Optimal Control.

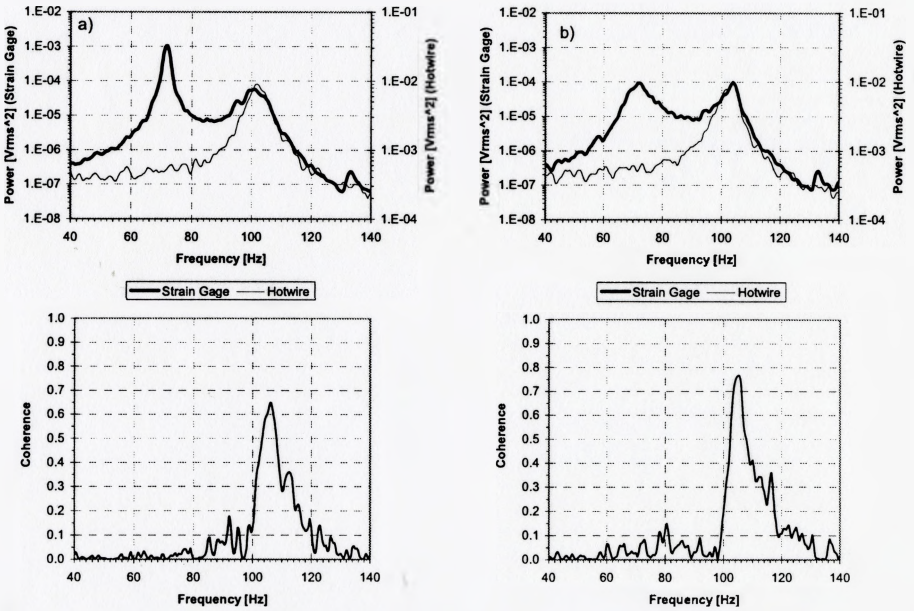

Figure D.26. Power spectra of and coherence between the strain gage and hotwire signals at X/D=1.25 and Z/D=1.25 for the long slit case. a) No Control. b) Optimal Control.

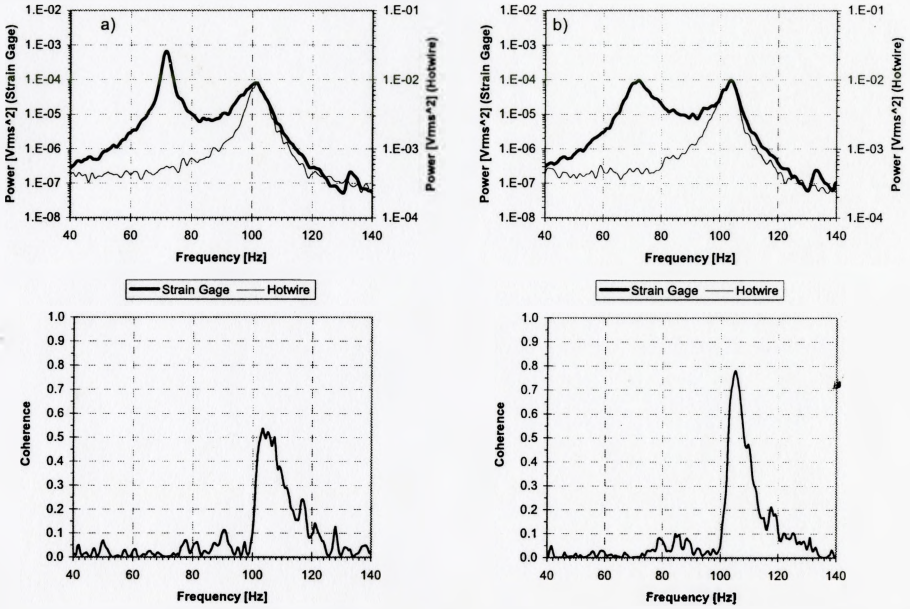

Figure D.27. Power spectra of and coherence between the strain gage and hotwire signals at X/D=1.25 and Z/D=2.5 for the long slit case. a) No Control. b) Optimal Control.

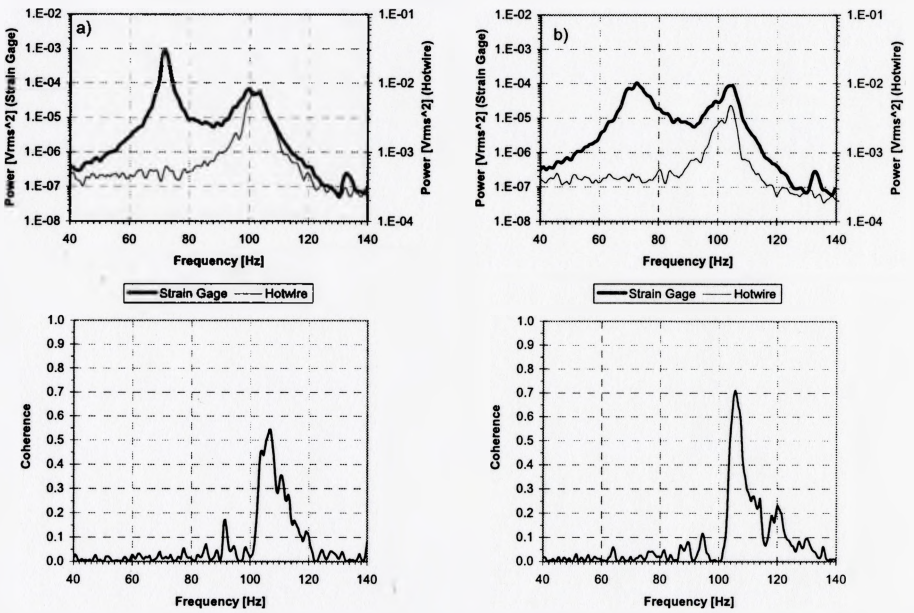

Figure D.28. Power spectra of and coherence between the strain gage and hotwire signals at X/D=1.25 and Z/D=3.75 for the long slit case. a) No Control. b) Optimal Control.

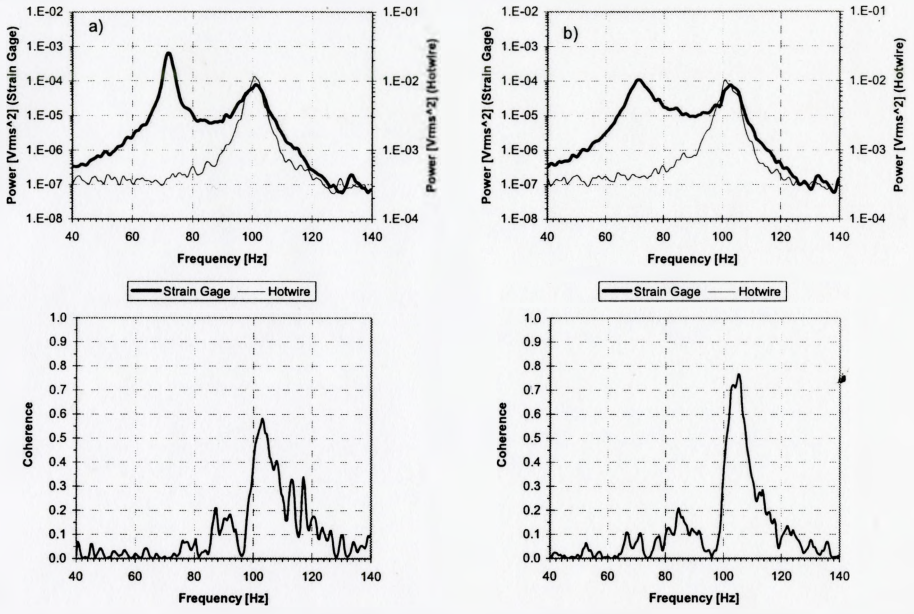

Figure D.29. Power spectra of and coherence between the strain gage and hotwire signals at X/D=1.875 and Z/D=0 for the long slit case. a) No Control. b) Optimal Control.

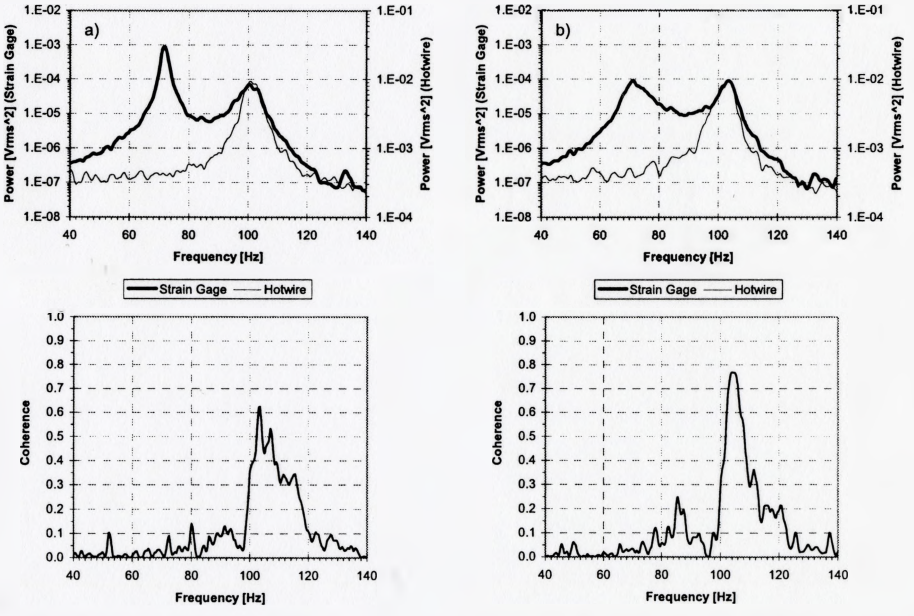

Figure D.30. Power spectra of and coherence between the strain gage and hotwire signals at X/D=1.875 and Z/D=1.25 for the long slit case. a) No Control. b) Optimal Control.

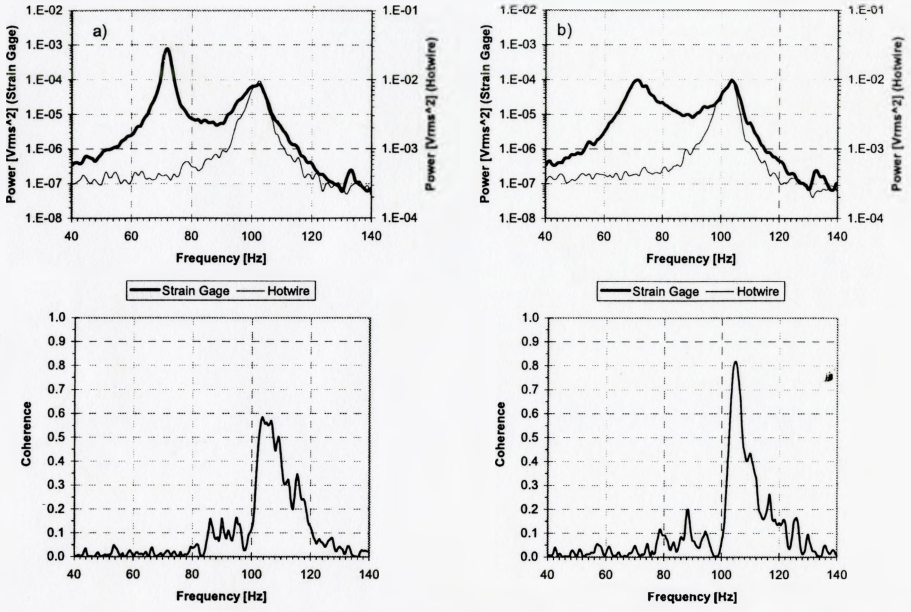

Figure D.31. Power spectra of and coherence between the strain gage and hotwire signals at X/D=1.875 and Z/D=2.5 for the long slit case. a) No Control. b) Optimal Control.

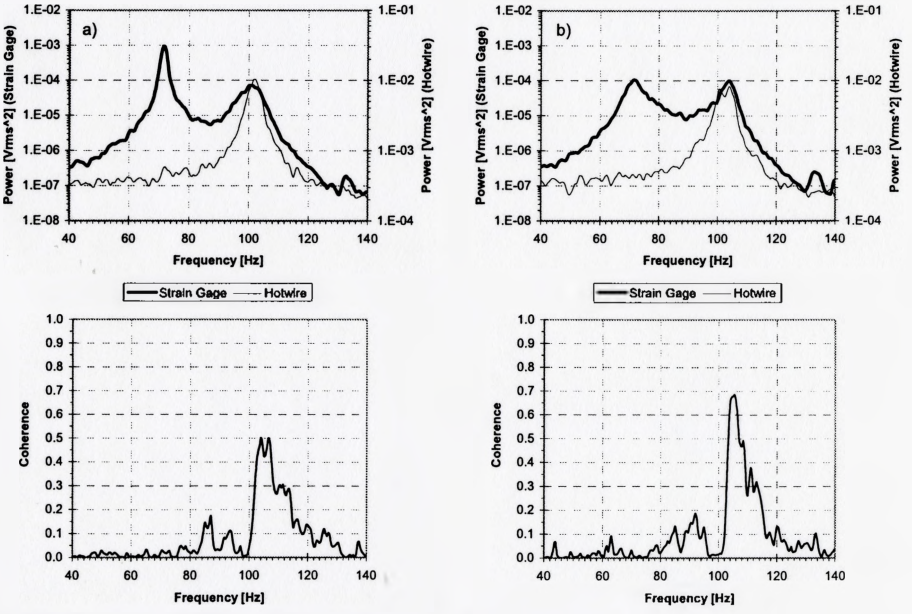

Figure D.32. Power spectra of and coherence between the strain gage and hotwire signals at X/D=1.875 and Z/D=3.75 for the long slit case. a) No Control. b) Optimal Control.